UNIVERSITY OF Southampton

University of Southampton Research Repository
ePrints Soton

Copyright © and Moral Rights for this thesis are retained by the author and/or other copyright owners. A copy can be downloaded for personal non-commercial research or study, without prior permission or charge. This thesis cannot be reproduced or quoted extensively from without first obtaining permission in writing from the copyright holder/s. The content must not be changed in any way or sold commercially in any format or medium without the formal permission of the copyright holders.

When referring to this work, full bibliographic details including the author, title, awarding institution and date of the thesis must be given e.g.

AUTHOR (year of submission) "Full thesis title", University of Southampton, name of the University School or Department, PhD Thesis, pagination

http://eprints.soton.ac.uk

GALLIUM AND TITANIUM DIFFUSED OPTICAL WAVEGUIDE DEVICES IN SAPPHIRE

Vasilis Apostolopoulos

A thesis submitted for the degree of Doctor of Philosophy

FACULTY OF ENGINEERING AND APPLIED SCIENCE

OPTOELECTRONICS RESEARCH CENTRE

UNIVERSITY OF SOUTHAMPTON

June 2003

UNIVERSITY OF SOUTHAMPTON

ABSTRACT

FACULTY OF ENGINEERING AND APPLIED SCIENCE
OPTOELECTRONICS RESEARCH CENTRE

Doctor of Philosophy

GALLIUM AND TITANIUM DIFFUSED OPTICAL WAVEGUIDE DEVICES IN SAPPHIRE

by Vasilis Apostolopoulos

This thesis describes new methods to realise an integrated Ti:Sapphire laser using thermal ionic diffusion. Passive and active waveguides were fabricated by thermal diffusion of gallium and titanium ions in sapphire.

Theoretical simulations were established which describe the potential of planar Ti:Sapphire waveguide lasers and intracavity wavelength selection devices. A diffusion study of gallium, titanium and gallium/titanium co-doping is presented; the diffusion coefficient of gallium ions in sapphire was calculated to be $3.3x10^{-17}$ m^2s^{-1} at 1600^0C and the diffusion coefficient of titanium ions in sapphire at 1600^0C was found to be $1.7x10^{-15}$ m^2s^{-1}.

Planar Ga:Sapphire passive waveguides were realised by thermal diffusion of gallium ions. The refractive index of sapphire at 800nm is approximately 1.766 and the index change induced by gallium doping was found to be up to $6x10^{-3}$ and the mode sizes of the waveguides were as small as 1μm at 488nm. A fabrication procedure based on SU-8 photolithography and ion beam milling was developed for micromachining the surface of sapphire. Using this fabrication technique Ga:Sapphire ridge waveguides were fabricated by diffusion of gallium and exhibited mode sizes as small as 2μm at 633nm. Using the same fabrication technique the realisation of the first Ti-diffused sapphire ridge waveguide lasers is reported. Finally, the fabrication of sapphire optical circuits using titanium and gallium co-doping is described and fluorescence characterisation of these waveguides is given.

CONTENTS

CHAPTER 1 INTRODUCTION

1.1 Introduction..1

1.2 Advantages of the waveguide geometry..1

1.3 Sapphire as a substrate material for integrated optics..3

1.3.1 Rare-earth doped sapphire devices..3

1.3.2 Ti and Cr doped integrated devices in Sapphire..4

1.4 Waveguides in sapphire by ionic diffusion..5

1.5 General overview of the thesis..7

References to Chapter 1..10

CHAPTER 2 TI: SAPPHIRE WAVEGUIDE LASER: THEORY AND MODELLING

2.1 Introduction..15

2.2 Material characteristics of sapphire..16

2.2.1 Sapphire as a mineral..16

2.2.2 Synthetic Sapphire and modern applications..17

2.2.3 Crystal structure of Sapphire..17

2.2.4 Physical properties of Sapphire and Ti:Sapphire..18

2.2.5 Spectroscopy of Titanium doped sapphire..19

i) Energy levels of the Ti^{3+} ion in sapphire..19

ii) Characteristics of the Ti:Sapphire laser..21

2.3 Waveguide Theory..24

2.3.1 Asymmetric slab waveguide model..24

2.3.2 WKB method..29

2.3.3 Beam Propagation Method (BPM) 30
2.4 Titanium Sapphire waveguide laser model..........33
2.4.1 Waveguide laser description..........33
2.4.2 Energy levels of Ti:Sapphire. 34
2.4.3 Gain and threshold of the waveguide laser..........35
i) Population inversion..........36
ii) Laser gain..........37
iii) Threshold of the laser..........38
iv) Pump and signal mode sizes..........39
v) Waveguide losses and mirror reflectivities. 40
vi) Device length..........42
2.4.4 Slope efficiency and waveguide losses..........43
2.5 Integrated wavelength selection..........43
2.5.1 Grating wavelength selection..........44
i) F-Matrix model..........45
ii) Phase shifted grating..........47
iii) Model results..........48
2.5.2 Coupled cavity integrated resonators..........51
i) Basic principles of y-junction resonators..........52
ii) Model for coupled cavity integrated resonators...........54
iii) Bent waveguides..........61
2.6 Conclusions..........62
References to Chapter 2..........64

CHAPTER 3 DIFFUSION OF TITANIUM AND GALLIUM IN SAPPHIRE

3.1 Introduction..67

3.2 Theory of Diffusion 68

3.2.1 Introduction..68

3.2.2 Mass flux and Fick's first law...68

3.2.3 The diffusion equation 69

3.2.4 Physical meaning of the diffusion coefficient. 70

3.2.5 The Arrhenius relation 71

3.2.6 Solutions to the diffusion equation. 72

3.3 Overview of diffusion in sapphire 74

3.3.1 Diffusion characterisation in sapphire 74

3.3.2 Literature review of cation diffusion in sapphire...............................75

3.3.3 Review of titanium diffusion in sapphire...77

i) Fabricated samples and characterisation techniques 77

ii) Concentration profiles of Ti in sapphire...79

3.3.4 Limitations of diffusion in sapphire..81

3.4 Diffusion of Gallium in sapphire 83

3.4.1 Introduction..83

3.4.2 Preparation of samples 84

3.4.3 Diffusion conditions..84

3.4.4 Characterization of diffusion profiles 86

3.5 Combined Titanium and Gallium diffusion in Sapphire 91

3.5.1 Introduction..91

3.5.2 Fabrication of samples 92

3.5.3 Preparation of samples for analysis by bevelling. 93

3.5.4 Diffusion profiles of gallium and titanium diffused samples 95
i) Sample 1, Ti diffusion 96
ii) Sample 2, Ga diffusion followed by Ti diffusion..................................... 99
iii) Sample 3, Ti diffusion followed by Ga diffusion.................................. 101
iv) Sample 4, Ga/Ti diffusion 103
v) Overview of results for Ga/Ti diffusion 105
3.6 Conclusions.. 106
References to Chapter 3 109

CHAPTER 4 GALLIUM DIFFUSED WAVEGUIDES IN SAPPHIRE

4.1 Introduction.. 111
4.2 Waveguide fabrication 112
4.2.1 Fabrication of slab waveguides.. 112
4.2.2 Fabrication of channel waveguides... 113
4.2.3 Overview of fabrication parameters.. 114
4.3 Characterisation of Ga:Sapphire waveguides 115
4.3.1 Introduction.. 115
4.3.2 Experimental procedure for optical measurements.................................. 116
4.3.3 Mode profiles of samples 1 to 4 between wavelengths of 700 and 850nm. 117
i) Experimental results 117
ii) Discussion of results.. 120
4.3.4 Mode profiles of samples 5 to 8 at 488 and 633nm 122
i) Experimental results 122
ii) Discussion of results.. 122

4.3.5 Channel waveguide mode profiles 123
i) Experimental results 123
ii) Discussion of results 124
4.4 Maximum index change of the Ga:Sapphire waveguides 124
4.5 Conclusions 126
References to Chapter 4 128

CHAPTER 5 GALLIUM-DIFFUSED RIDGE WAVEGUIDES IN SAPPHIRE

5.1 Introduction 129
5.2 Fabrication 130
5.2.1 Overview of the process 130
5.2.2 Details of SU-8 application 133
5.2.3 Fabricated samples 135
5.3 Characterisation of gallium diffused ridge waveguides 136
5.3.1 Mode profiles 136
5.3.2 Prism coupling 137
5.3.3 Propagation loss and spectral attenuation measurements 138
5.4 Beam Propagation Model. 141
5.5 Conclusions 143
References to Chapter 5 144

CHAPTER 6 ACTIVE TITANIUM-DIFFUSED RIDGE WAVEGUIDES IN SAPPHIRE

6.1 Introduction 145

6.2 Ga and Ti diffused ridge waveguides 146
6.2.1 Samples fabricated for characterisation of Ti and Ga co-diffusion. 146
6.2.2 Experimental fluorescence configuration 147
6.2.3 Fluorescence spectra of samples R1-R5 148
6.3 Ti:Sapphire ridge waveguide lasers 152
6.3.1 Fabrication overview of the titanium diffused ridge samples 152
6.3.2 Discussion of the fabrication procedure of the Ti-diffused ridge waveguides 154
i) Titanium diffusions 154
ii) SU 8 photolithography of the planar Ti:Sapphire waveguides 154
iii) Alignment and end-face polishing for active devices 155
6.3.3 Characterisation of the Titanium sapphire ridges 155
i) Mode profiles and loss measurements 155
ii) Fluorescence measurements 156
iii) Laser measurements 158
6.3.4 Summary and discussion on the results of the waveguide lasers 161
6.4 Conclusions 164
References to Chapter 6 165

CHAPTER 7 CONCLUSIONS

7.1 Introduction 166
7.2 Summary of the presented work 166
7.3 Proposed future research directions 168
7.3.1 Improvement of the Ti:Sapphire ridge waveguide laser 168
7.3.2 Gallium and titanium co-doping 168
7.3.3 Wavelength selection and tunability 169

References to Chapter 7 171

Publications, Conferences and Patents 172

ACKNOWLEDGMENTS

Finishing this PhD thesis I realise that I consider myself extremely lucky for the people I have or had around me. So, I would like first to thank James Wilkinson for being an excellent supervisor and an amazing person, I sincerely consider myself lucky to know him. I also thank my parents for being supportive in really all my decisions, I could not ask for more. Also thanks to all the people in our group, especially David Sager, happy to know him and work with him. Thanks to all my friends, here I will name only the ones that are work-related, meaning … Sakellaris Mailis, Tracy Melvin, Pavlos Lagoudakis. And I conclude with a somehow mysterious acknowledgment to the people that I lost during the PhD.

CHAPTER 1

INTRODUCTION

1.1 Introduction

The Ti:Sapphire laser was invented by Peter F. Moulton in 1982 [1,2] and quickly became commercially successful. Implementing the Ti:Sapphire laser in a waveguide geometry is expected to lead to a portable laser source with a tuning range from 650 to 1050nm with applications in spectroscopy, microscopy and sensing. This thesis describes the progress towards creating new methods to successfully realise active integrated devices in sapphire. In this thesis, fabrication of passive waveguides in sapphire by thermal diffusion of gallium is reported for the first time. Furthermore by micromachining the surface of the sapphire substrates ridge gallium diffused sapphire waveguides are fabricated and characterised for the first time. Finally using diffusion of titanium and surface micromachining the first rib waveguide titanium sapphire laser is realised.

1.2 Advantages of the waveguide geometry

The bulk titanium sapphire laser is a successful scientific laser and is used mainly in research as a tunable source. Furthermore, due to its broad tuning range the Ti:Sapphire laser is ideally suited to realise a pulsed source, which was confirmed in 1990 when self mode-locking was exhibited [3,4]. At present, femtosecond Ti:Sapphire lasers [5] are the principal research tools for investigation of ultra-fast

phenomena. Nevertheless, the applications of the titanium sapphire laser are restricted because of the investment required to support such a system. A Ti:Sapphire laser system is expensive (50-100k£), partly because it requires an expensive pump laser (Argon Ion or frequency doubled solid state laser).

The miniaturisation of the Ti:Sapphire laser is an ambitious and demanding project; nevertheless it is justified by the potential performance of the result. The implementation of a Ti:Sapphire laser in a waveguide geometry, compared to the bulk solution, provides flexibility that could lead to improved performance and reduced cost. The confinement of radiation in the waveguide increases the optical intensity, for a given pump power and, combined with low waveguide propagation losses, can give a laser with low lasing threshold and high slope efficiency. This opens up a wider choice of pump sources, and may allow replacement of the traditional laser schemes that are now used for pumping Ti:Sapphire lasers with smaller and more efficient pump sources. Small sources in the blue-green will shortly be available with sufficient power and reliability with the use of materials like GaN [6,7] and can be used for pump sources in order to produce a diode-pumped portable Ti:Sapphire laser. Further, in a waveguide geometry integrated wavelength selection can be introduced, and finally the geometry of such a device is ideal for conductive cooling due to the proximity of the waveguide structure to the surface.

1.3 Sapphire as a substrate material for integrated optics

Since the first demonstration of the bulk Ti:Sapphire laser, research has been performed in order to use Al_2O_3 in integrated optics and a diversity of approaches has been taken. Research was conducted aiming to realise a Ti:Sapphire laser in integrated geometry using a variety of fabrication methods [8-11]. There were also numerous attempts to use sapphire in bulk or film form as a host for other active ions [12]. There were successful attempts to grow Al_2O_3 films functioning as waveguides on Si/SiO_2 substrates for implementation of active integrated circuits with the introduction of rare earth ions, such as erbium [13].

1.3.1 Rare-earth doped sapphire devices

Sapphire films have been demonstrated to form high quality passive waveguides and also have the potential for incorporating rare earth ions, Er, in high concentrations [13-16]. Due to the applications such as amplifiers in the telecommunications industry, there has been a great interest in research for the implementation of rare earth doping in Al_2O_3 films. The optical properties of rare earth ions are very weakly dependent on the electric field of the host lattice as the electrons that undergo the laser transitions are in an inner energy shell. Consequently, the sapphire host films can be polycrystalline, which increases the freedom in the fabrication methods that can be used. Al_2O_3 films have been sputtered and subsequently doped using Er ion implantation [12,17]. Other methods used for the growth of the films are Chemical Vapour Deposition (CVD) or Plasma Enhanced Metallo-Organic CVD (PE-MOCVD) [18,19] and Pulsed Laser Deposition (PLD) [20-22]. Thermal annealing has been shown to enhance the performance of the doped (passive) or un-doped (active) sapphire film waveguides by reducing the losses or increasing the fluorescence yield of the active ions [23].

1.3.2 Ti and Cr doped integrated devices in Sapphire

Similar scientific work has been carried out into the incorporation of Ti and Cr ions inside the lattice of sapphire using alternative methods. A significant difference between transition metal ions (Ti and Cr) and rare earths is that in the case of transition metals the laser electronic transition is in the outer shell which is strongly affected by the local crystal field. In the trivalent state the Ti^{3+} ion has the electron configuration of Ar]$4s^2$ $3d^1$, and can be regarded as a closed shell plus a single 3d electron. The free space d-electron energy levels are five-fold degenerate (excluding spin) and there is no lower energy electron level to permit a radiative transmission. In the local crystal field of the sapphire the degeneracy is lifted and the levels are split thereby allowing laser transitions [24]. Consequently, single-crystal sapphire is needed as a host for these ions and the fabrication techniques are limited accordingly. At Southampton University work is being carried out into the fabrication of titanium sapphire waveguide lasers using pulsed laser deposition (PLD) [8,25,26]. A slab waveguide laser has been demonstrated using this technique, with 0.5W pump power threshold and fluorescence in ridge waveguides has been recently demonstrated using patterning and etching [27].

A passive waveguide can be formed in sapphire by ion implantation of a light ion, He, and an active region can be formed by implantation of a metal ion. The implantation in sapphire of numerous metal ions has been studied [10,28-44]. This technique is used combined with annealing because it creates high structural damage and therefore high propagation losses and amorphous layers in sapphire that inhibit the fluorescence of active ions such as Ti.

Another important approach, based on fibre geometry, aims at the fabrication of a low threshold, compact Ti:Sapphire source. A single crystal fibre was pulled using the laser heated pedestal method [11] and was operating as a Ti:Sapphire laser with 56nm of tuning range. Sapphire fibres are also important as probes, in sensing applications for measuring temperature in a wide temperature range, up to 1800^{0}C [45,46] and also in medical, surgical applications [47].

1.4 Waveguides in sapphire by ionic diffusion

Thermal diffusion is a promising fabrication process as it offers the potential for introducing a dopant inside a crystal without severely distorting the lattice of the host. The doping level and the depth of the diffusion can be controlled by appropriately selecting the parameters of the process such as time, temperature and thickness of the diffusion source. Diffusion in sapphire for fabrication of integrated devices is not thoroughly explored because until recently it was believed that in order to have the appropriate doping levels and diffusion depth required for waveguide fabrication forbiddingly high temperatures needed to be used. A first step towards this goal was achieved in the University of Southampton by Louise Hickey with the fabrication of the first Ti:Sapphire channel waveguide laser by thermal diffusion of titanium into a sapphire wafer [9,48-50]. The work presented here shows that titanium and gallium ions can be readily diffused to sufficient depths for waveguide fabrication [51,52].

A number of problems are identified and addressed in this work, thereby significantly advancing progress towards titanium sapphire laser integration by ionic diffusion. Channel waveguides and locally doped regions can be fabricated by photolithographic patterning of the diffusion source. Nevertheless, an inherent problem of titanium and

gallium diffusion in sapphire is the strong component of surface diffusion. This poses a limit to the horizontal confinement that can be achieved in the fabrication of a channel waveguide using a patterned diffusion source. In this work a technological solution was developed, which is based on the surface micromachining of sapphire, after photolithography using SU-8 photoresist [52].

Titanium diffusion in sapphire yields an index change of approximately 10^{-4} at the optimum concentrations to realise a laser [53]. The introduction of a second ion into sapphire with thermal diffusion in order to form a passive waveguide is expected to yield a number of significant advantages. By co-doping with an active ion and a waveguide ion the waveguide and the gain medium characteristics can be independently controlled, leading to greater design flexibility. Furthermore, a passive waveguide formed by introducing another ion can deliver pump power in waveguide circuits since it would not absorb at the pump wavelength. The active region could be localised in the centre of the sapphire chip and this would also benefit the thermal management of the device. This combined diffusion approach is used in waveguide lasers fabricated in lithium niobate where erbium and titanium are the active and the waveguide ion respectively [54,55]. A waveguide ion which would result in a higher index increase than Ti would also result in guided modes with smaller mode waists, which would potentially lead to the fabrication of low-threshold lasers and more densely integrated active optical circuits. Figure 1.1 shows a possible implementation of a waveguide coupled cavity realised by co-doping with titanium and gallium. This is an integrated device which could feature integrated wavelength selection and tunability (section 2.5.2). In this project the waveguide ion was successfully identified

as the Ga^{3+} ion and passive diffused planar and ridge waveguides were fabricated and characterised [51,52,56].

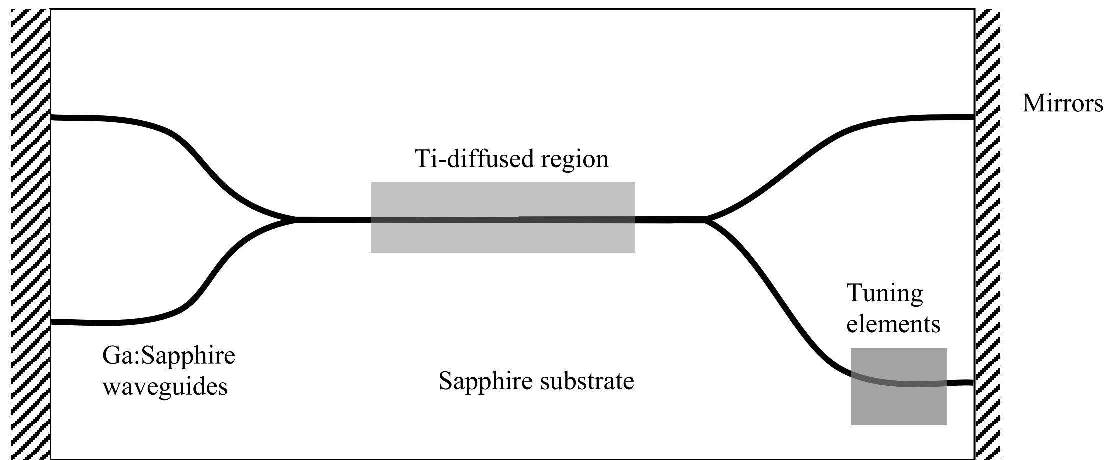

Figure 1.1. Possible implementation of an integrated tunable titanium sapphire coupled cavity.

1.5 General overview of the thesis

In this thesis passive and active waveguides were fabricated by thermal diffusion of gallium and titanium ions in sapphire. Chapter 2 gives a summary of theoretical principles that were used as design guidelines for this project and also uses theoretical simulations which outline the potential of the devices that are pursued in the present work. The chapter starts with the presentation of sapphire and titanium doped sapphire, giving details on the physical and optical properties. Waveguide theory is then briefly given and the waveguide models used in this thesis are described. Laser theory adapted to the case of titanium-doped sapphire is presented and a model for a waveguide laser is presented with simulation results that estimate the performance of such a configuration. Wavelength selection mechanisms are presented, including a model for gratings on sapphire integrated devices. Furthermore a theory of coupled cavity structures for wavelength selection is described and results from a model are

given in order to investigate a cavity design which may be suitable for a Ti:Sapphire laser.

Chapter 3 describes the characterisation of the diffusion processes of titanium and gallium in sapphire. The chapter starts with the classical theory of diffusion as a theoretical basis for the characterisation of the results. The diffusion study of gallium, titanium and gallium/titanium codoping is presented in the chapter. Diffusion coefficients for all these cases are given and the results are discussed in terms of realising titanium and gallium integrated devices.

Chapter 4 describes the fabrication and characterisation of planar Ga:Sapphire passive waveguides; it starts with the description of the fabrication procedure for the waveguide samples. The characterization of the waveguide samples was based on a series of experiments which relate the fabrication parameters to the guided modes. The optimization of the samples was achieved by increasing the refractive index change and consequently minimizing the size of the mode waists. At the end of this chapter the results obtained in these experiments are used in waveguide models in order to conclude the characterisation of the waveguides.

Chapter 5 describes the realisation and characterisation of Ga:Sapphire ridge waveguides by diffusion of gallium followed by photolithography and ion beam milling. The chapter starts with a description of the fabrication procedure which is a general technological tool for micromachining the surface of sapphire. The experimental characterisation of the ridges is given and the potential of these devices for fabrication of active integrated circuits is underlined.

Chapter 6 presents the realisation of the first Ti:Sapphire ridge waveguide lasers. The fabrication of the active devices is described and the experimental results giving the performance of the devices are given. The fabrication of sapphire circuits with titanium and gallium co-doping is included and fluorescence measurements on the waveguides are given.

Chapter 7 draws conclusions from the work presented in the thesis, and proposes future work which would exploit the devices realised in this project.

In summary, this thesis presents the successful realisation of gallium doped passive waveguides in sapphire, micromachining of the substrate surface for the implementation of channel waveguides and finally the first titanium sapphire ridge waveguide laser.

References to Chapter 1

1. P.F.Moulton. XXII Int. Quantum Electronics Conference. 1982. Munich, Germany.

2. P. F. Moulton, "Spectroscopic and Laser Characteristics of Ti-Al_2O_3," *Journal of the Optical Society of America B-Optical Physics* **3**, 125-133 (1986).

3. J. Goodberlet, J. Wang, J. G. Fujimoto, and P. A. Schulz, "Femtosecond Passively Mode-Locked Ti-Al_2O_3 Laser with A Nonlinear External Cavity," *Optics Letters* **14**, 1125-1127 (1989).

4. P. M. W. French, S. M. J. Kelly, and J. R. Taylor, "Mode-Locking of A Continuous-Wave Titanium-Doped Sapphire Laser Using A Linear External Cavity," *Optics Letters* **15**, 378-380 (1990).

5. D. E. Spence, P. N. Kean, and W. Sibbett, "60-Fsec Pulse Generation from A Self-Mode-Locked Ti-Sapphire Laser," *Optics Letters* **16**, 42-44 (1991).

6. Fasol G. "Room-temperature blue gallium nitride laser diode". *Science* **272**, 1751. (1996).

7. Nakamura S. "Blue light emitting laser diodes". *Thin solid films* , **345**. (1999).

8. A. A. Anderson, R. W. Eason, L. M. B. Hickey, M. Jelinek, C. Grivas, D. S. Gill, and N. A. Vainos, "Ti:sapphire planar waveguide laser grown by pulsed laser deposition," *Optics Letters* **22**, 1556-1558 (1997).

9. LMB Hickey, AA Anderson, and JS Wilkinson. "Ti:Sapphire channel waveguide laser by thermal diffusion of titanium into sapphire. post deadline paper" pd6. 1997. Stockholm. 8th European Conference on Integrated Optics.

10. H. Lee, S. M. Lee, E. T. Ada, B. Kim, M. Weiss, S. S. Perry, and J. W. Rabalais, "Shallow implantation of Ti+ ions in sapphire [alpha-Al_2O_3(0001)]," *Nuclear Instruments & Methods in Physics Research Section B- Beam Interactions with Materials and Atoms* **157**, 226-232 (1999).

11. L. S. Wu, A. H. Wang, J. M. Wu, L. Wei, G. X. Zhu, and S. T. Ying, "Growth and Laser Properties of Ti-Sapphire Single-Crystal Fibers," *Electronics Letters* **31**, 1151-1152 (1995).

12. G. N. vandenHoven, Snoeks, E., Polman, A., vanDam, C., vanUffelen, J. W. M., and Smit, M. K. "Optical gain in erbium-implanted Al_2O_3 waveguides." Proc.of 7th European Conference on Integrated Optics, Delft, Holland , 229-232. 1995.

13. G. N. vandenHoven, R. J. I. M. Koper, A. Polman, C. vanDam, J. W. M. vanUffelen, and M. K. Smit, "Net optical gain at 1.53 μm in Er-doped Al_2O_3 waveguides on silicon," *Applied Physics Letters* **68**, 1886-1888 (1996).

14. G. N. vandenHoven, E. Snoeks, A. Polman, J. W. M. vanUffelen, Y. S. Oei, and M. K. Smit, "Photoluminescence Characterization of Er-Implanted Al_2O_3 Films," *Applied Physics Letters* **62**, 3065-3067 (1993).

15. G. N. vandenHoven, E. Snoeks, A. Polman, C. vanDam, J. W. M. vanUffelen, and M. K. Smit, "Upconversion in Er-implanted Al_2O_3 waveguides," *Journal of Applied Physics* **79**, 1258-1266 (1996).

16. G. N. vandenHoven, J. A. vanderElsken, A. Polman, C. vanDam, K. W. M. vanUffelen, and M. K. Smit, "Absorption and emission cross sections of Er^{3+} in Al_2O_3 waveguides," *Applied Optics* **36**, 3338-3341 (1997).

17. A. Polman, "Erbium implanted thin photonic films", *Journal of Applied Physics* **82**, 1-39 (1997).

18. Muller R et al. "Spectroscopic study of the reduction of nickel and cobalt ions in sapphire." *J.Chem.Phys* **44**, 365 (1966).

19. M. Mahnke, S. Wiechmann, H. J. Heider, O. Blume, and J. Muller, "Aluminum oxide doped with erbium, titanium and chromium for active integrated optical applications," *Aeu-International Journal of Electronics and Communications* **55**, 342-348 (2001).

20. R. Serna, M. J. de Castro, J. A. Chaos, C. N. Afonso, and I. Vickridge, "The role of Er^{3+}-Er^{3+} separation on the luminescence of Er- doped Al_2O_3 films prepared by pulsed laser deposition," *Applied Physics Letters* **75**, 4073-4075 (1999).

21. M. J. de Castro, R. Serna, J. A. Chaos, C. N. Afonso, and E. R. Hodgson, "Influence of defects on the photoluminescence of pulsed-laser deposited Er-doped amorphous Al_2O_3 films," *Nuclear Instruments & Methods in Physics Research Section B- Beam Interactions with Materials and Atoms* **166**, 793-797 (2000).

22. R. Serna, M. J. de Castro, J. A. Chaos, A. Suarez-Garcia, C. N. Afonso, M. Fernandez, and I. Vickridge, "Photoluminescence performance of pulsed-laser deposited Al_2O_3 thin films with large erbium concentrations," *Journal of Applied Physics* **90**, 5120-5125 (2001).

23. E. Alves, R. C. da Silva, M. F. da Silva, and J. C. Soares, "Solubility and damage annealing of Er implanted single crystalline alpha-Al_2O_3," *Nuclear Instruments & Methods in Physics Research Section B- Beam Interactions with Materials and Atoms* **139**, 313-317 (1998).

24. F.J.Duarte, *Tunable lasers handbook*, (Academic press, 1995).

25. A. A. Anderson, R. W. Eason, M. Jelinek, C. Grivas, D. Lane, K. Rogers, L. M. B. Hickey, and C. Fotakis, "Growth of Ti:sapphire single crystal thin films by pulsed laser deposition," *Thin Solid Films* **300**, 68-71 (1997).

26. M. Jelinek, R. W. Eason, J. Lancok, A. A. Anderson, C. Grivas, C. Fotakis, L. Jastrabik, F. Flory, and H. Rigneault, "Waveguiding pulsed laser deposited Ti : sapphire layers on quartz," *Thin Solid Films* **322**, 259-262 (1998).

27. C. Grivas, D. P. Shepherd, T. C. May-Smith, R. W. Eason, M. Pollnau, A. Crunteanu, and M. Jelinek, "Performance of Ar+-milled Ti : sapphire rib waveguides as single transverse-mode broadband fluorescence sources," *IEEE Journal of Quantum Electronics* **39**, 501-507 (2003).

28. Y. Saito, H. Kumagai, and S. Suganomata, "Coloration of Sapphire by Metal-Ion Implantation," *Japanese Journal of Applied Physics Part 2-Letters* **24**, L880-L882 (1985).

29. A. P. Mouritz, D. K. Sood, D. H. Stjohn, M. V. Swain, and J. S. Williams, "Ion-Implantation of Low Melting-Point Metals Into Sapphire," *Nuclear Instruments & Methods in Physics Research Section B- Beam Interactions with Materials and Atoms* **19-2**, 805-808 (1987).

30. T. Miyano, T. Matsumae, H. Yokoo, Y. Andoh, M. Kiuchi, and M. Satou, "Effect of High-Energy Ion-Implantation on Sapphire," *Nuclear Instruments & Methods in Physics Research Section B- Beam Interactions with Materials and Atoms* **59**, 1167-1172 (1991).

31. Y. Saito, H. Horie, and S. Suganomata, "Coloration of Sapphire by Co Ion-Implantation," *Nuclear Instruments & Methods in Physics Research Section B- Beam Interactions with Materials and Atoms* **59**, 1173-1176 (1991).

32. M. Bauer, S. M. M. Ramos, B. Canut, J. L. Loubet, L. Romana, L. Gea, P. Kapsa, and P. Thevenard, "Titanium and Niobium Implantation Into Alpha-Al_2O_3 - Structural and Mechanical-Properties," *Nuclear Instruments & Methods in Physics Research Section B- Beam Interactions with Materials and Atoms* **65**, 301-304 (1992).

33. G. W. Arnold, "Ion-Implantation Effects in Al2O3 - Hydration and Optical-Absorption," *Nuclear Instruments & Methods in Physics Research Section B-Beam Interactions with Materials and Atoms* **80-1**, 1036-1039 (1993).

34. E. Alves, M. F. daSilva, G. N. vandenHoven, A. Polman, A. A. Melo, and J. C. Soares, "Incorporation and stability of erbium in sapphire by ion implantation," *Nuclear Instruments & Methods in Physics Research Section B-Beam Interactions with Materials and Atoms* **106**, 429-432 (1995).

35. C. J. McHargue, J. D. Hunn, D. L. Joslin, E. Alves, M. F. daSilva, and J. C. Soares, "Etching of amorphous Al_2O_3 produced by ion implantation," *Nuclear Instruments & Methods in Physics Research Section B- Beam Interactions with Materials and Atoms* **127**, 596-598 (1997).

36. J. D. Demaree, S. R. Kirkpatrick, A. R. Kirkpatrick, and J. K. Hirvonen, "Modification of single-crystal sapphire by ion implantation," *Nuclear Instruments & Methods in Physics Research Section B- Beam Interactions with Materials and Atoms* **127**, 603-607 (1997).

37. D. Z. Xie, D. Z. Zhu, H. C. Pan, H. J. Xu, and Z. X. Ren, "Enhanced etching of sapphire damaged by ion implantation," *Journal of Physics D-Applied Physics* **31**, 1647-1651 (1998).

38. S. Nakao, M. Ikeyama, M. Tazawa, P. Jin, H. Niwa, S. Tanemura, Y. Miyagawa, S. Miyagawa, and K. Saitoh, "High-energy co-implantation of Ti and O ions into sapphire," *Materials Chemistry and Physics* **54**, 342-345 (1998).

39. J. C. McCallum and L. D. Morpeth, "Synthesis of Ti : sapphire by ion implantation," *Nuclear Instruments & Methods in Physics Research Section B-Beam Interactions with Materials and Atoms* **148**, 726-729 (1999).

40. J. Tian, Q. Z. Wang, Y. F. Chen, and Q. J. Xue, "Reaction in Al_2O_3 surface layers upon ion implantation," *Journal of Materials Chemistry* **10**, 565-569 (2000).

41. M. Ando, Y. Kanemitsu, T. Kushida, K. Matsuda, T. Saiki, and C. W. White, "Sharp photoluminescence of CdS nanocrystals in Al_2O_3 matrices formed by sequential ion implantation," *Applied Physics Letters* **79**, 539-541 (2001).

42. L. D. Morpeth and J. C. McCallum, "Ti : sapphire formation via the co-implantation of Ti and O ions into sapphire," *Nuclear Instruments & Methods in Physics Research Section B- Beam Interactions with Materials and Atoms* **175**, 537-541 (2001).

43. C. Marques, M. M. Cruz, R. C. da Silva, and E. Alves, "Optical changes induced by high fluence implantation of Co ions on sapphire," *Surface & Coatings Technology* **158**, 54-58 (2002).

44. M. Ikeyama, S. Nakao, and M. Tazawa, "Optical property changes in sapphire induced by triple-energy Cu and O implantation," *Surface & Coatings Technology* **158**, 720-724 (2002).

45. Y. H. Shen, L. M. Tong, Y. Q. Wang, and L. H. Ye, "Sapphire-fiber thermometer ranging from 20 to 1800 degrees C," *Applied Optics* **38**, 1139-1143 (1999).

46. J. H. Sharp, C. W. P. Shi, and H. C. Seat, "Er-doped sapphire fibre temperature sensors using upconversion emission," *Measurement & Control* **34**, 170 (2001).

47. J. Fitzgibbon and G. Hayes, "Sapphire optical fibers: Rugged fiber expands surgical and sensor applications," *Photonics Spectra* **33**, 118-119 (1999).

48. L. M. B. Hickey and J. S. Wilkinson, "Titanium diffused waveguides in sapphire," *Electronics Letters* **32**, 2238-2239 (1996).

49. L. M. B. Hickey, E. Martins, J. E. Roman, W. S. Brocklesby, and J. S. Wilkinson, "Fluorescence of Ti^{3+} ions thermally diffused into sapphire," *Optics Letters* **21**, 597-599 (1996).

50. Louise M.B.Hickey, PhD thesis, "Ti:Sapphire waveguide laser by the thermal diffusion of Ti into sapphire", (Optoelectronics Research Centre, University of Southampton, 1998).

51. V. Apostolopoulos, L. M. B. Hickey, D. A. Sager, and J. S. Wilkinson, "Gallium-diffused waveguides in sapphire," *Optics Letters* **26**, 1586-1588 (2001).

52. V.Apostolopoulos, L.M.B.Hickey, D.A.Sager, and J.S.Wilkinson. "Gallium diffused ridge waveguides in Sapphire". CLEO Long Beach California. 2002.

53. Louise MB Hickey. "Report on Activities in Southampton during the 1851 fellowship award". 1999.

54. Becker P et al. "Er-Diffused Ti-$LiNbO_3$ Wave-Guide Laser of 1563 and 1576 nm emission wavelengths". *Applied Physics Letters* **61**, 1257 (1992).

55. R. Brinkmann, W. Sohler, and H. Suche, "Continuous-Wave Erbium-Diffused $LiNbO_3$ Wave-Guide Laser," *Electronics Letters* **27**, 415-417 (1991).

56. V.Apostolopoulos, Mini-thesis, "Gallium diffused waveguides in Sapphire" (Electronics and Computer Science, University of Southampton, 2000).

CHAPTER 2

TI: SAPPHIRE WAVEGUIDE LASER: THEORY AND MODELLING

2.1 Introduction

In this chapter the theoretical background to the different concepts surrounding the realisation of active waveguide devices in sapphire is presented. Further, in order to outline the potential performance of a Ti:Sapphire waveguide laser, theoretical simulations were developed and the modelling results are given.

The chapter starts with an introduction of the fundamental material properties of pure and doped sapphire. The basic physical properties of sapphire are given as well as its chemical composition and crystal structure. Following this introduction to the substrate material, the basic theory of the optical waveguide is included. A range of waveguide models are described, starting with the simple theory of the slab waveguide model and continuing with the description of increasingly complex and powerful models. Subsequently basic laser theory is presented and in particular a theoretical model of a 4-level laser system that is expanded into waveguide geometry. This simulation analyses the potential performance of the integrated Ti:Sapphire laser, which is realised in this thesis.

In the final part of this chapter the potential for integrated wavelength selection mechanisms is explored. The first configuration analysed is a Distributed FeedBack laser (DFB) in which the wavelength selection element is a surface relief grating. The theory of DFB lasers is presented with modelling results. The second possible wavelength selection mechanism is a coupled cavity configuration in waveguide geometry and is described using a novel theoretical analysis and simulation for the specific device.

2.2 Material characteristics of sapphire

2.2.1 Sapphire as a mineral

Sapphire and ruby in mineral science are considered to be variations of corundum; the chemical composition of corundum is Al_2O_3. Corundum is a very well documented mineral and gemstone, which can be found in nature in a magnificent variety of colours. Historically, corundum or sapphire is known as a precious stone. A very important characteristic of sapphire is that it is the second hardest material that can be found in nature after diamond and it is chemically inert to any etchant at room temperature [1]. Sapphire rates 9 in the Moh scale; as a comparison, diamond rates 15 (definition of the scale's maximum) and common glasses rate approximately 4 [1,2].

Sapphire is a very bright gemstone because of its high refractive index (~1.766 at 800nm) and high purity natural crystallisation. Mineral sapphire is a blue-coloured corundum that takes its colour from the combination of iron and titanium ions. Ruby has a pink to red colour that is created by the presence of chromium ions in the lattice.

2.2.2 Synthetic Sapphire and modern applications

Synthetically grown, single crystal sapphire without any dopants, appeared at the beginning of the 20th century. Although sapphire is known in mineralogy as form of corundum containing Ti and Fe ions, synthetic sapphire is single crystal Al_2O_3 also known as α-alumina. The single crystal is hard, chemically inert, and has high thermal conductivity and excellent electrical resistivity. These characteristics make sapphire a successful insulating substrate for microelectronic components. Furthermore it is an excellent material for fabrication of optical windows in applications where robustness and high optical transmission is needed. Sapphire became important in optoelectronics when ruby was reinvented as the first laser material in 1960 [3]. Following this, in 1982 the Ti doped sapphire laser was discovered by Peter F. Moulton, and very rapidly became a successful scientific laser [4-6]. Due to this variety of applications, today high quality synthetic sapphire can be readily obtained at relatively low prices (approximately £100), usually in wafer form and surface polished to optical flatness.

2.2.3 Crystal structure of Sapphire

The crystal structure of sapphire can be simplified as a hexagonal close packed structure. The lattice consists of layers of close packed oxygen ions with aluminium sites between each oxygen plane. Only two out of every three aluminium sites are occupied in order to preserve electrical neutrality. The exact description of the lattice system of corundum is trigonal - hexagonal Scalenohedral the point group symbol is -3 2/m in international symbols or C_{3v} in Schoeflies symbols; the space group of sapphire is R3_c [1,2,7,8]. Figure 2.1 shows a sketch of the lattice of sapphire, indicating the different crystal planes.

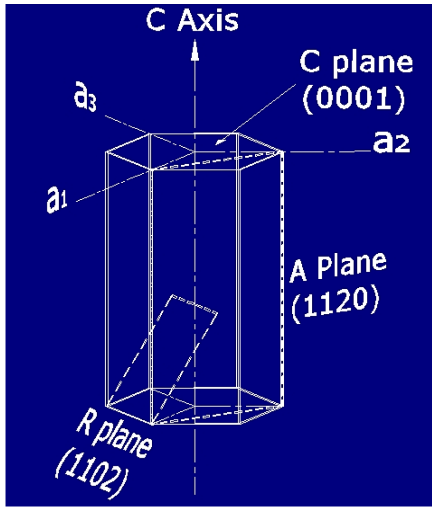

Figure 2.1. Lattice of sapphire, from [1,2].

2.2.4 Physical properties of Sapphire and Ti:Sapphire.

Sapphire is a uniaxial material with a weak negative birefringence, the extraordinary refractive index being about 0.01 lower than the ordinary index at a wavelength of 633nm [9]. The refractive index of sapphire is near 1.75 at visible wavelengths and in Figure 2.2 a graph of refractive index versus wavelength is depicted. The refractive index of sapphire in Figure 2.2 is calculated using the Sellmeier equation with the appropriate parameters [1].

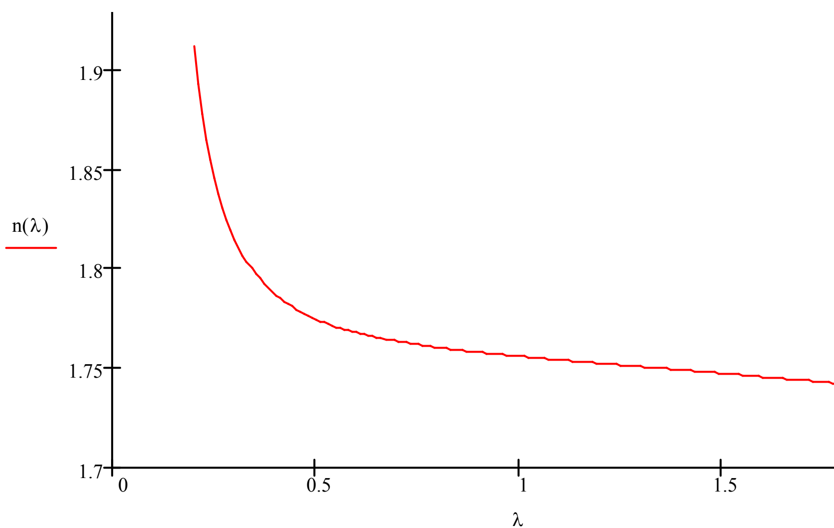

Figure 2.2. Ordinary refractive index of sapphire vs. wavelength

The refractive index of sapphire is dependent on stresses, defect concentration and impurities. The dependency on impurities can be used as an advantage for the realisation of waveguides in sapphire, by introducing dopants. Waveguides have been fabricated in the course of this project using the diffusion of Ti and Ga ions [10-12]. Furthermore the refractive index of a Ti:Sapphire crystal increases with illumination at blue-green wavelengths near the absorption of the active ion, Ti^{3+} [13,14]. The refractive index also increases with temperature, which can have a significant effect on the performance of a laser based on sapphire since it can result in thermal lensing [15,16]. Generally Ti:Sapphire lasers are sensitive to heating and the performance of the first fabrication attempts of Ti:Sapphire lasers was dependent on liquid nitrogen cooling (77K) [17]. However the excellent heat conductivity of sapphire is convenient for successful cooling of the device and at present commercial laser systems use water cooling. In addition, the waveguide geometry is excellent for efficient conductive heat extraction as the laser structure is near the surface of the substrate.

2.2.5 Spectroscopy of titanium doped sapphire.

i) Energy levels of the Ti^{3+} ion in sapphire

Single crystal sapphire is transparent from wavelengths of 200nm to about 7μm [1]; in the optical region, characteristic absorptions occur when the crystal is doped with metal ions, as in the cases of mineral sapphire and ruby. When sapphire is doped with titanium ions, for the preservation of local charge neutrality the Ti^{3+} ion is incorporated substitutionally in the Al sites. In the trivalent state the Ti^{3+} ion has the electron configuration of Ar]$4s^2$ $3d^1$, and can be regarded as a closed shell plus a single 3d electron. The free space d-electron energy levels are five-fold degenerate (excluding spin) and there is no lower energy electron level to permit a radiative

transmission. In the local crystal field the degeneracy is lifted and the levels are split thus allowing laser transitions [18]. The site of the trivalent titanium ion has trigonal- and cubic- symmetry components [8,19,20]. The first splitting of the degenerate energy levels of the 3d electron results from the cubic field that splits the energy levels into a triply degenerate $^{2}T_{2}$ ground state and a doubly degenerate ^{2}E excited state. The trigonal field splits the $^{2}T_{2}$ ground state into two levels. The lower energy level of the ground state, $^{2}T_{2}$, is then split again by spin-orbit interaction. The doubly degenerate ^{2}E excited state is finally split by the dynamic Jahn-Teller effect. The five-fold initial degeneracy of the free electron is completely lifted. In Figure 2.3 a schematic diagram for the splitting of the energy levels is shown. The energy states of the electron are coupled with phonon states, thus the transitions are significantly broadened and Ti:Sapphire is considered to be a vibronic laser [18].

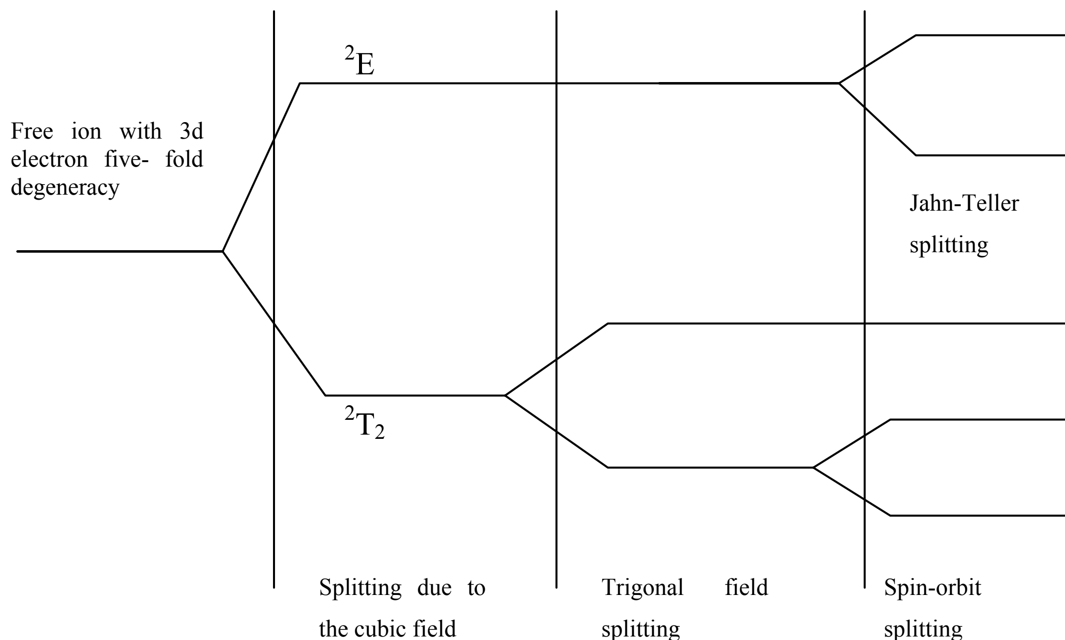

Figure 2.3. A schematic diagram showing how the crystal field lifts the degeneracy of the energy levels of the titanium ion.

ii) Characteristics of the Ti:Sapphire laser

It can be observed that sapphire is an exceptional host for the Ti^{3+} ion; because of the energy level splitting a laser transition is possible with the $^2E \rightarrow ^2T_2$ transition. Data on fluorescence for this transition was first reported by Gachter and Koningstein in 1974 [20] and the first Ti:Sapphire laser was reported, as mentioned, in 1982 by Moulton [4]. In Figure 2.4 the characteristic absorption and emission spectra of Ti doped sapphire is shown from [5]. The peak of the absorption curve is very near 488nm, which is a characteristic line of an Argon ion laser. Typical pumping lasers for a Ti:Sapphire system are Argon ion lasers and more recently CW frequency-doubled solid state sources (Nd:YLF) are used. The π-polarisation is more strongly absorbing than the σ-polarisation and the peak absorption cross-section is approximately 10^{-20} cm^{-2} [21].

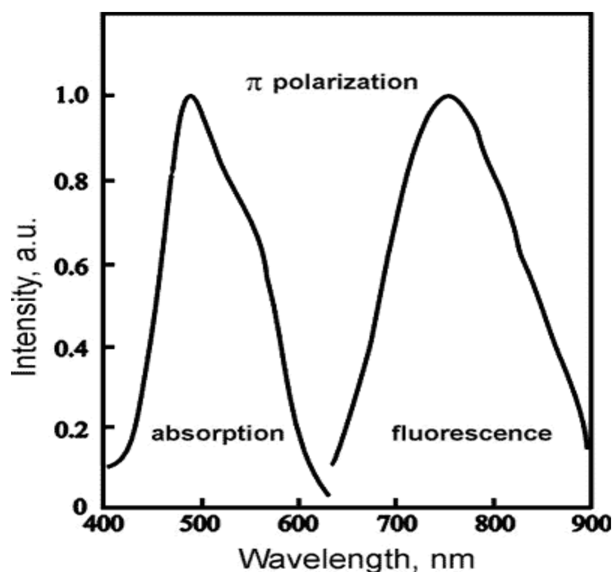

Figure 2.4. Absorption and fluorescence spectra of Ti:Sapphire for the π-polarisation, from [5].

The titanium ions are incorporated in the crystal in the same sites resulting in the line of each atom being broadened the same way, therefore Ti:Sapphire lasers can be approximated as a homogeneously broadened laser. An impurity ion in an ionic

crystal demonstrates collision broadening which is a case of homogeneous broadening and the lineshape of the transition is theoretically described by a Lorentzian distribution [22] .

The peak of the emission curve is near 770nm and the most impressive characteristic of the Ti:Sapphire laser is that the emission curve stretches over approximately 450nm, from 650nm to 1100nm. This bandwidth of 200THz makes the Ti:Sapphire laser a very attractive tunable source with applications in spectroscopy, microscopy and sensing. Furthermore, Ti:Sapphire systems are the most attractive solutions for the generation of ultra-short pulsed sources, this is because the minimum duration of a mode-locked pulse is inversely proportional to the bandwidth of the emission spectrum. Mode-locked, Q-switched Ti:Sapphire lasers are used for the generation of ultra-short pulses in the femtosecond and, recently, in the attosecond region [23-26]. These systems are used for white light generation and spectroscopy, observation of ultra-fast phenomena and very demanding laser machining applications. The laser linewidth increases with temperature as with most laser systems, for example ruby, Nd:YAG etc. The product of the absorption cross-section and the emission lifetime is considered to be a characteristic of the laser medium. The cross-section gives the efficiency with which the pump radiation will raise an ion to the upper level and the lifetime of the transition gives the available time for a successful population inversion to happen. Therefore, a high $\sigma \cdot \tau$ product indicates the potential for a low threshold and high slope efficiency laser, as in the case of the Nd:YAG laser. The lifetime of a laser transition is inversely proportional to the width of the line (FWHM), and for a collision broadened transition, is given by [22]

$$\Delta \nu_0 = \frac{1}{\pi \tau} \quad \textbf{(2.1)}$$

Therefore in the case of Ti:Sapphire the broadband spectrum indicates a trade-off in the lifetime of the transition. The measured lifetime for Ti:Al_2O_3 lasers is approximately 3μs at room temperature and as the lifetime decreases with temperature, the linewidth increases [27].

The titanium ion in the sapphire lattice is in the trivalent state as it occupies the site of a trivalent ion, aluminium. Due to lattice defects, it is probable that traces of Ti^{4+} exist in the crystal. The ion induces a distortion in the lattice field and causes a shift of the absorption of nearby Ti^{3+} ions towards the infrared. This shift in absorption results in an overlap with the emission band of the laser [28,29]. Figure 2.5 shows the absorption due to the Ti^{3+}-Ti^{4+} pairs which can be seen to have a peak near 800nm. This effect limits the performance of the laser as it increases the losses in the cavity. An important characteristic of a titanium doped sapphire crystal is the ratio of peak absorption in the blue-green region (488nm) and the parasitic peak absorption near 800nm. This ratio is called Figure of Merit (FOM) and characterises the quality of the crystal, at present crystals with FOM near 1000 can be fabricated, although they are highly priced.

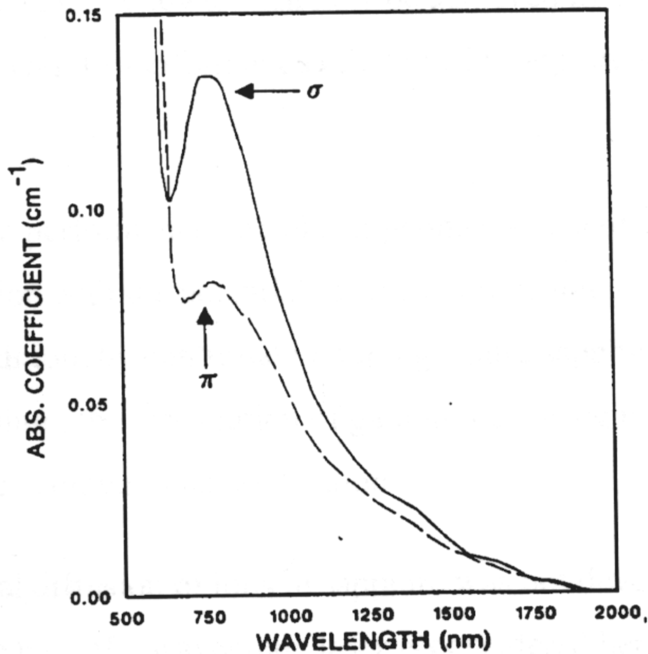

Figure 2.5. Absorption spectra of Ti^{3+}-Ti^{4+} pairs, from [5].

2.3 Waveguide Theory

In the previous sections the characteristics of sapphire as a material and the basic spectroscopic characteristics of the Ti:Sapphire laser were presented. The aim of this project is the realisation of diffused Ti:Sapphire ridge waveguide laser using gallium or titanium as the waveguide ion and in this section the theory of optical waveguides is presented. This section starts with the analysis of simple models and a geometrical approach to the waveguide theory, continuing with increasingly complex models that are sufficiently flexible to solve the more complex waveguide structures that are studied in this project.

2.3.1 Asymmetric slab waveguide model

Light can be confined or guided in a material with higher dielectric coefficient than its surroundings. Everyday structures like a glass plate or a jet of water surrounded by air are, or can be, waveguide structures. Modern optical waveguides are planar structures

in which a thin layer has higher refractive index than the substrate material. Similarly, in the case of optical fibre the core of the silica thin rod has a dopant that increases its refractive index and is capable of supporting guided modes.

Guiding is based upon the phenomenon of total internal reflection (TIR). For angles greater than a critical angle, light can be guided inside the structure. However, guiding does not occur for all angles above the critical angle but for discrete angle values. This gives rise to the presence of discrete guided modes, each waveguide mode corresponding to one angle of reflection inside the structure. One way to understand why only discrete angles can give guiding is to imagine the waveguide in the direction vertical to the propagation direction as a cavity. In this cavity the incident and the reflected wave should interfere constructively; that corresponds to only a set of angles which give the correct path lengths in order for a stationary wave to be built.

The symmetric and asymmetric slab waveguide are the simplest models for analysis of waveguide structures. The waveguide model presented here is based on an approximation to a hypothetical Ga:Sapphire diffused waveguide. In this case the simplest model that can be used is the asymmetric slab waveguide. Figure 2.6 shows a sketch depicting the geometry of a Ga:Sapphire slab waveguide. The propagation direction is along the z-axis and the TE-modes are polarized along the y-axis.

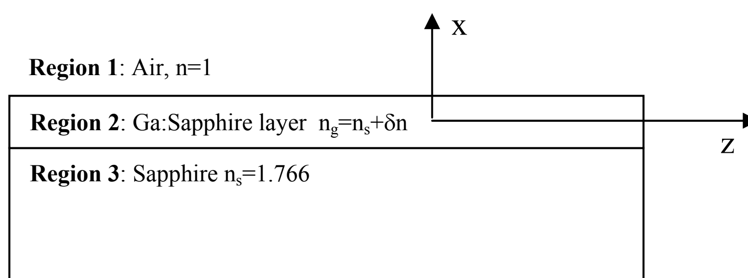

Figure 2.6. Slab waveguide geometry for Ga:Sapphire waveguides.

Waveguides created by diffusion do not have a step-like index profile assumed in the development of the slab waveguide model. The index profile of the gallium and titanium sapphire waveguides described in this thesis varies smoothly in a plane perpendicular to the direction of propagation [10,12,30]. Nevertheless the profile may be approximated by a step function, as shown in Figure 2.7.

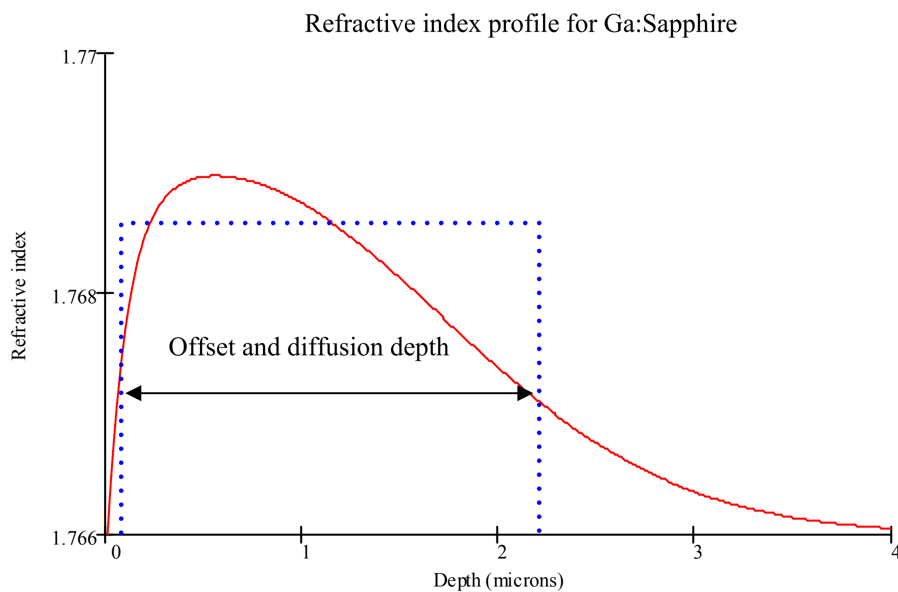

Figure 2.7. Step index approximation for a hypothetical Ga:Sapphire waveguide.

The basic equations of the slab waveguide model are derived, based on the analysis of Donald L Lee [31]. In the slab waveguide an oscillatory behaviour in the core region 2 is assumed and exponentially decaying fields in regions 1 and 3 (Figure 2.6). The field distribution for TE modes of the waveguide is assumed in the form

$$E_y(x,z) = \begin{Bmatrix} A_1 e^{-a_{1x}x} \\ A_2 \cos(k_{2x}x + \psi) \\ A_3 e^{-a_{3x}x} \end{Bmatrix} e^{-jk_z z} \qquad \begin{matrix} x > d/2 \\ |x| \le d/2 \\ x < -d/2 \end{matrix} \qquad \textbf{(2.2)}$$

Where the transverse wavenumbers are defined with the dispersion relation in each region

$$\begin{aligned} a_{1x} &= \sqrt{k_z^2 - \omega^2 \mu_1 \varepsilon_1} \\ k_{2x} &= \sqrt{\omega^2 \mu_2 \varepsilon_2 - k_z^2} \\ a_{3x} &= \sqrt{k_z^2 - \omega^2 \mu_3 \varepsilon_3} \end{aligned} \qquad \textbf{(2.3)}$$

Continuing with these equations and taking boundary conditions at x=±d/2 for the electric field of equation (2.2) and also for the magnetic field which is derived with Maxwell's curl equation the guidance condition for the TE modes of the waveguide is derived,

$$2k_{2x}d - \Phi_1^{TE} - \Phi_3^{TE} = 2p\pi \qquad \textbf{where } \boldsymbol{p = 0, 1, \ldots} \qquad \textbf{(2.4)}$$

Where the factor, $2k_{2x}d$, is the phase change of the field inside region 2 (waveguide region). The other two factors are the phase change from total internal reflection at the interface with the regions 1 and 3. The value of p represents different waveguide modes; in general there is more than one solution to the equation for different waveguide modes. The guidance condition for the TM modes is derived with the same reasoning, and takes the same form with the phase changes on total internal reflection but with different boundary conditions.

The guidance equation can be solved graphically or numerically and yields the dispersion relation of the asymmetric slab waveguide. Three new quantities must be introduced for the solution of the equation, a frequency parameter, v, normalized to the film thickness that is defined by

$$v = k_0 d \sqrt{(\varepsilon_2 - \varepsilon_3)/\varepsilon_0} \quad \textbf{where} \quad k_0 \equiv \omega\sqrt{\mu\varepsilon_0} \qquad \textbf{(2.5)}$$

the next parameter introduced is b, which is dependent on the effective index of the waveguide

$$b = (\varepsilon_{eff} - \varepsilon_3)(\varepsilon_2 - \varepsilon_3) \qquad \textbf{(2.6)}$$

and finally an asymmetry measure α given by the relation

$$\alpha = (\varepsilon_3 - \varepsilon_1)(\varepsilon_2 - \varepsilon_3) \qquad \textbf{(2.7)}$$

With these normalizations introduced, a set of normalised curves for the first three TE modes and for different asymmetry measures is depicted in Figure 2.8. It can be observed that the fundamental mode for a symmetrical refractive index profile does not have a cutoff, an example of this case is the index profile of an optical fibre.

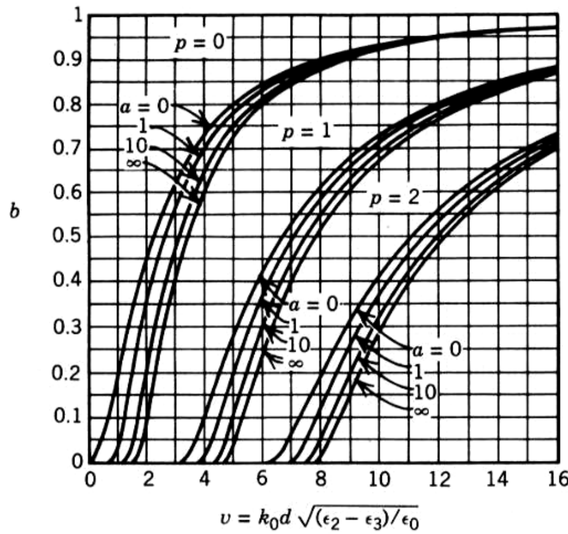

Figure 2.8. Graphical solution of the guidance condition of a slab waveguide, from [31].

2.3.2 WKB method

Although the slab model is frequently used with graded-index waveguides, it can only give precise results for waveguide structures that have a step index profile. The WKB model is an efficient method to solve problems of graded-index waveguides. The WKB method has the assumption that the guiding region is imbedded at a sufficient depth in the substrate so that the influence of the discontinuity of the substrate-air interface can be ignored. In our case the waveguide is very shallow and is probably

buried only for 0.5μm. A WKB model was developed and the air-substrate index profile discontinuity was lifted as the profile was generated using a logistic and not a step function (Figure 2.7). Therefore the WKB model is used to compare with the results of the slab model.

In a waveguide where the index variation is smooth, the boundaries of the guiding region cannot be easily defined. However if they are found, then it is expected that the field should oscillate within the boundaries or turning points and decay away exponentially. In a WKB simulation the refractive index profile of the waveguides is given as input and the modal effective indices are calculated with the following equation [27,28].

$$k_0 \int_{x_a}^{x_b} \sqrt{n^2(x) - n_{eff}^2}\, dx = (p + 0.5)\pi \quad p=0,\ 1,\ 2,\ \ldots \qquad \textbf{(2.8)}$$

Where x_a and x_b are the turning points defined by the following relation.

$$n(x_a) = n(x_b) = n_{eff} \qquad \textbf{(2.9)}$$

p is the number of the mode and $n(x)$ is the refractive index profile. The algorithm used tests the equality defined in equation (2.8) for different turning points and effective refractive indices. This method is used in Chapter 3, with a refractive index profile similar to the one depicted in Figure 2.7, for the calculation of the effective indices of the slab Ga:Sapphire diffused waveguides.

2.3.3 Beam Propagation Method (BPM)

Beam propagation is a more sophisticated model that can deal with optical propagation problems that have nearly arbitrary parameters. Waveguide channels realised in this project are based on the Ion Beam Milling technique for the realisation

of ridge waveguides. These structures cannot be analysed with the methods described above so that commercial BPM packages were used. Here the theory of the Beam Propagation Method will be briefly described following the analysis of Reinhard Marz and of Katsunari Okamoto [32,33]. The mathematical procedure used was developed for underwater acoustics and seismology before it was adapted to optical waveguide problems. BPM yields the response of a given device to an external optical signal used as an input, in a way which closely parallels practical application.

The BPM is based in the forward Helmholtz equation which describes the propagation of the optical field in respect to the propagation direction. The vector Helmholtz equations are derived from Maxwell's equations by eliminating the electric or magnetic field. Solutions of the vector Helmholtz equations without a longitudinal component are called transverse or scalar waves. In layered waveguide media two types of scalar waves can be found, the transverse electric, usually referred as TE, and the transverse magnetic, usually referred as TM.

For the electrical field the three-dimensional scalar wave equation (Helmholtz equation), is given by

$$\frac{\partial^2 E}{\partial x^2}+\frac{\partial^2 E}{\partial y^2}+\frac{\partial^2 E}{\partial z^2}+k^2 n^2(x,y,z)E=0 \quad \textbf{(2.10)}$$

The electric field can be separated into two parts,

$$E(x,y,z)=\Phi(x,y,z)\exp(-jkn_0 z) \quad \textbf{(2.11)}$$

where the axially slowly varying envelope term is $\Phi(x, y, z)$ and the rapidly varying term is $exp(-jkn_o z)$, where n_0 is the refractive index of the cladding. Substituting the electric field in the Helmholtz equation yields,

$$\nabla^2\Phi - j2kn_0\frac{\partial\Phi}{\partial z}+k\left(n^2-n_o^2\right)\Phi=0 \quad \textbf{(2.12)}$$

Assuming the weakly guiding condition it can be approximated that $\left(n^2 - n_o^2\right) \cong 2n_o\left(n - n_o\right)$ and equation (2.12) can be written as

$$\frac{\partial \Phi}{\partial z} = -\frac{j}{2kn_0}\nabla^2\Phi - jk\left(n - n_o\right)\Phi \quad \textbf{(2.13)}$$

When $n = n_o$ only the first term of the right hand side will remain, which represents free-space propagation in a medium having refractive index, n_o. The second term gives the influence of the region having refractive index $n(x, y, z)$. Both terms affect simultaneously the propagation of light, however in BPM the influence of the two terms is separated. Each term affects the light propagation separately and alternately during the propagation step, Δz, furthermore during this step the dielectric profile is assumed to be constant. Figure 2.9 shows an example illustrating the operation of the algorithm of the classical BPM. Figure 2.9 (a) shows light propagation in an actual tapered waveguide and Figure 2.9 (b) shows the BPM simulation for light propagation in the tapered waveguide.

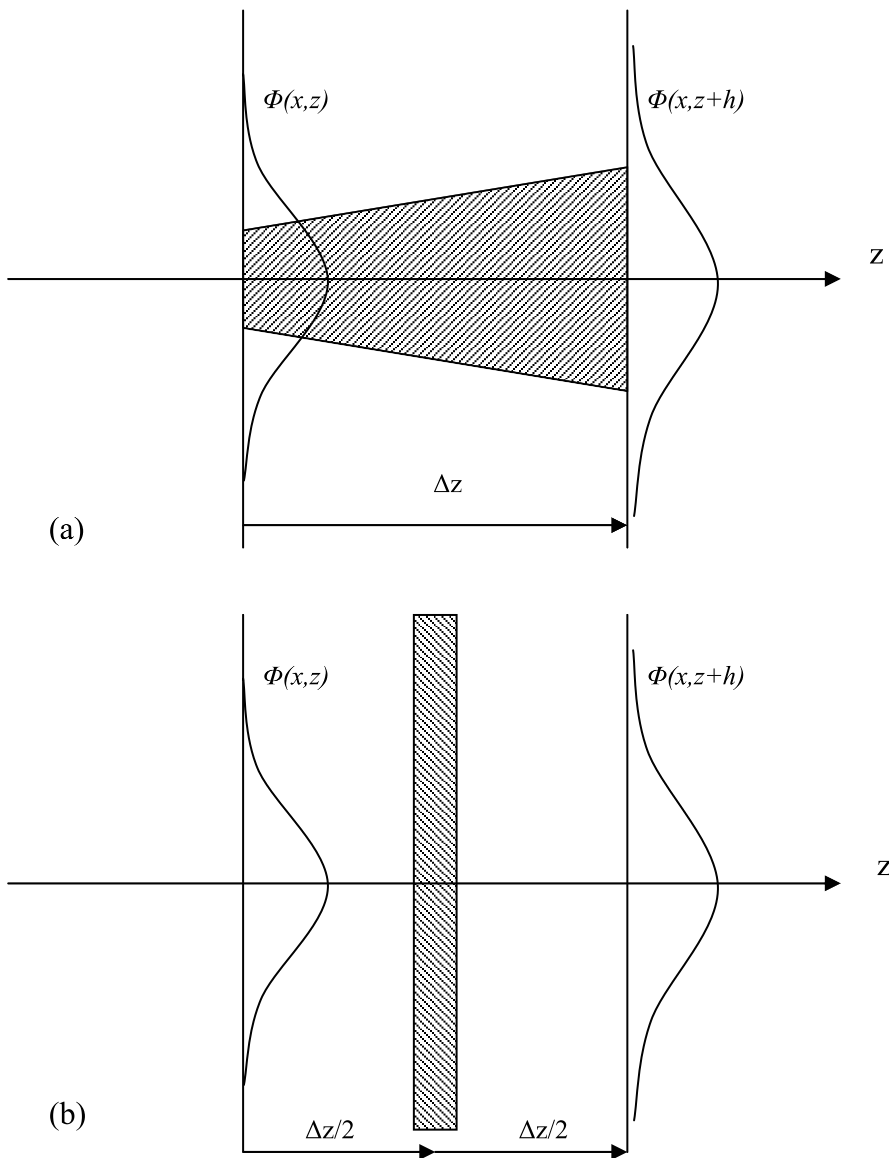

Figure 2.9. Schematic representation of the operation of a classical BPM algorithm.

In BPM analysis the field, *Φ(x,y)*, is free-space propagated over a distance of Δz/2, then the portrait of the field is corrected at the centre of propagation for the entire distance, Δz, and again for a distance the field is propagated in free space. The propagation of the optical field inside the waveguide is replaced by a sequence of free space propagation steps and phase corrections. The optical field takes the information of the propagation environment every propagating step, so that the BPM method is

very sensitive to the appropriate choice of propagation step. For small and smooth index changes found in diffused waveguides the classical BPM is very successful but for abrupt index changes (that can be found in semiconductor devices) cannot successfully work except if a sufficiently small propagation step is chosen.

The method works like a simulated experiment, an optical field is launched inside the waveguide and the efficiency of the coupling depends, as in real conditions, on the overlap of the selected launch field with the waveguide supported modes. The optical field is propagated until a stable state is reached and a solution for a waveguide mode is obtained. If the length of propagation is not adequate or the launching field is not appropriately selected the simulation will not give a solution for a supported mode. This implies that results from a BPM model should be treated with more caution than the other simulation methods presented.

A commercial simulation package called BeamProp was used for propagation problems in planar and ridge waveguides created by ionic diffusion in sapphire. Results of the BPM simulations will be shown in the following chapters.

2.4 Titanium Sapphire waveguide laser model

2.4.1 Waveguide laser description

In this section a model for a Ti:Sapphire laser system in a waveguide geometry is derived. It is important to derive the relation of the expected laser threshold and gain per unit length of this configuration, dependent on the waveguide characteristics [22,34-36]. A schematic of a waveguide Ti:Sapphire laser is depicted in Figure 2.10. It is a simple cavity in which pump radiation is coupled to the waveguide usually

using a microscope objective lens. The pump radiation and fluorescence is confined in the waveguide region and plane dielectric mirrors provide the signal feedback at the polished ends of the waveguides. The spectral characteristics of the mirrors are high reflectivity at the signal wavelength (near 750nm) and high transmission at the pump wavelengths. Once the total gain per round trip is higher than the losses of the waveguide and of the mirrors, laser operation will commence.

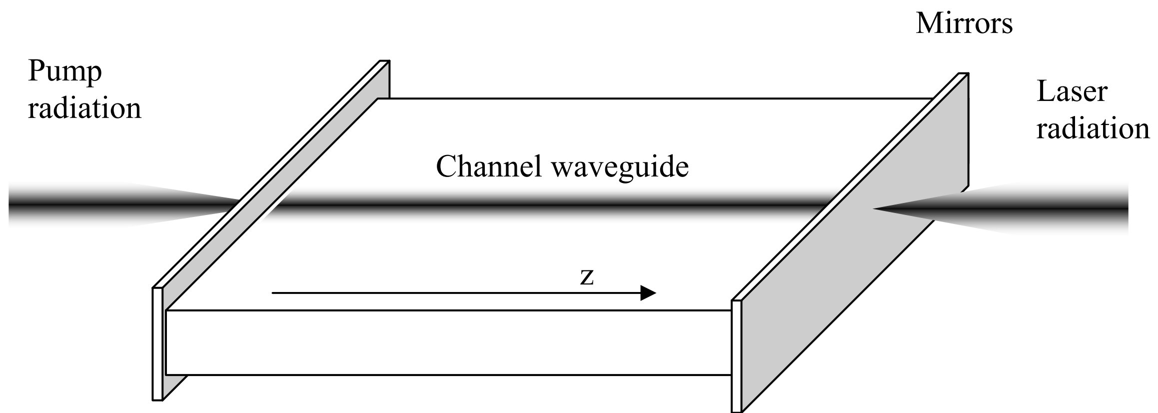

Figure 2.10. Schematic for a Ti:Sapphire laser in waveguide geometry.

2.4.2 Energy levels of Ti:Sapphire.

Titanium has only one d electron, hence it is, at a first approximation a two-level system that theoretically cannot lase since population inversion cannot be achieved. However when Ti is incorporated into the lattice of sapphire each electron energy level is coupled to lattice vibrations leading to splitting of the energy levels (section 2.2.5). Therefore Ti:Sapphire is a laser in a vibronic transition and operates as a 4-level laser. Figure 2.11 shows the energy level diagram of the Ti:S laser.

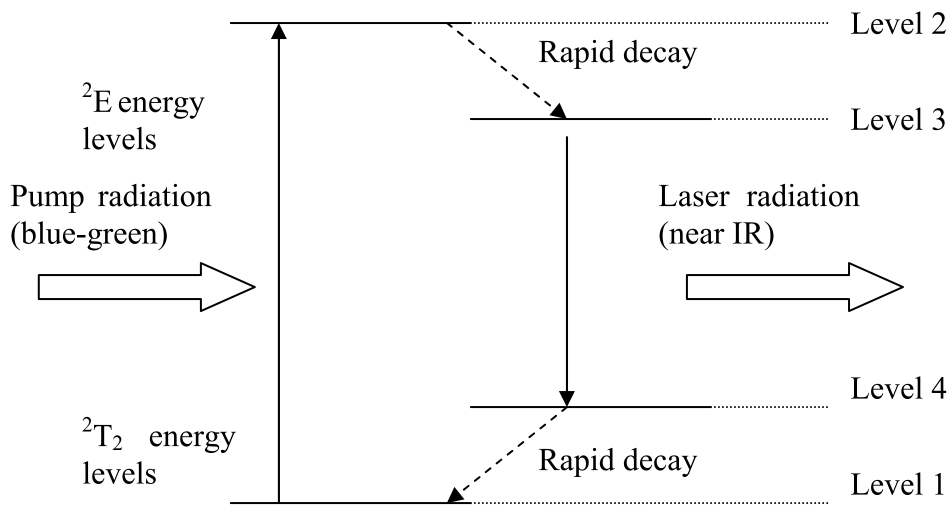

Figure 2.11. Energy levels and pumping scheme of a Ti:Sapphire laser.

The ground state, level 1, is a low vibrational state of the $^2T_2$ electronic energy and, in the presence of pump radiation, electrons are excited to level 2 which is an excited vibrational state of the electronic level ^2E. The electrons then undergo a rapid non-radiative decay to a lower level of the state ^2E, level 3. The transition from level 3 to level 4 is the laser transition that can occur with stimulated emission. Level 4 is an excited vibrational state of the $^2T_2$ electronic energy level and the electrons follow a non-radiative rapid decay back to level 1.

2.4.3 Gain and threshold of the waveguide laser

In this section a model is presented which describes how characteristics of the laser such as threshold are dependent on characteristics of the configuration such as pump, signal mode sizes of the waveguide, device length etc. A model is derived for this 4-level laser using the analysis of L. Hickey and M. Digonnet [22,35,36]; it is assumed that the system is in thermal equilibrium, so that the rate of excitation is equal to the

rate of decay. The population of ions in level 1 is N_0-$N(x,y,z,t)$ where N_0 is the concentration of Ti ions in the substrate and $N(x,y,z,t)$ is the number of excited ions. Supposing that the depopulation of the ground state is negligible yields that $N(x,y,z,t) << N_0$, therefore $N_0 - N(x,y,z,t) \approx N_0$. Level 2, at any given moment, is assumed to have negligible population because any ion in this state rapidly decays to level 3. Level 3 is the level that holds the population of the excited ions, $N(x,y,z,t)$. Level 4 is also assumed to have negligible population because of the short lifetime of the excited vibronic level.

i) Population inversion

Equation (2.14) gives the rate at which ions move from level 1 to level 3; this rate is proportional to the intensity of the pump radiation, ion concentration, quantum efficiency and absorption cross section of the transition.

$$\left.\frac{dN}{dt}\right|_{1\rightarrow 3} = \frac{I_p(x,y,z)\sigma\eta N_0}{h\nu_p} \qquad \textbf{(2.14)}$$

The laser transition rate from level 3 to level 4 has two components, the spontaneous emission rate and the stimulated emission rate. It is assumed that for low pump powers (up to threshold pump power) and for thermal equilibrium, the stimulated emission rate is negligible. The spontaneous emission decay rate is given by the following equation.

$$\left.\frac{dN}{dt}\right|_{3\rightarrow 1} = \frac{N(x,y,z)}{\tau} \qquad \textbf{(2.15)}$$

and in a thermal equilibrium state,

$$\left.\frac{dN}{dt}\right|_{3\rightarrow 1} = \left.\frac{dN}{dt}\right|_{1\rightarrow 3} \Rightarrow N(x,y,z) = \frac{I_p(x,y,z)\sigma\eta N_0\tau}{h\nu_p} \qquad \textbf{(2.16)}$$

Therefore with this equation the population inversion of the laser may be estimated. The intensity of the pump radiation is $I_p(x,y,z)$ and that of the signal radiation is $I_s(x,y,z)$. The intensities can be related to the power densities using the expression $I(x,y,z)= P(z)S(x,y)$, where the modal distributions of the pump and signal radiation in the waveguide are $S_p(x,y)$ and $S_s(x,y)$ respectively, and are normalised such that $\int\int S(x,y)dxdy = 1$. Furthermore $P(z)$ is the power of the signal or pump radiation. Therefore using equation (2.16) and substituting the above expression for the pump radiation yields,

$$N(x,y,z) = \frac{P_p(z)S_p(x,y)\sigma\eta N_0\tau}{h\nu_p} \quad \textbf{(2.17)}$$

ii) Laser gain

The signal gain is the rate of growth of the signal due to the level of stimulated emission and is proportional to the interaction of the incident signal $I_s(x,y,z)$, and the population inversion, using the stimulated emission cross section.

$$\frac{dP_s(z)}{dz} = \iint N(x,y,z)I_s(x,y,z)\sigma_s dxdy - \left(\beta_s + \frac{N_0\sigma_p}{FOM}\right)P_s(z) \quad \textbf{(2.18)}$$

The second term of equation 2.18 shows the loss due to the propagation loss of the waveguide in signal wavelength and due to reabsorption of the signal due to Ti^{3+}-Ti^{4+} pairs, which is given by the FOM. Substituting for the population inversion $N(x,y,z)$ and the intensity of the signal radiation

$$\frac{dP_s(z)}{dz} = P_s(z)\left(\frac{\sigma_p\sigma_s\eta N_0\tau}{h\nu_p}P_p(z)\iint S_p(x,y)S_s(x,y)dxdy - \left(\beta_s + \frac{N_0\sigma_p}{FOM}\right)\right) \quad \textbf{(2.19)}$$

The pump power, $P_p(z)$, in the waveguide decays due to waveguide losses at the pump wavelength and due to pump absorption from the Ti ions, assuming that the ground state in not significantly depopulated.

$$P_p(z) = P_p(0)\exp(-(N_0\sigma_p + \beta_p)z) \qquad \textbf{(2.20)}$$

In order to find an expression for the total gain in the waveguide laser equation (2.19) has to be integrated over the length of the waveguide.

$$\int_{P(0)}^{P(L)} \frac{1}{P_s(z)} dP_s(z) = \frac{\tau\sigma_p\sigma_s\eta N_0}{h\nu_p} \int_0^L P_p(z)dz \iint S_p(x,y)S_s(x,y)dxdy - \int_0^L \left(\beta_s + \frac{N_0\sigma_p}{FOM} \right) dz \qquad \textbf{(2.21)}$$

Using equation (2.20), which gives the pump power as a function of the propagation distance, and solving equation (2.21) yields,

$$\ln G = \frac{\tau\sigma_p\sigma_s\eta N_0}{h\nu_p} \frac{\left(1-\exp(-(N_0\sigma_p + \beta_p)L)\right)P_p(0)}{N_0\sigma_p + \beta_p} \iint S_p(x,y)S_s(x,y)dxdy - \left(\beta_s + \frac{N_0\sigma_p}{FOM} \right) L \qquad \textbf{(2.22)}$$

This equation gives the gain for the laser in which, the first term $\frac{\tau\sigma_p\sigma_s\eta N_0}{h\nu_p}$, gives the material characteristics, the second term $\frac{\left(1-\exp(-(N_0\sigma_p + \beta_p)L)\right)P_p(0)}{N_0\sigma_p + \beta_p}$ describes the pump absorption, the integral $\iint S_p(x,y)S_s(x,y)dxdy$ calculates the overlap of the waveguide modes at the pump and signal frequencies and finally the last term $\left(\beta_s + \frac{N_0\sigma_p}{FOM} \right) L$ gives the loss of the signal wavelength due to the loss of the waveguide and also due to signal reabsorption due to the Ti^{3+} and Ti^{4+} pairs.

iii) Threshold of the laser

Using equation (2.22) the gain of the laser can be calculated as a function of the device characteristics such as length, concentration and loss. The threshold pump power is achieved when the gain is sufficient to overcome the extra loss of the mirrors. Therefore the threshold will occur when

$$2G = \ln(R_1 R_2) \qquad \textbf{(2.23)}$$

Using equation (2.23), and solving equation (2.22) for the pump power, the expression for the laser threshold is derived.

$$P_{th} = \frac{h\nu_p}{\tau\sigma_p\sigma_s\eta N_0} \frac{N_0\sigma_p + \beta_p}{1-\exp(-(N_0\sigma_p + \beta_p)L)} \frac{1}{\iint S_p(x,y)S_s(x,y)dxdy} \left[\left(\beta_s + \frac{N_0\sigma_p}{FOM} \right) L - \frac{\ln(R_1R_2)}{2} \right] \quad \textbf{(2.24)}$$

In the following sections the expressions that give the gain and the threshold of the laser will be analysed in order to determine how different characteristics of the system affect the performance of the laser.

iv) Pump and signal mode sizes

As described above, the term $\iint S_p(x,y)S_s(x,y)dxdy$ is the overlap integral between the waveguide modes at the signal and pump wavelengths. Assuming that the waveguide has modes that can be approximated with concentric Gaussian functions the normalised mode distribution at the pump wavelength can be written as

$$S_p(x,y) = \frac{1}{\pi w_{px} w_{py}} \exp\left[-\left(\frac{y^2}{w_{py}^2} + \frac{x^2}{w_{px}^2} \right) \right] \quad \textbf{(2.25)}$$

where the waists are defined at *1/e* of the maximum intensity. Then the solution for the overlap integral is,

$$\iint S_s(x,y)S_p(x,y)dxdy = \left[\pi w_{px} w_{py} w_{sx} w_{sy} \left(\frac{1}{w_{px}^2} + \frac{1}{w_{sx}^2} \right)^{0.5} \left(\frac{1}{w_{py}^2} + \frac{1}{w_{sy}^2} \right)^{0.5} \right]^{-1} \quad \textbf{(2.26)}$$

In order to be able to describe the effect that the waveguide size will have on the gain and threshold of the laser more clearly, the expression will be simplified by assuming that the waveguide modes are not astigmatic, so that $w_{px}=w_{py}=w_p$ and $w_{sx}=w_{sy}=w_s$, in which case equation (2.26) can be written as

$$\iint S_s(x,y)S_p(x,y)dxdy = \left[\pi\left(w_p^2 + w_s^2\right)\right]^{-1} \quad \textbf{(2.27)}$$

Therefore equation (2.24) which gives the threshold of the waveguide can be writtern as,

$$P_{th} = k(w_p^2 + w_s^2) \quad \textbf{(2.28)}$$

where k is a proportionality constant. From this expression it is clear that the threshold of the laser system is proportional to the square of the pump and signal mode sizes. Therefore a waveguide with a smaller mode dimension will result in a reduced threshold power. As expected, from equation (2.22) the gain of the laser is also increased as the waveguide mode waists decrease. In the case of gallium diffused waveguides in sapphire a mode size of 2μm is expected at the pump wavelength and 4μm at the signal wavelength [section 5.3.1]. In Figure 2.12 a plot of the gain of two laser systems with different mode sizes is depicted, the graph indicates the importance of mode size on the performance of a waveguide laser device.

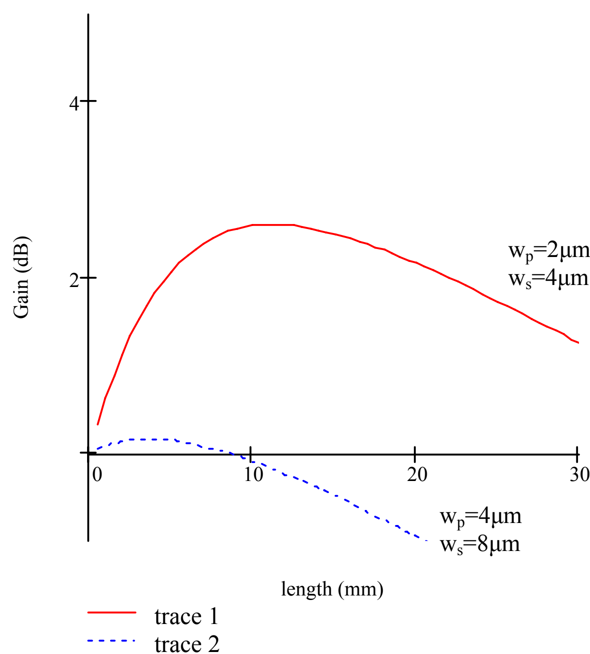

Figure 2.12. Gain of the device versus length for waveguides with different mode sizes. Trace 1 is for a waveguide with waists w_p=2μm and w_s=4μm and trace 2 with w_p=4μm and w_s=8μm.

v) Waveguide losses and mirror reflectivities.

From the threshold equation of the laser, equation (2.24), it is clear that as the losses of the waveguide at the signal and pump wavelength increase the laser threshold also increases. Figure 2.13 shows the laser gain versus length for devices with increasing propagation loss. The threshold of the laser decreases as the mirror reflectivities increase, the value of the mirror reflectivity can be chosen so that it gives a low threshold. Nevertheless high reflectivity mirrors will have a performance trade-off as they reduce the slope efficiency. An important engineering consideration in a laser device is the efficiency with which the mirrors couple the reflected radiation back in the waveguide. Poor coupling of the reflected radiation increases the losses and results in poor laser performance. Problems of bad coupling of the mirrors exist due to mirror and waveguide separation, mirror tilt and curvature on the waveguide end-faces. In Figure 2.14 threshold plots can be compared for devices that have the same characteristics except mirror reflectivities.

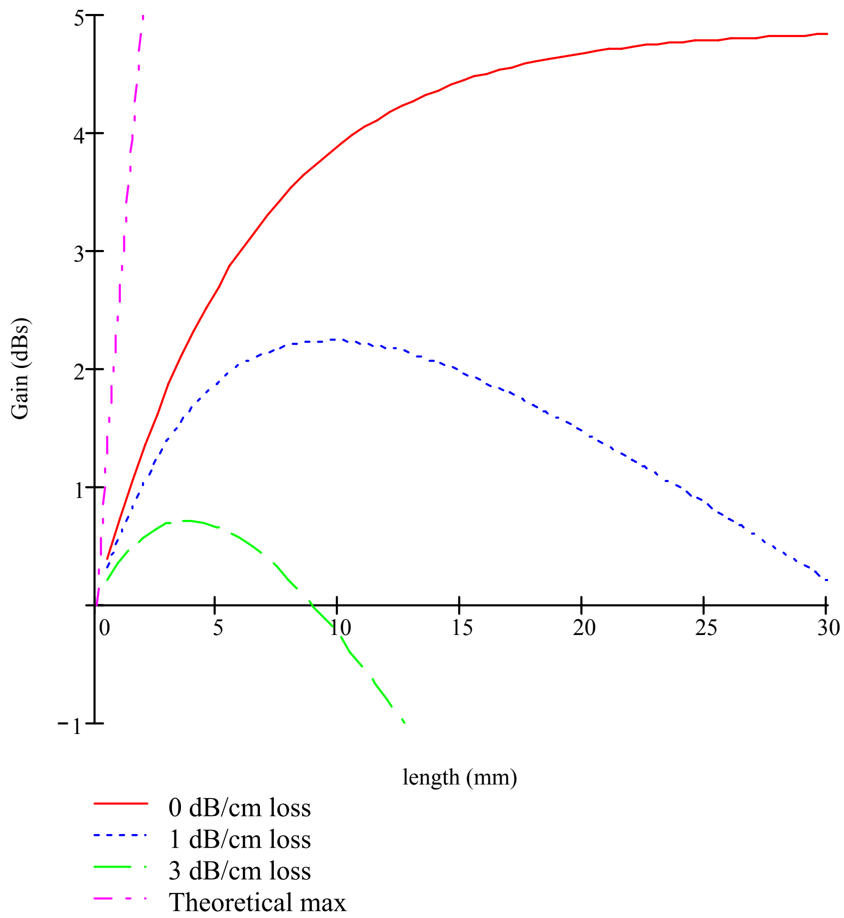

Figure 2.13. Gain versus length, for waveguides with different loss, with a maximum theoretical curve assuming complete population inversion. The pump power is in all cases 0.5W.

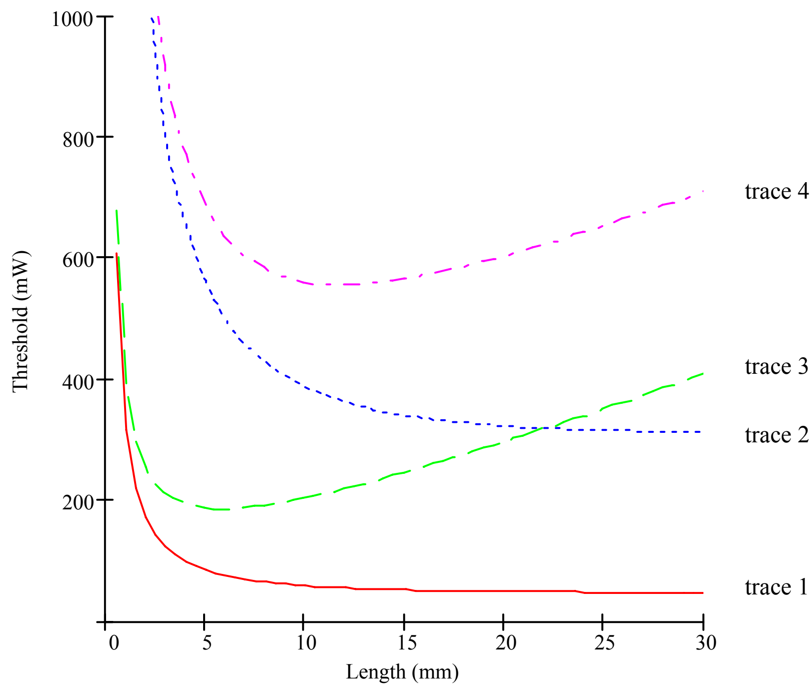

	Loss (dB/cm)	Reflectivity (%)
trace 1	0	90
trace 2	0	50
trace 3	1	90
trace 4	1	50

Figure 2.14. Threshold versus length for devices with different losses and mirror reflectivities

vi) Device length

In a waveguide without losses the threshold of the waveguide laser decreases as the length of the cavity is increased. In Figure 2.14 for the two curves (trace 1 and 2) representing a waveguide without propagation losses the threshold becomes minimum as the length of the cavity becomes infinite. Conversely in a waveguide with non-negligible propagation losses, which is the general case, the laser threshold becomes minimum at an optimum length. In Figure 2.14 for traces 3 and 4, which represent waveguides with 1 dB/cm losses, there is an optimum length (approximately 5 and 10mm respectively) that the laser threshold becomes minimum.

2.4.4 Slope efficiency and waveguide losses

The slope efficiency of the laser is defined as the rate of increase of the laser power versus the launched pump power, above threshold. For a waveguide laser in which the round trip cavity losses are assumed to be low the slope efficiency is given by [36]

$$\eta_s = \eta \frac{t_2}{\delta} \frac{v_s}{v_p} \qquad \textbf{(2.29)}$$

where v_s, v_p are the signal and pump frequencies, t_2 is the transmission of the output mirror, η is the quantum efficiency of pumping and finally δ is the round trip loss in the cavity given by the following equation.

$$\delta = 2\beta_s l - \ln(R_1 R_2) \qquad \textbf{(2.30)}$$

Therefore the slope efficiency is not directly dependent on the laser material fluorescence properties and the mode characteristics. The slope efficiency is dependent on losses and can be increased with the fabrication of low-loss waveguides. It should be noted that the selection of cavity mirrors with high reflectivity that are beneficial to the threshold of the laser result in a device with poor slope efficiency; this indicates that a laser cavity should be optimised according to its specific application.

2.5 Integrated wavelength selection

In waveguide technology, lasers with a single transverse mode output can be fabricated using appropriate selection of geometry in channel waveguides (opening, depth). In a simple waveguide cavity though, created with two mirrors and a straight channel waveguide, it is very likely that the gain curve of the laser will be broader than the cavity mode spacing, hence the laser will exhibit multiple longitudinal modes. Integrated wavelength selection can be used to implement compact waveguide

devices with a potential to function as linewidth lasers and is also the first step for the realisation of a compact tunable source. In the following sections two different wavelength selection mechanisms that can be integrated in a waveguide device are described. The first approach is the fabrication of surface relief gratings; an introduction in grating theory and DFB lasers is presented with simulation results. The second possible wavelength selection mechanism is a 4-port coupled cavity configuration in waveguide geometry and a brief theoretical analysis is described with a novel simulation for this type of device.

2.5.1 Grating wavelength selection

A promising approach for integration of wavelength selectivity in lasers is the fabrication of surface relief grating structures. Distributed feedback lasers (DFB) oscillate predominantly in one longitudinal mode; single frequency operation is induced by an index-grating that provides feedback only at the Bragg wavelength. A distributed feedback laser consists of an active medium and the index grating which is usually achieved by a periodic thickness variation produced during fabrication. Any perturbation of a waveguide structure can locally affect the value of the effective index of the guided modes, this can be used to induce coupling of the propagated light into other directions, modes or layers. If the disturbance of the refractive index is periodic then a forward guided wave can be reflected at a specific wavelength, called the Bragg wavelength. The vectorial relation for this operation is

$$\bar{k}_b = \bar{k}_{Bragg} + \bar{K}_f \rightarrow n_{eff}\frac{\pi}{\lambda} = \frac{\pi}{\Lambda} - n_{eff}\frac{\pi}{\lambda} \rightarrow \Lambda = \frac{\lambda}{2n_{eff}} \qquad \textbf{(2.31)}$$

Where k_f, k_b, k_{Bragg} are the k-vectors for the forward and backward propagating waves and the k-vector of the grating, respectively. The free space wavelength is λ, n_{eff} is the effective refractive index of the propagating mode and Λ is the grating period.

In order to model the behaviour of grating structures the most widely used theoretical techniques are coupled mode theory and the matrix method. The model used in the thesis is based on the matrix method and on the work of Makoto Yamada and Kyohei Sakuda [37].

i) F-Matrix model

The method used is a unified approach to obtain characteristics of grating structures that are almost periodic. In this approach the waveguides are divided into segments in the propagation direction over which the grating can be considered constant. The fundamental matrix is derived for each short segment of the grating, then to derive the fundamental matrix of the whole structure all the matrices of the small segments are multiplied under specific phase conditions at the interface between adjacent segments. In Figure 2.15 a short segment of a uniform sinusoidal grating is depicted, with the forward and backward propagating waves at the beginning and the end of the grating. The definition of the fundamental matrix approach lies in the following relation

$$\begin{pmatrix} E_A(0) \\ E_B(0) \end{pmatrix} = [F] \begin{pmatrix} E_A(L) \\ E_B(L) \end{pmatrix} \qquad (2.32)$$

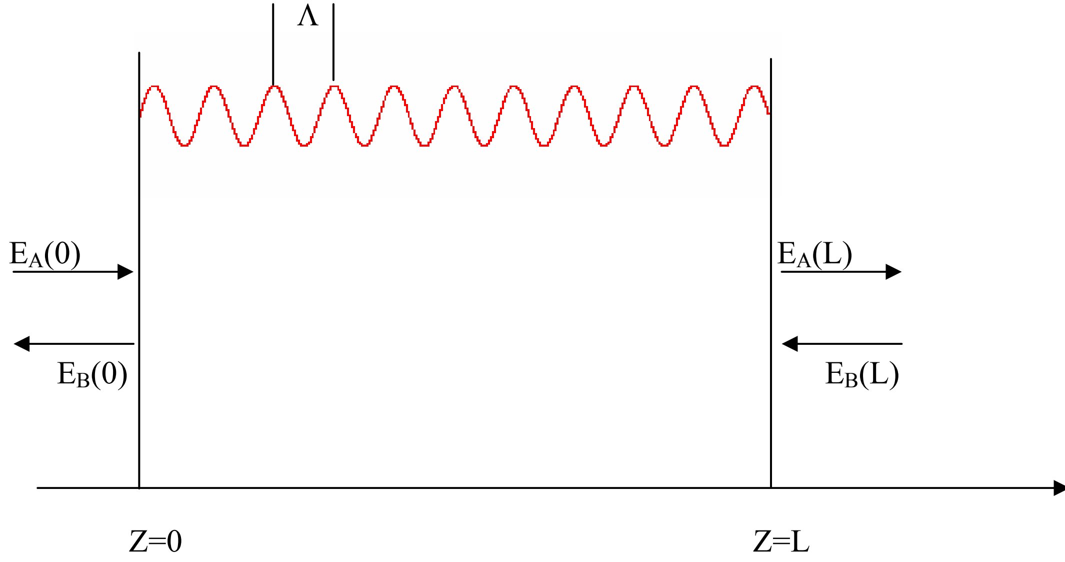

Figure 2.15. Segment of uniform sinusoidal grating, with the forward and backwards propagating waves.

[F] is a 2X2 matrix that describes a uniform grating of length L and period Λ. It gives the relation of the "input" fields in the grating at $z=0$ and the "output" fields of the grating at $z=L$. The relief gratings are assumed to be sinusoidal and, in order to find the elements of the matrix, the basic coupled wave equations for a uniform grating with period Λ and with gain per unit length, g, are used.

$$\frac{dE_A}{dz} = k\exp[i(2\Delta\beta z - \varphi]E_B + gE_A$$
$$\frac{dE_B}{dz} = k\exp[-i(2\Delta\beta z - \varphi]E_A - gE_B \qquad \textbf{(2.33)}$$
$$\Delta\beta = \beta - \beta_B = \beta - N\pi/\Lambda$$

Where β is the propagation constant in the z-direction that is equal to $n_{eff}\pi/\lambda$, where n_{eff} is the effective index of the propagating mode and λ is the free space wavelength. Then $\Delta\beta$ is the difference between the propagation constant β and the Nth Bragg

frequency $N\pi/\Lambda$ of the grating. Furthermore k is a coupling coefficient between forward and backward waves and finally φ is the grating phase.

The coupled wave equations are solved and the solutions of the propagating waves are replaced in equation (2.32), yielding the elements of the F-matrix, which are

$$\begin{aligned} F_{11} &= \left[\cosh(\gamma L) + i\Delta\beta' L \sinh(\gamma L)/(\gamma L)\right]\exp(i\beta_B L) \\ F_{12} &= -kL\sinh(\gamma L)\exp\left[-i(\beta_B L + \varphi)\right]/(\gamma L) \\ F_{21} &= -kL\sinh(\gamma L)\exp\left[i(\beta_B L + \varphi)\right]/(\gamma L) \\ F_{22} &= \left[\cosh(\gamma L) - i\Delta\beta' L \sinh(\gamma L)/(\gamma L)\right]\exp(-i\beta_B L) \end{aligned} \quad \textbf{(2.34)}$$

Where

$$\begin{aligned} \Delta\beta' &= \Delta\beta + ig \\ \gamma^2 &= k^2 - (\Delta\beta')^2 \end{aligned} \quad \textbf{(2.35)}$$

From equation (2.34) the transmission and reflection coefficients of the grating are given by the F-matrix elements

$$\begin{aligned} T &= 1/F_{11} \\ R &= F_{21}/F_{11} \end{aligned} \quad \textbf{(2.36)}$$

ii) Phase shifted grating

In a wavelength selective laser source the F-matrix model is well suited to simulate the case of a phase shifted grating. A waveguide laser with a constant grating lases in two lines around the Bragg wavelength, as shown in Figure 2.16. This is because there are two modes (standing waves) subjected to a different average refractive index. As can be seen in the second part of Figure 2.16 in the case of a λ/4 phase shifted grating there is only one mode that will see an effective index equal to the one that gives the Bragg wavelength [22,38].

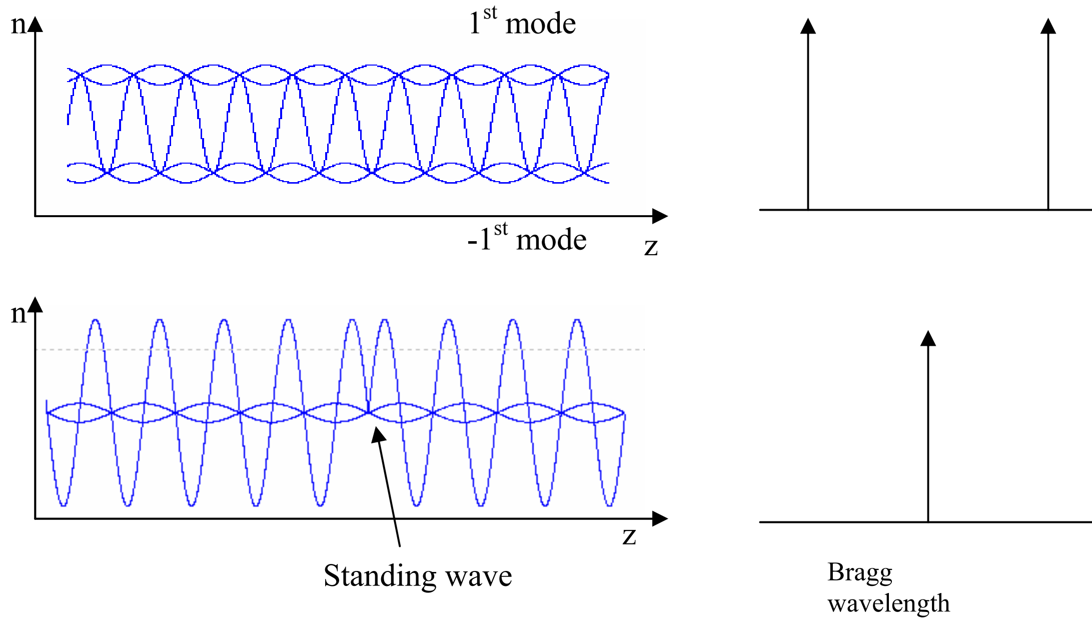

Figure 2.16. Representation of the refractive index change, mode patterns and corresponding resonance wavelengths for a laser with a uniform grating and for a laser with a phase shifted grating from [22].

In order to obtain the F-matrix and therefore the transmission and reflection characteristics of the phase shifted grating is to multiply the F-matrices of the two constant segments are multiplied using the correct phase for the start of the second segment, which for the case of a π-phase shift is

$$\varphi = \pi + 2\beta_{Bragg} L \qquad \textbf{(2.37)}$$

iii) Model results

The strength or efficiency of a grating is a function of the strength of the interaction of the waveguide mode with the surface relief. Usually a waveguide with good mode confinement gives gratings of higher efficiency for the same relief because of a better

overlap of the mode with the grating structure. In order to obtain model results for a waveguide device the grating model has to be combined with BPM results from the waveguide models for the ridge diffused sapphire waveguides [12]. The effective refractive index of the guided modes should be known at the places where the grating has a relief, n_{effh}, or a depression, n_{effl}. The difference of the effective indices is $\Delta n_{eff} = n_{effh} - n_{effl}$ and determines the strength of the grating. A BPM simulation for the planar diffused waveguide is used, with parameters that match experimental results of the waveguides. The value for the substrate refractive index is 1.766, the maximum index change that is achieved in the planar waveguides is $6\text{x}10^{-3}$,and the diffusion depth of the gallium ions is 3μm. The effective refractive indices are calculated for gratings with a relief height ranging from 20 to 300nm. The difference in effective refractive index, Δn_{eff}, between the etched and unetched section versus the relief of the grating is shown in Figure 2.17. The curves have approximately the same linear fit, $\Delta n=10^{-6} \text{ x } h$, where h is the height of the grating relief.

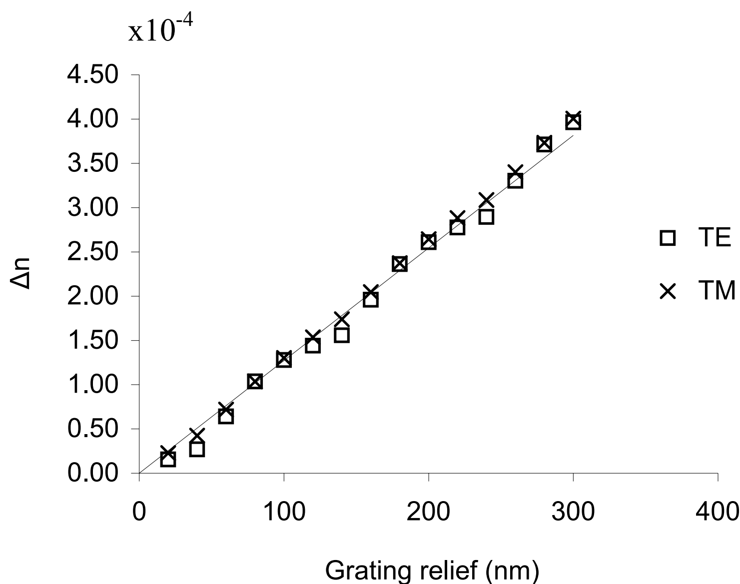

Figure 2.17. Difference in effective refractive index vs. grating relief

A promising fabrication technique for creating a relief pattern in sapphire with the required period and the required height is probably e-beam writing combined with etching. A photoresist sensitive to an electron beam is patterned appropriately and then the pattern is transferred to the substrate using ion beam milling. It is expected that a grating height of approximately 50-100nm can be achieved on sapphire, and from Figure 2.17 this is expected to give a refractive index difference in the order of 10^{-4}. Using these values the grating can be modelled using the matrix method and in Figure 2.18 the transmission and reflection of a uniform grating can be seen. The length of the grating is 7mm and the effective index difference is 10^{-4}, resulting in a grating reflection of approximately 90%. In Figure 2.19 two segments of the previous grating are used with a π phase shift in between, giving a total device length of 14mm; the reflection of the device is near 100%. This result shows great promise for future implementation of gratings on sapphire integrated devices.

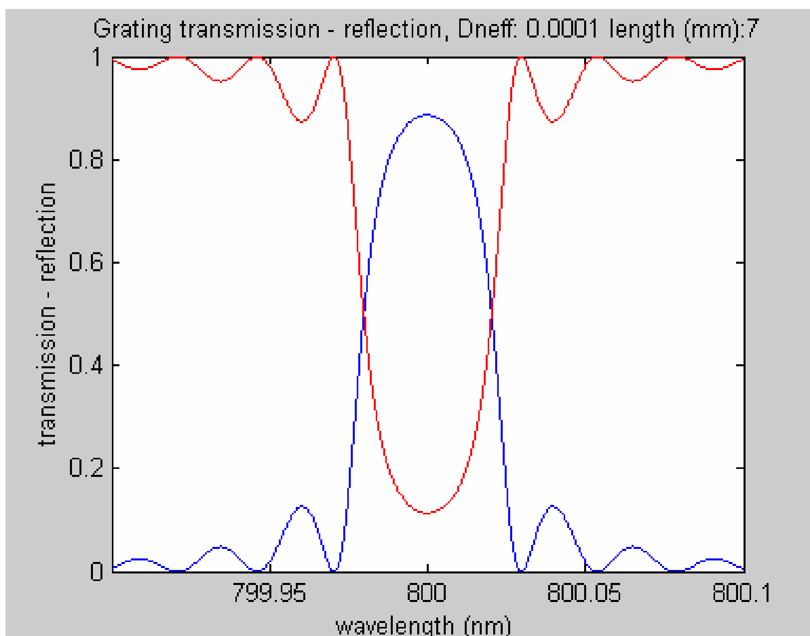

Figure 2.18. Theoretical transmission and reflection of a uniform grating on a hypothetical Ga diffused sapphire waveguide with a grating height of 100nm.

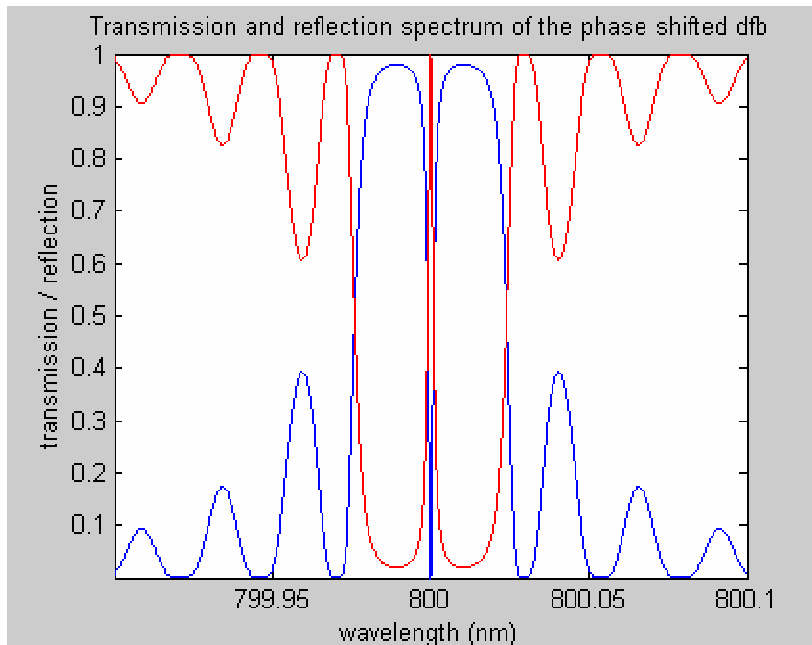

Figure 2.19. The theoretical transmission and reflection spectra of a π-phase shifted grating on a Ga-diffused sapphire waveguide. The π-phase shifted grating gives the desired transmission band at 800nm.

2.5.2 Coupled cavity integrated resonators

Coupled cavity resonators are a successful configuration for implementation of wavelength selection in lasers [39]. A coupled cavity resonator is based in the principle that the laser light is propagated in to more than one optical path which have a common section. In this common section the light that propagates in the different optical paths should be in-phase and interfere constructively. A simple form of coupled cavity resonator is when two or more simple Fabry-Perot resonators are superimposed so that the longitudinal modes of the combined resonator are the common longitudinal modes of the two resonators. In this section an appropriate device that implements a coupled cavity resonator in an integrated geometry is described.

i) Basic principles of y-junction resonators

The Y-junction is the simplest kind of branching element in a waveguide geometry; it is a simple configuration of one single mode input waveguide gradually separated into two single mode output waveguides. Each waveguide has a width, *w*. A tapered waveguide with length *l* and a width varying from *w* to *2w* is at the branching point. In Figure 2.20 a Y-junction is depicted. Y-junctions are a simple way to implement coupled resonators in integrated geometry. As can be seen in Figure 2.20, the device forms two optical paths with a common region, which, with the exception of mirrors are the elements needed to build a coupled cavity.

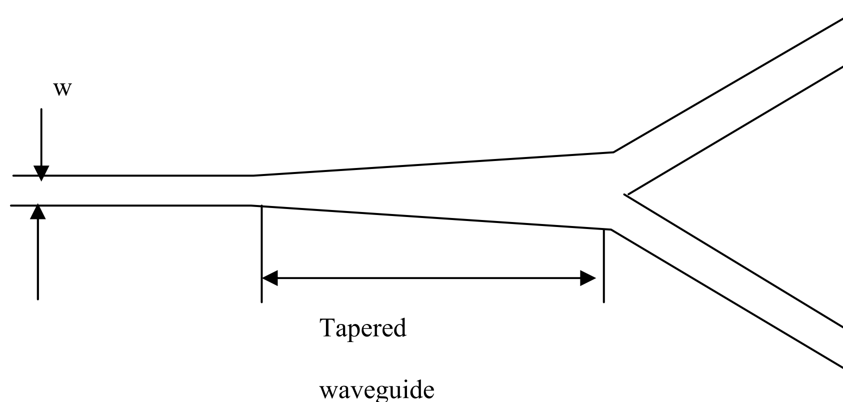

Figure 2.20. The geometry of a Y-branch.

In Figure 2.21 a drawing of a Y-junction integrated resonator is depicted. It can be seen that two cavities are formed, the first is between ports 1 and 2 and the second is between the ports 1 and 3. This configuration can be used for wavelength selection in integrated lasers [40,41]; the arm length difference, ΔL, defines the spectral response of the coupled cavity.

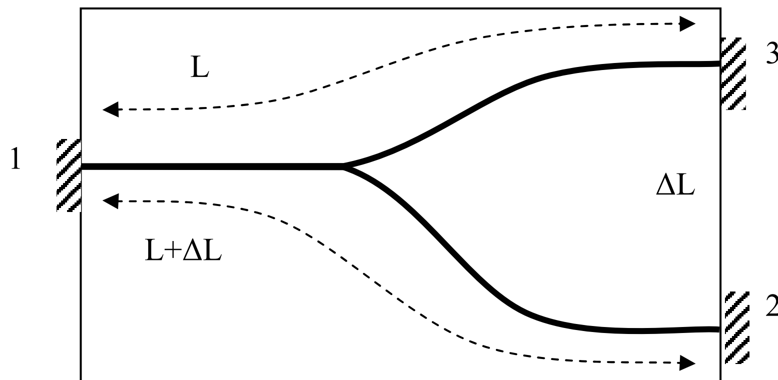

Figure 2.21. Drawing of a waveguide y-junction cavity.

This coupled cavity integrated configuration cannot always give adequate wavelength selectivity, especially in cases where the laser material has a very broad gain band. In these cases more complex coupled cavity designs are employed, that can propagate the optical field in more than two optical paths. The configuration of the back to back Y-junction resonator is very promising for implementation in sapphire active circuits that use gallium diffused waveguides. In Figure 2.22 a sketch of a back to back Y-junction integrated resonator is depicted; a model was developed in order to simulate the spectral response of this configuration.

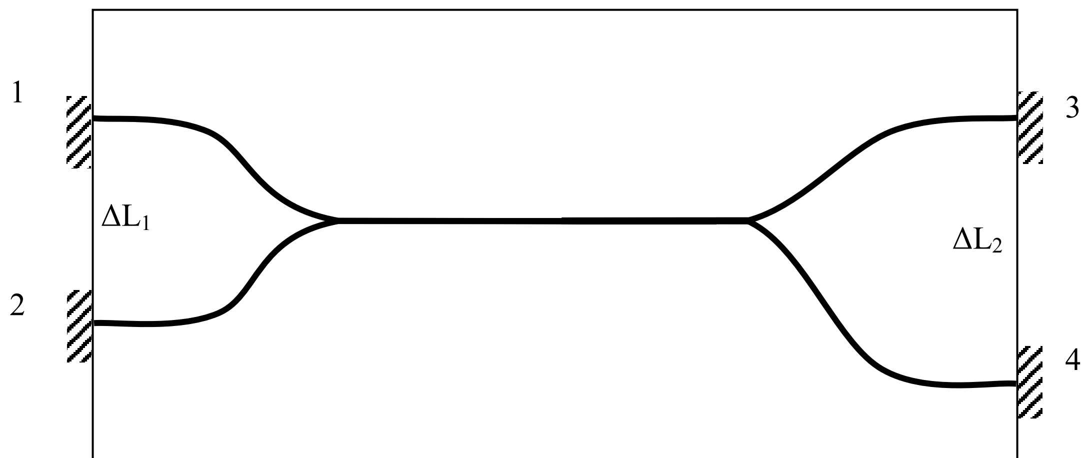

Figure 2.22. A drawing of an integrated back to back Y-junction with different arm lengths.

ii) Model for coupled cavity integrated resonators.

To model the behavior of the devices the formulae and the method used is analogous to the study of multi-port devices in the field of guided microwaves [41-43]. The model uses the concept of the transfer matrix that relates the input at one port to the output of the other ports. The purpose of the model was to calculate the spectral response of the back to back Y-junction as a function of the path difference between the arms of the Y-branches. This type of model was used for the first time to simulate the spectral response for this configuration. The computer model for the device was implemented in Matlab. The program takes as input the required supermode spacing and central wavelength and calculates the path differences of the branches. It gives, as output, graphs for the anticipated spectral response of the resonator. The program takes also as input from the user the resolution for the calculations, the central wavelength for the graph and finally the number of points to be calculated.

For the better understanding of these resonators the model will be used to simulate the spectral response of a Fabry-Perot, a Y-junction and finally a back to back Y-junction resonator. This is performed by appropriately selecting the path differences of the branches of the device shown in Figure 2.22. Further, in each of the following sections, a theoretical brief overview of each resonator will be given along with results from the model.

Fabry Perot resonator

In a simple laser resonator, defined by only two mirrors, the wavelengths supported by the cavity are related to the Length of the cavity, L, by the following relation [39].

$$\frac{2\omega L}{c} = m2\pi \quad \textbf{or} \quad L = m \cdot \frac{\lambda}{2} \qquad \textbf{(2.38)}$$

where m is an integer. The frequencies (or wavelengths) that satisfy this relation are called axial or longitudinal modes. They represent the resonant frequencies at which there is an integer number, m, of half wavelengths between the two mirrors. Under these conditions there is constructive interference between multiple reflected waves, which can lead to laser action in a suitable gain medium [39]. The wavelength difference between two sequential longitudinal modes that can be supported by the cavity is:

$$\Delta\lambda = \lambda_m - \lambda_{m+1} = \frac{2L}{m(m+1)} \qquad \textbf{(2.39)}$$

By defining in the model that all path differences of the configuration are equal to zero, the model simulates a Fabry-Perot resonator. In Figure 2.23 the results of the model are shown for such a simulation, of an integrated Fabry-Perot cavity in sapphire with length of 23mm. It can be seen that the separation of the cavity modes is approximately 0.1Å, clearly the gain curve of most laser materials is broader than

the cavity mode spacing therefore a laser using a Fabry-Perot resonator will be multimode. The mode spacing of the cavity modes can also be calculated using equation (2.39).

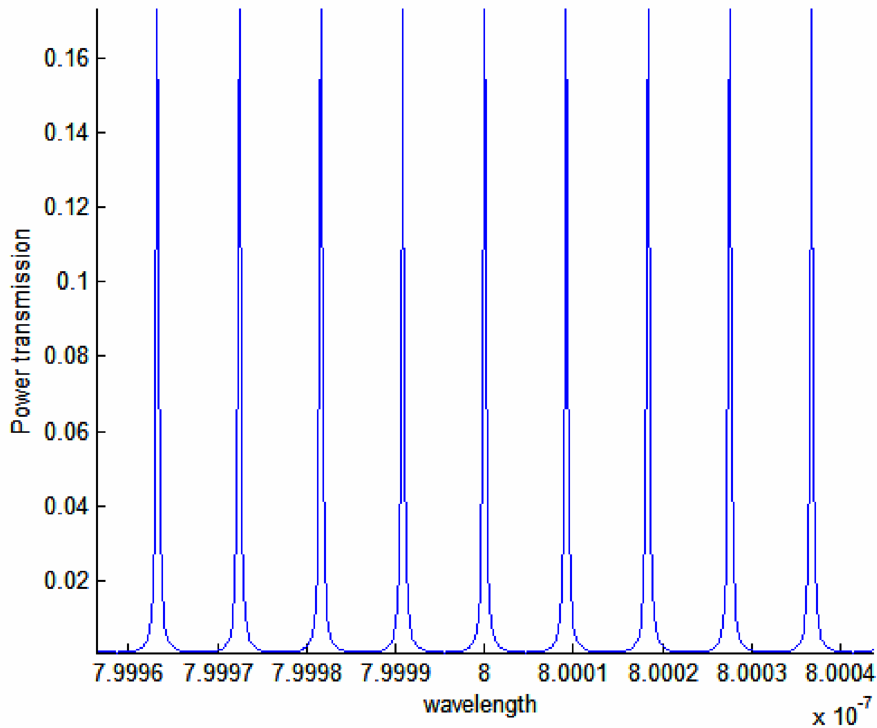

Figure 2.23. Power transmission versus wavelength for a Fabry-Perot cavity in sapphire.

Y-junction resonator

Now the operation of a Y-junction cavity will be theoretically examined. Based on Figure 2.21, if the lengths of the cavities defined between ports 1 and 2 and ports 1 and 3 have lengths L_1 and L_2 ($L_1 > L_2$) respectively, then equation (2.38) yields

$$L_1 = n \cdot \frac{\lambda}{2} \text{ and } L_2 = m \cdot \frac{\lambda}{2} \quad \textbf{(2.40)}$$

These conditions must be both satisfied, thus both individual cavities must be resonant at a specific wavelength for the coupled cavity to be resonant. When this wavelength is transmitted in the common region of the two cavities there is constructive interference. The path difference between the two cavities is

$$\Delta L = k \cdot \frac{\lambda}{2} \qquad \textbf{(2.41)}$$

Where $n - m = k$ and $L_1 - L_2 = \Delta L$. The device will support all the wavelengths that can satisfy this equation rendering k an integer; these solutions are frequently called supermodes. The Y-junction resonator will suppress the modes of its individual cavities that are between sequential solutions of the relation. The configuration applies a response envelope in the spectrum of its individual cavities, the spectral response of the cavity in the wavelength $\lambda_n + d\lambda$, where $d\lambda << \Delta\lambda$, is an attenuated output. The above relations with basic algebraic manipulations yield the following relation for frequency selectivity.

$$\Delta\lambda = \lambda_k - \lambda_{k+1} = \frac{2\Delta L}{k} - \frac{2\Delta L}{k+1} = \frac{2\Delta L}{k(k+1)} = \frac{\lambda_k^{\ 2}}{2\Delta L + \lambda_k} \qquad \textbf{(2.42)}$$

Therefore by choosing the path difference between the arms, ΔL, the supermode spacing, $\Delta\lambda$, induced by the Y-junction cavity can be controlled; the path difference and the supermode spacing are inversely proportional.

The Y-junction resonator can be simulated by the model by choosing one of the path differences to be zero, $\Delta L_1 = 0$, and selecting an appropriate value for the other path difference ΔL_2 (Figure 2.22). A path difference of 2.1162μm was calculated by the model to give a supermode spacing of 100nm at a central wavelength of 800nm. The result of the simulation is given in Figure 2.24; it can be seen that the spectral peak at 800nm has a FWHM of approximately 20nm, most likely a Ti:Sapphire laser would be multimode using this scheme. A larger path difference, of 14.267μm, is calculated to give a supermode spacing of 15nm, centred again at 800nm. In Figure 2.25, the simulation results are shown and in this case the FWHM of the peak at 800nm is 3nm and the wavelength selection is improved. Though a Ti:Sapphire laser, having a large

bandwidth, probably will lase in all the spectral peaks of the scheme at 785nm, 800nm and 815nm.

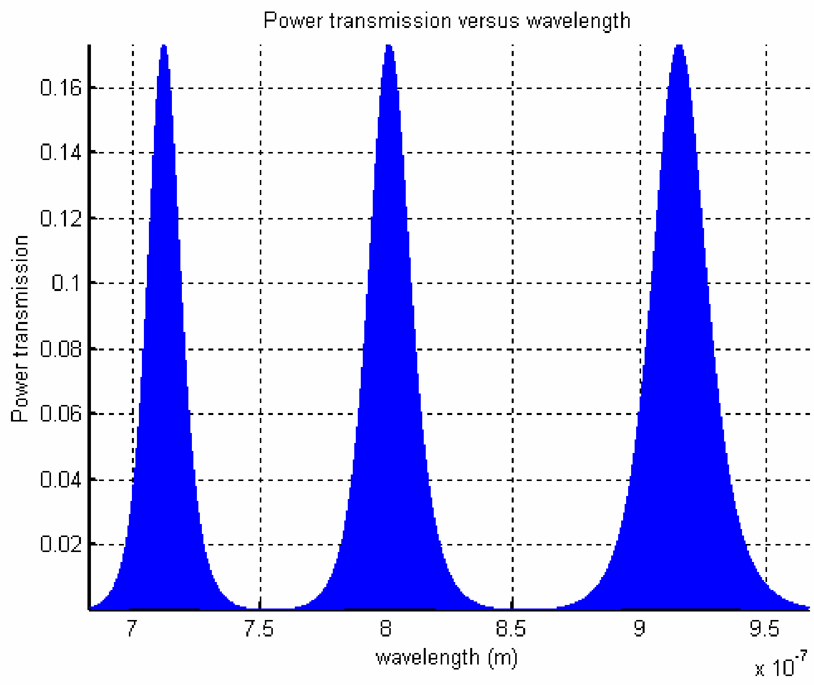

Figure 2.24. Modelling of a Y-junction cavity in sapphire with arm length difference of ΔL=2.1162μm; this length difference results in supermode spacing of approximately 100nm.

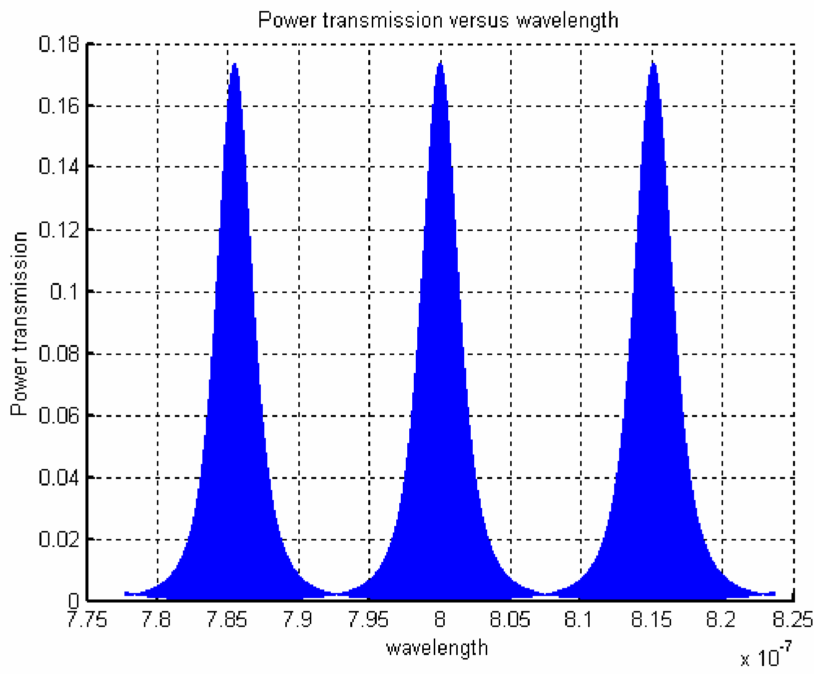

Figure 2.25. Modelling of a Y-junction cavity in sapphire with arm length difference of ΔL=14.267μm; this length difference results in supermode spacing of approximately 15nm.

As shown from the modelling results a Y-junction resonator cannot achieve the required wavelength selectivity for a true single-moded laser especially in cases like the Ti:Sapphire laser where the gain curve is broad. The back to back Y-junction, a more complex coupled waveguide device, can give the wavelength selectivity that is required

Back to Back Y-junction resonator

The advantage of this configuration (Figure 2.22) is that it combines the spectral responses of the two Y-junctions that are modelled in the previous paragraph. A convenient way to understand the spectral response of the back to back Y-junction is to see it as a combination of two simple Y-junctions. Therefore, using the already calculated arm differences of 2.1162μm and 14.267μm, the resulting spectral response is given in Figure 2.26. The result exhibits better wavelength selectivity by far better suppression of the side-modes and is a step closer to the implementation of a single longitudinal mode laser. The results of the model are regarded as very promising; it is likely that this cavity design has the required wavelength selectivity for a wavelength selective Ti:Sapphire laser.

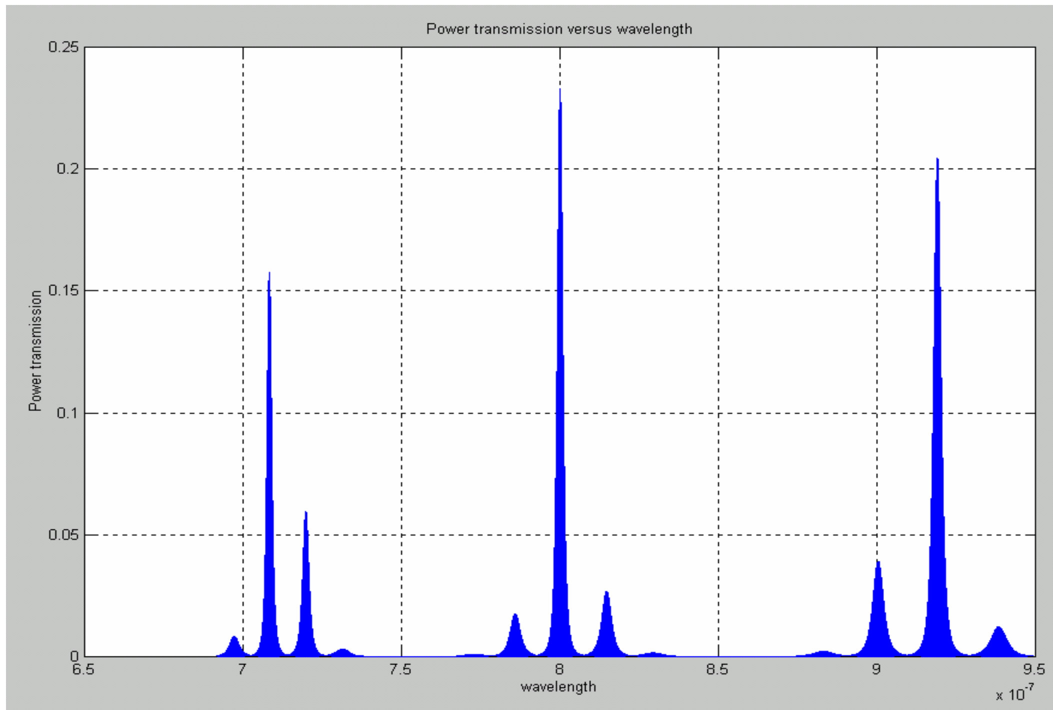

Figure 2.26. Model results for a back to back y-branch cavity that combines the spectral response of the two previously modeled y-junctions. The 100nm and 15nm spacing between the modes of the back to back Y-junction can be observed, from [43].

iii) Bent waveguides

For the implementation of the simulated coupled cavity s-bend waveguides should be fabricated in sapphire, therefore, design parameters such as the length of the curves and the curvature radius must be considered. The path differences of the arms are introduced by fabricating curves of a variable length in each branch. Radiation bending loss increases with the decrease of the curvature radius, furthermore it is a function of the mode size of the waveguide, so that for small bend radii high Δn waveguides are required; Figure 2.27 shows the field distribution of a guided mode in a bent waveguide. The index change of the waveguide is the limiting factor on the curvature of the bends and therefore on the dimensions of the device. Consequently it is very important to have a waveguide with an adequate index change in order to

implement such devices in a sapphire substrate. Gallium-diffused waveguides in sapphire have the potential for the implementation of these integrated circuits, and the length of the simulated back to back Y-junction was calculated to be 2cm. The bend radius used for the calculation was 30mm, and is appropriate for index changes more than 10^{-3} [44]. Further, when having a large index contrast waveguide in the horizontal direction, like a Ga:Sapphire ridge waveguide [12], the radius may be reduced further [45].

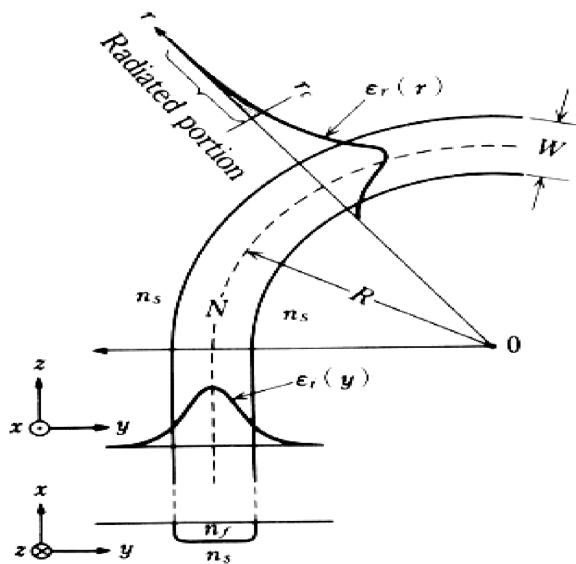

Figure 2.27. Radiation loss of a bent waveguide, from [45].

2.6 Conclusions

In this chapter the basic theory for lasers, waveguides and wavelength selection mechanisms is given and furthermore this theory is expanded into models useful for the design of devices and for comparison with experimental results that are presented in the following chapters. In addition this chapter aims to outline the potential for implementation of integrated devices in sapphire.

The properties of the substrate material, sapphire and titanium-doped sapphire are presented and explained at the beginning of the chapter. Subsequently waveguide theory and models are presented with specific examples based on Ga diffused sapphire waveguides. The performance of a waveguide laser is simulated and outlines the potential of Ti:Sapphire integration and the promise of such a configuration for low threshold operation. Based on modelling results of the waveguide model and using an F-matrix simulation method the possibility of successful fabrication of gratings on gallium diffused sapphire waveguides is presented. This approach may lead to an all integrated linewidth titanium sapphire laser. As an alternative approach also the theory and a model of a coupled cavity design is also given, which is based on the integration of a back to back y-junction resonator.

References to Chapter 2

1. Union Carbide, Datasheet, "Properties of Sapphire".

2. Mineralogy Database, http://webmineral.com, "Properties of corrundum", 2002.

3. Maiman,T.H., "Stimulated Optical Radiation in Ruby", *Nature*, **187**, 493, (1960).

4. P.F.Moulton. XXII Int. Quantum Electronincs Conference. 1982. Munich, Germany.

5. P. F. Moulton, "Spectroscopic and Laser Characteristics of Ti-Al2O3," *Journal of the Optical Society of America B-Optical Physics* **3**, 125-133 (1986).

6. P. F. Moulton, "Tunable Solid-State Lasers," *Proceedings of the IEEE* **80**, 348-364 (1992).

7. Martin J.Buerger, *Introduction to crystal symmetry*, (Mc Graw Hill, 1971).

8. B.Henderson and G.F.Imbusch, *Optical spectroscopy of inorganic solids*, (Clarendon Press, 1989).

9. I.H.Malitson. "Refraction and dispersion of synthetic sapphire". *J.Opt.Soc.Am* **52**, 1377 (1962).

10. V.Apostolopoulos, Mini-thesis, "Gallium diffused waveguides in Sapphire", (Electronics and Computer Science, University of Southampton, 2000).

11. V. Apostolopoulos, L. M. B. Hickey, D. A. Sager, and J. S. Wilkinson, "Gallium-diffused waveguides in sapphire," *Optics Letters* **26**, 1586-1588 (2001).

12. V.Apostolopoulos, L.M.B.Hickey, D.A.Sager, and J.S.Wilkinson. "Gallium diffused ridge waveguides in Sapphire". CLEO, Long Beach, California, 2002.

13. H.Eilers. "Photoelastic effect in Ti^{3+-} doped sapphire". *Phys.Rev.B* **45**, 9604 (1982).

14. K.F.Wall. "Optically induced non-resonant changes in the refractive index of $Ti:Al_2O_3$". *Optics Letters* **14**, 180 (1982).

15. J.Tapping and M.L.Reilly. "Index of refraction measurement of sapphire between 24 and 1060^0C for wavelengths of 633nm and 799nm". *J.Opt.Soc.Am* **3,** 610 (1986).

16. M.A.Jeppeson. "Some optical, thermo-optical and piezo-optical properties of synthetic sapphire". *J.Opt.Soc.Am* **48**, 629-632 (1958).

17. Schulz P. A. and Henion S R. "Liquid-nitrogen-cooled Ti:Al_2O_3 laser". *IEEE J.Quantum Electronics* **27**, 1039-1047 (1991).

18. F.J.Duarte, *Tunable lasers handbook*, (Academic press, 1995).

19. R.M.McFarlane et al. "Dynamic Jahn-Teller effect in octahedrally coordinated d^1 impurity systems". *Phys.Rev.* **166**, 250 (1968).

20. B.F.Gachter et al. "Zero-phonon transitions and interacting Jahn-Teller phonon energies from the fluorescence spectra of Al_2O_3:Ti^{3+}". *J.Chem.Phys* **60,** 2003 (1974).

21. R.L.Aggarwal, A Sanchez, R E Fahey, and A J Strauss. "Magnetic and optical measurements on Ti:Al_2O_3 crystal for laser applications: Concentration and absorption cross section of Ti^{3+} ions". *Applied Physics Letters* **48**, 1345-1347 (1986).

22. Orazio Svelto, *Principle of Lasers*, (Plenum Press, 1998).

23. J. Goodberlet, J. Wang, J. G. Fujimoto, and P. A. Schulz, "Femtosecond Passively Mode-Locked Ti-Al_2O_3 Laser with A Nonlinear External Cavity," *Optics Letters* **14**, 1125-1127 (1989).

24. P. M. W. French, J. A. R. Williams, and J. R. Taylor, "Femtosecond Pulse Generation from A Titanium-Doped Sapphire Laser Using Nonlinear External Cavity Feedback," *Optics Letters* **14**, 686-688 (1989).

25. D. E. Spence, P. N. Kean, and W. Sibbett, "60-Fsec Pulse Generation from A Self-Mode-Locked Ti-Sapphire Laser," *Optics Letters* **16**, 42-44 (1991).

26. N.A.Papadogiannis, B.Witzel, C.Kalpouzos, and D.Charalambidis. "Observation of Attosecond Light Localization in Higher Order Harmonic Generation". *Physical review Letters* **83**, 4289-4292 (1999).

27. P.Albers et al. "Continuous wave laser operation and quantum efficiency of titanium doped sapphire". *Journal of the Optical society of America B* **3**, 134 (1986).

28. R.L.Aggarwal et al. "Residual infra-red absorption in as-grown and annealed crystals of Ti:Al_2O_3". *IEEE J.Quantum Electronics* **24**, 1003 (1988).

29. M.Yamaga et al. "Optical and electron-spin resonance spectroscopy of Ti^{3+} and Ti $^{4+}$". *J.Appl.Phys* **75**, 1111 (1994).

30. V.Apostolopoulos, L.M.B.Hickey, and J.S.Wilkinson, "Gallium diffused waveguides in sapphire," *European Conference in Integrated Optics, Paderborn, Germany* (2001).

31. Donald L.Lee, *Electromagnetic principles of integrated optics*, (Wiley, 1986).

32. Reinhard Marz, *Integrated optics: Design and Modelling*, (Artech House, 1995).

33. Katsunari Okamoto*, Fundamentals of Optical Waveguides,* (Academic Press, 2000)

34. Louise MB Hickey. "Report on activities in Southampton during the 1851 fellowship award". 1999.

35. Louise M.B.Hickey, PhD thesis, "Ti:Sapphire waveguide laser by thermal diffusion of Ti into sapphire", (Optoelectronics Research Center, University of Southampton, 1998).

36. M. J. F. Digonnet and C. J. Gaeta, "Theoretical-Analysis of Optical Fiber Laser-Amplifiers and Oscillators," *Applied Optics* **24**, 333-342 (1985).

37. Makoto Yamadda and Kyohei Sakuda. "Analysis of almost periodic distributed feedback slab waveguides via a fundamental matrix approach". *Applied Optics* **26**, 3474 (1987).

38. Amnon Yariv, *Quantum electronics*, (John Wiley and Sons, 1988).

39. Anthony E.Siegman, *Lasers*, (University Science books, 1986).

40. J. Amin, M. Hempstead, J. E. Roman, and J. S. Wilkinson, "Tunable Coupled-Cavity Wave-Guide Laser at Room-Temperature in Nd-Diffused Ti-$LiNbO_3$," *Optics Letters* **19**, 1541-1543 (1994).

41. Eustace K.Mwarania and J.S.Wilkinson. "Modeling of Y-junction Waveguide resonators". *J.Lightwave Tech* **10**, 1700 (1992).

42. Eustace K.Mwarania, "PhD thesis," (Optoelectronics Research Centre, University of Southampton, 2003).

43. V.Apostolopoulos, "MSc project," (Electronics and Computer Science, University of Southampton, 1999).

44. Hiroshi Nishihara, Masamitsou Haruna, and Toshiaka Suhara, *Optical integrated circuits*, (McGRAW-HILL, 1989).

45. Richard Syms and John Cozens, *Optical guided waves and devices*, (McGraw Hill, 1992).

CHAPTER 3

DIFFUSION OF TITANIUM AND GALLIUM IN SAPPHIRE

3.1 Introduction

In this chapter diffusion coefficients for diffusion of gallium in sapphire and codiffusion of titanium and gallium in sapphire are presented for the first time. The main fabrication process used in this work was the diffusion of ions in sapphire for the implementation of passive and active waveguides. Therefore the characterization of ionic diffusion in sapphire was an important step in understanding the advantages and the restrictions that this fabrication method gives. The main purpose of the experimental study of diffusion is to identify how the diffused dopant profile in sapphire is related to the fabrication conditions. Diffusion of gallium into sapphire was selected in order to obtain passive waveguides, and diffusion of titanium into sapphire was used for the realisation of active waveguides [1-5].

This chapter begins with a theoretical introduction giving the basics of classical diffusion theory [6-8] as a background for the analysis and understanding of the data obtained by Secondary Ion Mass Spectroscopy (SIMS). A brief review of the literature on the diffusion of cations into sapphire is also included. Diffusion of titanium has already been characterised by Louise Hickey [3,9] and in this chapter some of those results are presented as a part of the review. In the present work

gallium diffusion was characterised, using SIMS analysis, and the results of the experiments are presented here. The characteristics of combined titanium and gallium diffusion were also investigated, again using the SIMS technique, and are given in the last section of the chapter with analysis and discussion.

3.2 Theory of Diffusion

3.2.1 Introduction

Diffusion is a kinetic process that leads to the homogenisation of a material with different chemical components. In comparison with heat flow in a temperature gradient (Fourier, 1807 [10]) a mass flux will exist in a concentration gradient. Any system of chemical components will tend to reach a dynamic equilibrium where the concentration gradient is zero. A simple everyday diffusion example that is often observed is the rapid dilution of a drop of dye in a glass of water. Adolf Fick was the first scientist to report a system of salt-water undergoing diffusion. The description of the system in his published work in 1855 [11] included the first use of the diffusion coefficient, D. In contrast with diffusion in gases or in liquids, where diffusion can be observed microscopically and macroscopically, diffusion in solids takes place only at a microscopic, atomic scale.

3.2.2 Mass flux and Fick's first law.

The mass flux, $\boldsymbol{J}(x,y,z)$, is the mass flowing per unit time per unit area. By observation it is found that the mass flux is proportional to the concentration gradient. This

observation actually comprises Fick's first law which, assuming an isotropic material, can be written in vector form, as

$$\mathbf{J} = -D\nabla C \qquad \textbf{(3.1)}$$

where D is the diffusion coefficient and C is the concentration. Assuming now a 1-D problem, equation 3.1 can be simplified further to the form:

$$J = -D\frac{dC}{dx} \qquad \textbf{(3.2)}$$

3.2.3 The diffusion equation

If we consider an arbitrarily small volume in a diffusing system the difference of inflow and outflow of mass gives the mass accumulation rate. This statement constitutes a general constraint, the conservation of mass.

$$-\nabla\mathbf{J} = \frac{\partial C}{\partial t} \qquad \textbf{(3.3)}$$

The interpretation of this statement is that if there is a converging flow of mass at a point, $\nabla\mathbf{J} < 0$, then the concentration rises with time. If there is a divergent flow, $\nabla\mathbf{J} > 0$, then the concentration will fall with time.

If we combine the conservation of mass statement, equation 3.3, with Fick's first law, equation 3.1 we have:

$$\frac{\partial C}{\partial t} = D\nabla^2 C \qquad \textbf{(3.4)}$$

This equation is Fick's second law, which is also called the diffusion equation; in 1-D the equation simplifies to:

$$\frac{\partial C}{\partial t} = D\frac{\partial^2 C}{\partial x^2} \qquad \textbf{(3.5)}$$

3.2.4 Physical meaning of the diffusion coefficient.

Phenomena such as diffusion or heat flow are the direct consequence of the random movement of atoms. As an example, a simple 1-D simulation in Matlab is made. A population of atoms (50000) is situated at the beginning of an axis system starting a random walk. The time unit is defined as the loop of the program; in each loop each particle may, with equal possibilities, stay where it is, move one square left or right. The result of the simple model is depicted in Figure 3.1 where the final distributions of the particles are shown for a different number of loops (100-1000). As predicted from diffusion equation the result follows Gaussian curves.

The diffusion coefficient gives the rate of movement of the diffusing atoms. It was introduced by Fick as a phenomenological constant describing the diffusion system. The exact physical interpretation was established much later; using a stochastic process like a Markov random walk. Describing one important and relatively simple result of this theory, the diffusion coefficient can be related to microscopic quantities. The diffusion coefficient is related to characteristics of the random walk by Einstein's formula,

$$D = \frac{1}{6}\left(\frac{n}{t}\right)\lambda^2 \qquad \textbf{(3.6)}$$

Where, n, is the number of steps that the particle took on the random walk and t is the time needed to complete this walk. Therefore n/t is the step rate and finally λ the length of each step. Now the parameters used in the random walk theory can be related to microscopic quantities to reveal the physical meaning of the diffusion coefficient. At a microscopic level n/t is the atomic jump frequency and λ the microscopic jump length. The microscopic jump length, λ, in crystals may be the

distance between adjacent lattice sites or interstices, in glasses it may be the mean distance of atoms in the glass matrix and finally in gases it may be interpreted as the mean free path between molecular collisions.

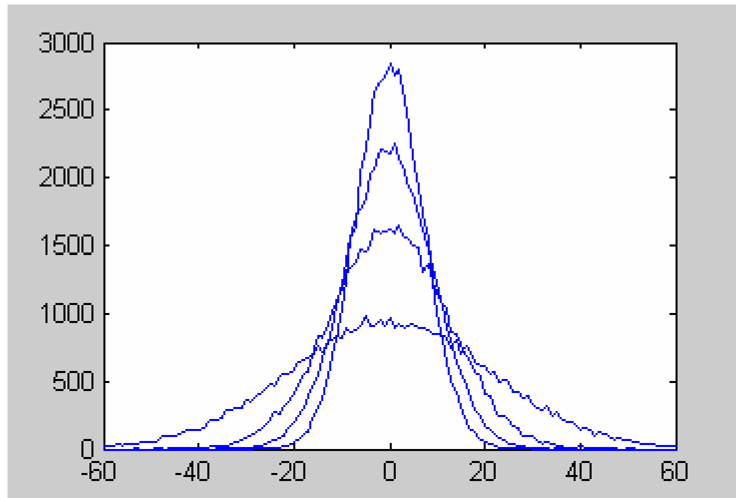

Figure 3.1 Simple model of random walk in 1-D of 50000 particles. The curves represent the distribution of particle on different time instances.

3.2.5 The Arrhenius relation

The Arrhenius relation is a general statement applying to many different physical processes. In diffusion theory it gives the temperature dependence of the diffusion coefficient.

$$D = D_o e^{-\frac{Q}{RT}} \qquad \textbf{(3.7)}$$

Where Q is the molar activation energy, R is the gas constant, T the temperature and D_0 a constant with units of diffusivity. For a diffusion problem we find the parameters of the Arrhenius relation by fitting equation (3.7) to the experimental data. Diffusion systems start exhibiting non-Arrhenius behaviour at high temperatures, $T>0.7T_m$, where T_m is the melting point. This is due to the fact that the Arrhenius relation does

not take into account the change of phase of the material, it is assumed that the mechanism of the diffusion is the same for all the range of temperatures.

3.2.6 Solutions to the diffusion equation.

In the case of gallium diffusion into sapphire the one dimensional diffusion equation must be solved considering the diffusion of a thin film on a planar substrate. This problem will be solved here theoretically, first for the case where the planar source is infinite and never depleted during the diffusion and second for the case in which the source is instantaneously depleted.

a) Unlimited diffusion source

When at the end of a diffusion process the surface is covered with residue of the source then it can be assumed that during the diffusion the supply of diffusing atoms on the surface was constant. Therefore at the interface between the source and the substrate the diffusant concentration is equal to the maximum solid solubility at the diffusion temperature. The solution of the diffusion equation, applying these boundary conditions, is a complementary error function, erfc. Therefore the general solution for the diffusion profiles in this case will be:

$$C(x,t) = C_s\left[1 - \int \exp\left(-\frac{x^2}{4Dt}\right)dx\right]$$

or $C(x,t) = C_s erfc\left(\frac{x}{2\sqrt{Dt}}\right)$ **(3.8)**

Where, C_s, is the maximum solid solubility of the diffusing substance at the temperature of the diffusion. The factor $2\sqrt{Dt}$ is called the effective diffusion depth and gives the depth at which the maximum concentration C_s has fallen to

$erfc(1)C_s = 0.157C_s$. In Figure 3.2 graphical examples of these concentration profiles for different times are depicted.

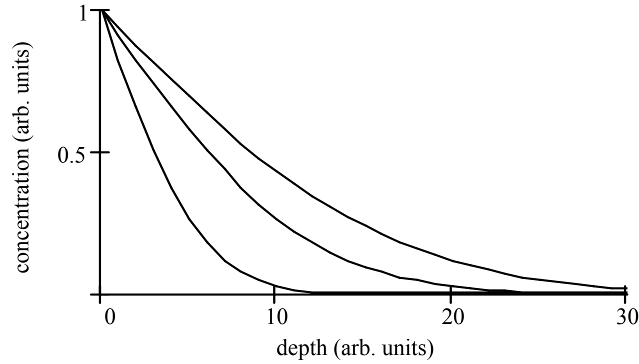

Figure 3.2. Concentration profiles of diffusion with an undepleted source, for different time periods.

b) *Solution for an instantaneous source*

In contrast to the previous case, where a film with sufficient thickness gives a constant supply of diffusant atoms to the substrate, here a diffusion source that is instantaneously depleted is assumed. The solution of the diffusion equation for these conditions is then a Gaussian function [6].

$$C(x,t) = \frac{Q}{2\sqrt{\pi Dt}} \exp\left(-\frac{x^2}{4Dt}\right) \qquad \textbf{(3.9)}$$

where Q is the total number of atoms supplied per unit area. The peak concentration is always at the surface and decreases with time. The diffusion profile is also characterized by the effective diffusion depth, $2\sqrt{Dt}$, that gives the depth at which the surface concentration is decreased by a ratio of 1/e. Therefore when at the end of a diffusion procedure there is no residue left on the surface of the substrate, we can

assume that the concentration profiles will follow a Gaussian fit. Figure 3.3 shows graphical examples of this diffusion profile.

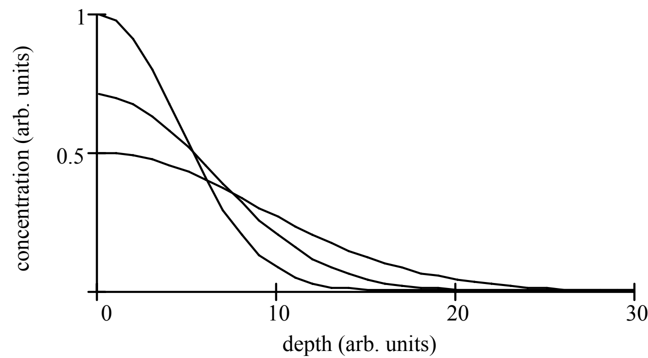

Figure 3.3. Concentration profiles for different time periods for an instantaneous source diffusion problem.

3.3 Overview of diffusion in sapphire

3.3.1 Diffusion characterisation in sapphire

In the case of ionic diffusion in sapphire, the most efficient experimental technique for composition analysis is Secondary Ion Mass Spectrometry (SIMS). The basic principles of this method will be outlined here [12]. SIMS is an established high depth resolution and high sensitivity, destructive technique that is used for analysing compositions of solids. A stream of high energy ions, usually O_2, Ga or Cs ions, is focused onto the surface of the sample. The high-energy incident ions lose their kinetic energy when bombarding the surface and ions from the surface of the sample are released. The ions are then accelerated towards an aperture close to a high negative or positive potential (depends if the species under investigation is electropositive or electronegative) and are identified by mass spectroscopy. Depth

profiling is made possible using this characterisation method by steadily etching the material to build a crater. At the end of the process the etch rate is measured by measuring the depth of the crater with the assumption that the etch rate is constant during the process. Profiles in sapphire that are in the order of 1μm or less can be readily obtained. However, because the etching process is slow, this method is inefficient, in time and funds, for measuring any profile that extends inside sapphire for more than a few micrometers. In this work SIMS was used to characterise gallium and titanium ion diffusion.

3.3.2 Literature review of cation diffusion in sapphire

In the literature there are data describing the diffusion of several ions into sapphire. Previous studies were performed for the diffusion of Al, Ni, Cr, Fe, Ag, Cu, Y, Pt and Ga into sapphire [13-28]. Here some of these reports (diffusion of trivalent species: Al, Cr, Y and Ga) will be examined briefly in order to be able to compare the results with gallium and titanium diffusion.

Palandino studied aluminum self-diffusion in polycrystalline alumina in 1962 [13]. Le Gall in more recent work studied aluminum self-diffusion in sapphire in 1994 [22]. The diffusion coefficient of Al self-diffusion is of special interest for the study of diffusion into sapphire because it indicates the mobility of defects in the lattice. The activation energy for aluminum is $510 kJmol^{-1}$, which can be used as a comparison for the other impurities that diffuse into sapphire.

There are several reports that give the lattice diffusion of chromium [15-17,23] in sapphire. The Arrhenius equation obtained by the study of Moya [23] is:

$$D(1000-1500°C)m^2s^{-1}{}_{Moya} = 1.2\cdot 10^{-10}\exp(-\frac{(290\pm 30)kJmol^{-1}}{RT})\left(m^2s^{-1}\right) \quad \textbf{(3.10)}$$

Figure 3.4 includes all the measured lattice diffusion rates for Cr and the self-diffusion of aluminum. Chromium doping of sapphire by diffusion is a promising procedure because of the very high solid solubility of Cr ions in the sapphire lattice. In the figure, it can be observed that although the diffusion coefficients reported vary significantly in magnitude, the slopes that yield the activation energy are in close agreement. In general, the variation of the diffusion coefficients in different studies is explained by the fact that small differences in the quality of material and the parameters of the diffusion can cause a large difference in the results of the diffusion. Nevertheless, in different studies the activation energy is approximately the same if the studies are performed for the same range of temperatures.

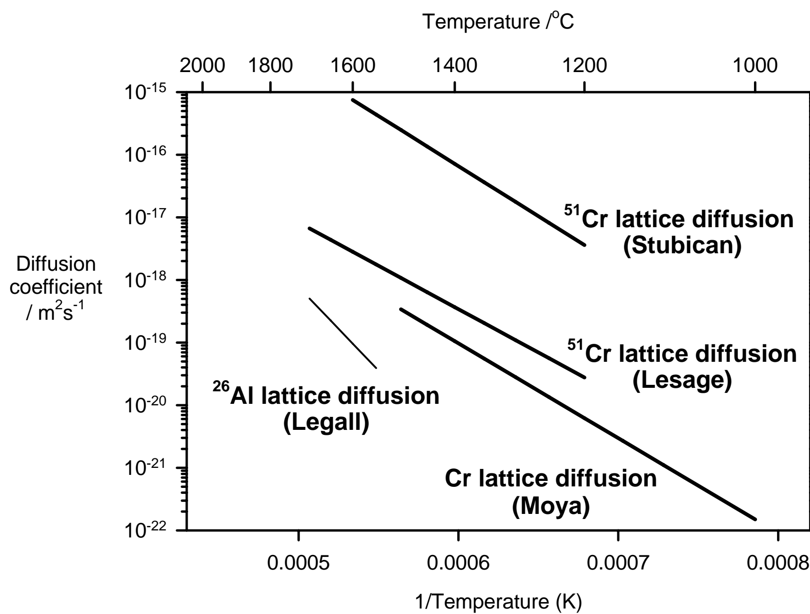

Figure 3.4 Arrhenius relations for Cr and Al diffusion into sapphire, from [3].

The other two reports that are of great interest for this work are the diffusion of gallium and yttrium [15,25,26]. Yttrium diffusion was studied by Moya [26], using

SIMS for the characterization of the diffusion profiles, in the range from 1150 to 1500°C. The diffusion coefficients obey the following Arrhenius relation:

$$D(1150-1500°C)_{Moya} = 1.2\cdot 10^{-10}\exp(-\frac{295kJmol^{-1}}{RT})\left(m^2 s^{-1}\right) \quad \textbf{(3.11)}$$

These values are in close agreement with the chromium diffusion results obtained by the same group of researchers [23] although the yttrium ion is larger than the chromium ion. Yttrium solid solubility in sapphire is reported to be low (<10ppm) [26] and for this reason yttrium doping of sapphire is not a very promising candidate for waveguide fabrication.

There are not many published data concerning Ga diffusion into sapphire except a recent report where gallium diffusion into sapphire has been investigated by Fung et al [25] by x-ray energy dispersive spectroscopy (XEDS). In this work gallium diffusion was investigated as a characteristic of the process of growing GaN films on sapphire substrates by metalorganic chemical vapour deposition (MOCVD). In this process the temperature is elevated to 1050°C and the gallium diffusion coefficient obtained was 2.3x10^{-13} cm^{2}sec^{-1}. In this report the parameters of the diffusion are not close to those used in our work therefore the results can not be directly applied. Nevertheless it gives useful information on the high solid solubility of gallium in sapphire (also mentioned in earlier publications [29]).

3.3.3 Review of titanium diffusion in sapphire

i) Fabricated samples and characterisation techniques

The characterisation of titanium diffusion in sapphire was performed by Louise Hickey [3,9,30], and a brief overview of this work is included in this section focusing

on some results of this research that are useful in the present study. Diffusion concentration profiles of titanium ions are presented that were obtained by SIMS analysis or fluorescent imaging. The fabrication parameters of the samples of interest are given in Table 3.1.

Sample #	Temperature (^{0}C)	Time (hrs)	Ti source thickness (nm)	Cooling
1	1950	2	41	slow
2	1950	2	41	fast
3	1605	1	13	slow
4	1605	8	13	slow

Table 3.1. Fabrication parameters of Ti-diffused sapphire samples, from [3,9].

Although the SIMS technique seems to be the optimum choice for characterising ionic diffusion in sapphire, there is another interesting option especially for the case of titanium ions in sapphire. This technique uses the fact that Ti^{3+} is a fluorescent ion when incorporated substitutionally to the aluminium ion in sapphire lattice. If a laser in the blue-green is used to excite them then the titanium ions will emit in the near infrared. Figure 3.5 shows the experimental configuration for depth profiling which takes advantage of the fluorescence of titanium in order to map the concentration of the ions versus depth in a polished cross-section. This technique can be used for characterisation of the diffusion of titanium in sapphire, if the assumption that all the titanium ions are in the 3+ state and also that they are substituting for aluminium sites is valid. Usually this is not the case as titanium will also diffuse in the 4+ state and through defects, so that technique usually is not ideally suited for diffusion coefficient calculations. Nevertheless, if the scope of the study is to fabricate an active device it can give valuable complementary information in comparison with SIMS analysis. It is

an excellent way to relate the ratio of Ti^{3+} to the total titanium to the fabrication conditions.

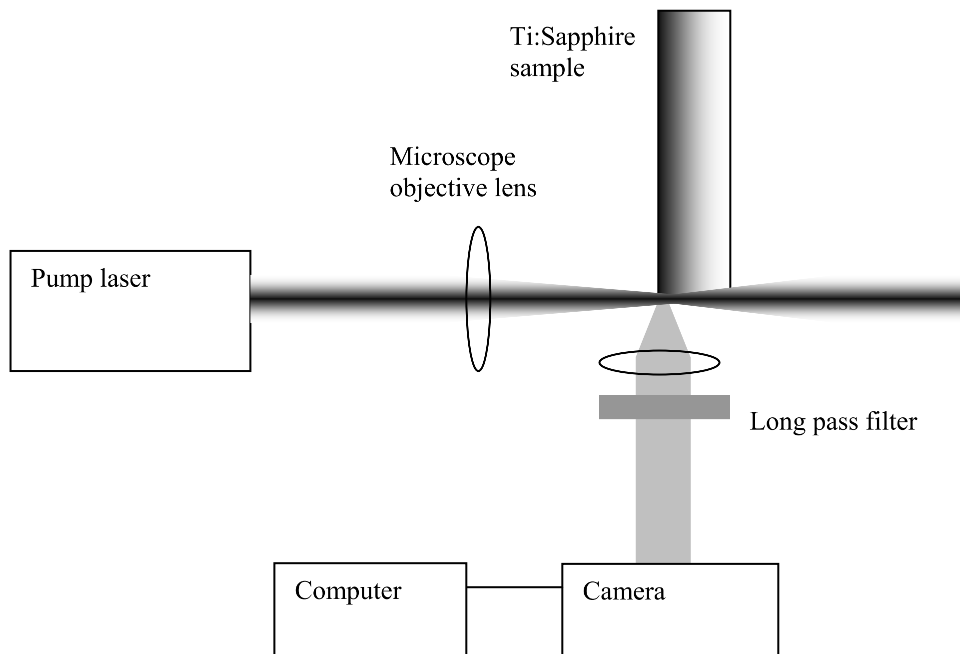

Figure 3.5 Experimental configuration of spectroscopic characterisation of Ti^{3+} concentration profiles [3].

ii) Concentration profiles of Ti in sapphire

In Figure 3.6 two graphs are shown with diffusion concentration profiles for samples 1 and 2. These two samples had identical diffusion conditions (41nm, 1950^0C, 2hrs) except that sample 1 was slow-cooled at the end of the annealing and sample 2 was fast-cooled. The titanium ion concentration profiles were measured using SIMS analysis and also fluorescence imaging. From the two graphs it can be deduced that fast cooling is increasing the ratio of fluorescent to total titanium in sapphire. In the case of slow cooling it seems that near the surface most of the titanium ions are not fluorescing. An appropriate explanation, although not tested, is that titanium near the surface is creating and is situated in defects in the crystal. Another characteristic of the profile of sample 2 that was subjected to fast cooling is that the shape of the

profile indicates a depletion of Ti ions near the surface region. These observations are very important to the analysis of gallium and titanium diffusion in sapphire that was performed in this work, and will be referenced in section 3.4.4.

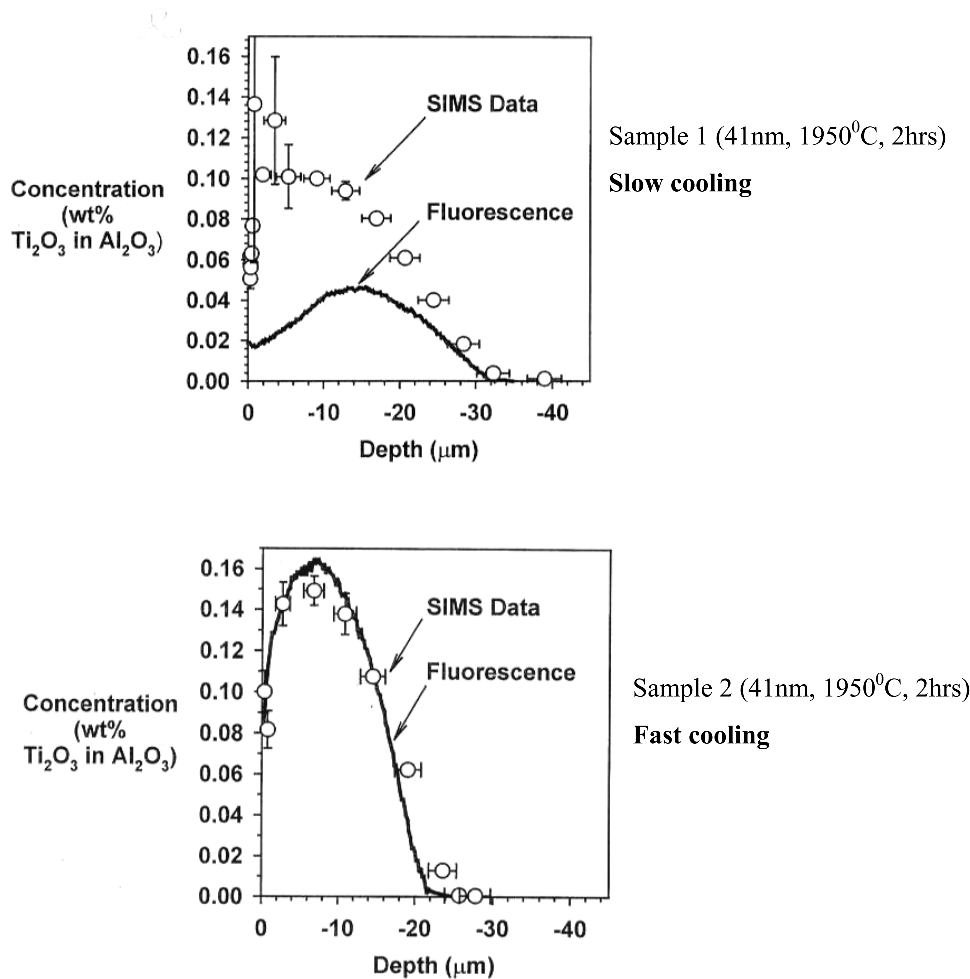

Figure 3.6. Comparison of titanium concentration obtained from SIMS and fluorescence imaging for samples 1 and 2, from [3].

Finally in Figure 3.7 the diffusion concentration profiles of titanium ions, obtained by SIMS, from samples 3 and 4 are depicted. From these profiles the diffusion coefficient of titanium in sapphire at 1605^{0}C was calculated and is (3±1) x 10^{-15} m^2s^{-1} [9]. This value is close to the data obtained in this work on titanium which are presented in section 3.5.

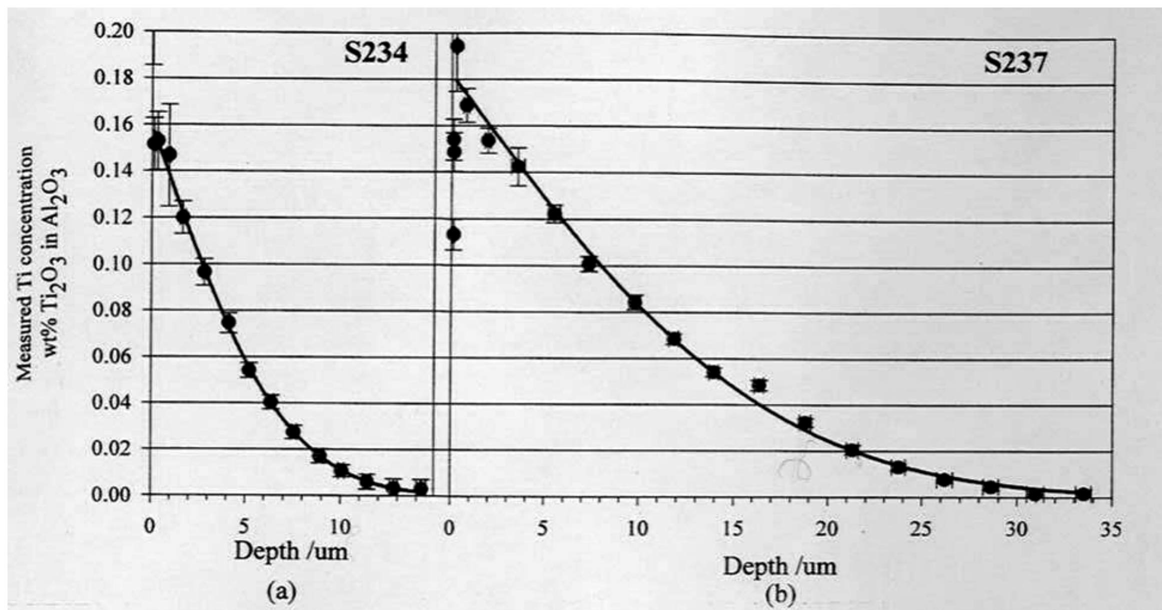

Figure 3.7 Diffusion profiles of samples 3 and 4, diffused at 1605^{0}C, for 1 and 8hrs respectively, from [9].

3.3.4 Limitations of diffusion in sapphire

There are two important limitations in titanium diffusion which are not yet solved and pose an important problem in the optimisation of optical devices. Gallium or titanium diffusion in sapphire have a strong component of lateral diffusion. When a patterned diffusion source is used in sapphire there is a very strong component of lateral diffusion. This poses a limit to the horizontal confinement that can be achieved in the fabrication of a channel waveguide. The effect is observed in the fabrication of gallium channel waveguides, mentioned in section 4.3.5, or titanium channel waveguides [3]. This effect is believed to originate from a high surface defect concentration of the substrate that provides a fast surface diffusion route [31,32].

Furthermore, titanium diffusion leaves on the surface of sapphire strong surface residue which results in strong surface roughness that gives rise to the dominant propagation losses in optical waveguides. In Figure 3.8 some microscope images of surface features that are characteristic for titanium diffusion are shown. Images (a), (b) and (c) are showing titanium diffusion from a 10nm thick diffusion source and image (d) is of a sample diffused for the same conditions (at 1600^{0}C) but with a 50nm thick diffusion source. Especially interesting seems to be image (c) where bright lines in the surface of sapphire can be observed, which appear to follow the symmetry of the lattice of sapphire and indicate slips of the lattice which are revealed or created during the annealing process. Image (a) shows the most commonly encountered surface roughness and features on sapphire after diffusion of a thin film (~10nm) of titanium. Comparing images (a) and (d), it can be deduced that the only way to avoid strong propagation losses in the fabrication of titanium waveguides is to try to limit the thickness of the diffusion source. Any attempt to chemically etch the surface residue features using strong chemicals like fuming nitric acid or hydrofluoric acid did not give any result. This indicates that the surface residue is not titanium metal but a chemical reaction between the diffusion source and sapphire, which is expected at the temperature of the annealing.

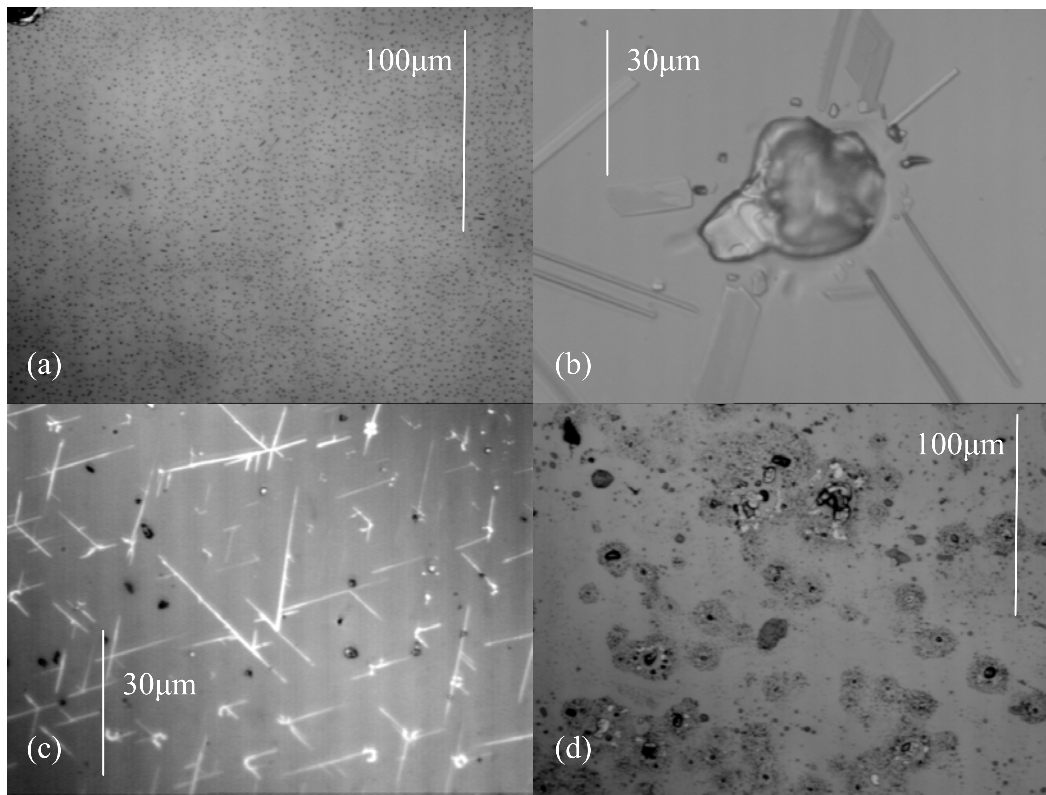

Figure 3.8 Image (a) shows typical surface features of a sample diffused with a 10nm ti film and images (b) and (c) are strange features of the same sample at higher magnification. Image (d) shows typical surface features of a 50nm film diffused sample. The images are enhanced since they are not used in any quantitative measurement.

3.4 Diffusion of gallium in sapphire

3.4.1 Introduction

The purpose of the work described in this section is to investigate the feasibility of gallium doping of sapphire substrates using thermal diffusion for the fabrication of passive optical waveguides. The first objective is to obtain diffusion coefficients for gallium diffusion profiles in sapphire in the range of 1400-1600^{0}C. This range of temperatures was chosen because it was expected to result in the diffusion depths that are needed (depths in the order of 1 micron are usually sufficient for waveguide fabrication [33]) in reasonable diffusion times. Using temperatures above this range

could provide shorter periods of annealing but because few furnaces can reach such high temperatures the flexibility of the fabrication procedure would be decreased. This was the first time that the diffusion of gallium in sapphire was investigated at this range of conditions and using the SIMS technique.

3.4.2 Preparation of samples

Samples of dimensions $1x1cm^2$ and thickness ~330μm were cut from commercial c-cut sapphire wafers. A thin film of gallium oxide was thermally evaporated on the optically polished face of the samples. All the films were deposited in vacuum using a thermal evaporation coater. The evaporation material, gallium oxide in the form of fine powder, was placed in a tantalum boat and the chamber was pumped down to a pressure of approximately $2x10^{-6}$ mbars. It is expected that the thin film consists of a mixture of gallium oxide phases, as the source is expected to lose oxygen during the evaporation. The thickness of the thin film produced was 50±5nm according to the measurements of a surface profilometer.

Gallium oxide was selected as the diffusion material because it has a sufficiently high melting point of 1900^0C and the thin films created by thermal evaporation are of good quality. If gallium metal is used, it would be in liquid form at the temperature of the diffusion as it has a low melting point of 30^0C.

3.4.3 Diffusion conditions

The furnace used for the diffusions was a heated tube furnace with molybdenum disilicide filaments capable of operating up to 1700^0C. The tube is a high purity

ceramic and was flushed continuously with inert or oxidizing gases. The diameter of the tube is 75mm and the length about 1m. The hot-zone of the furnace provides a uniform temperature distribution (±5^{0}C) across approximately 10cm. All the characterized samples were diffused in an argon atmosphere although a true inert atmosphere is difficult to be achieved due to the porosity of the tube. During the diffusion, the samples were held in the furnace using a platinum boat.

All the diffusions were performed with very fast heating and cooling (~100^{0}C/sec). The samples were introduced into the furnace when it had already reached the diffusion temperature and were removed whilst the furnace was running at diffusion temperature. Due to sapphire's excellent heat conductivity it was a rare occasion that a sample would crack or break. The diffusions were performed for a variety of time periods and temperatures and a subset was selected for characterisation by SIMS. One criterion used for choosing the diffusion conditions was to have no residue left on the samples after the diffusion. Further, the samples were selected to have small diffusion depths because SIMS analysis in a hard material like sapphire can be very time consuming and expensive for large diffusion depths. The characterized set consisted of 3 samples diffused at temperatures 1400^{0}C, 1500^{0}C and 1600^{0}C for times of 4hrs, 4hrs and 1hr respectively.

The SIMS analysis of the penetration profiles was carried out with a Cameca IMS 4f apparatus at Loughborough Surface Analysis Limited. A thin coating of silver was deposited on the samples in order to minimise sample-charging effects. The analysis of the samples was performed using O^- primary ion bombardment and positive secondary ion detection as these conditions give reasonable sensitivity to

electropositive species whilst minimizing sample charging effects that otherwise occur with bulk insulators. The depth scales were determined using interference microscopy and stylus based measurements of the sputtered craters.

3.4.4 Characterization of diffusion profiles

A characteristic of gallium diffusion into sapphire is that after the annealing, due to the high solid solubility of gallium in sapphire, no residue of gallium remains on the surface and the roughness of the surface remains unaltered. This renders gallium a promising candidate for waveguide fabrication as minimal surface roughness lowers the propagation loss and high solid solubility gives a wide selection range of the doping level. All the samples characterized by SIMS had no residue on the surface therefore the diffusion source was depleted. According to the diffusion equation, when the diffusion source is depleted the solution is a Gaussian function. Therefore according to the classical theory of diffusion it is expected that the data given by the SIMS analysis would have a Gaussian fit.

Figure 3.9, Figure 3.10 and Figure 3.11 show the diffusion profiles for the 1400^0C, 4 hrs, 1500^0C, 4hrs and 1600^0C, 1hr samples. From the profiles of these samples the diffusion coefficient of gallium into sapphire is derived. According to the classical theory of diffusion the maximum concentration will be on the surface. The diffusion profiles have maxima inside the bulk of sapphire at which depth aluminium counts have already reached their maximum value. The only plausible explanation for the surface depleted profiles of gallium is that during the diffusion process evaporation or sublimation is taking place from the diffusion source and also from the part of sapphire near the surface. Thus the maximum in the concentration profile may be found inside the bulk of the sapphire. Since evaporation should take place near the

surface the maximum of gallium should be found inside the sample approximately as deeply as the thin layer of gallium, 50nm, and to be weakly dependent on time and temperature.

The data shown do not fully support the explanation that evaporation occurred during the whole period of the diffusion. It can be observed that on the 1500^0C profile (Figure 3.10) the maximum is at a depth of 150nm; for the 1600^0C profile (Figure 3.11) the maximum is at a depth of 350nm. Furthermore, the depleted gallium regions of the 1600^0C and 1500^0C samples are unexpectedly steep. According to the hypothesis that evaporation is taking place during the whole annealing period smoother profiles would be expected.

Referring back to the titanium diffusion data that were shown in section 3.3.3, and specifically to Figure 3.6, there is a similar characteristic in the concentration profiles. This observation clearly leads to the conclusion that this effect is not a feature only of gallium but also of titanium diffusion, if not a general feature of cationic diffusion in sapphire. Therefore, it is logical to assume that the feature seen in the diffusions of titanium and gallium has the same physical origin. In Figure 3.6 it can be seen that the depleted titanium region extends some microns into the bulk of sapphire and is not confined to the surface region. It was mentioned again in section 3.3.3 that this feature appears only in the titanium profiles where fast cooling was performed. The Ga-diffused samples analysed here were also fabricated using fast cooling, consequently, the effect of surface depletion of titanium and gallium ions is connected with the cooling process.

A more plausible explanation of this diffusion feature arises if it is assumed that the lattice of sapphire is severely distorted near the surface during diffusion. According to this hypothesis, during fast cooling a "recrystallisation" process is taking place; as the temperature is rapidly decreased, the concentration of defects in equilibrium is also decreased [34]. The gallium or titanium ions that are located in defect sites, near the surface, are "pushed" out of the bulk of sapphire as the lattice contracts. Oppositely in a slow cooling process the crystal is accommodating for the defect sites that are occupied with titanium or gallium ions. From Figure 3.6, comparing the SIMS data curve to the titanium fluorescence curve can be deduced that a significant number of titanium ions are occupying defect and not lattice sites when slow cooling is used. This hypothesis of "recrystallisation" explains the feature and also the steep profiles encountered in Figure 3.10 and Figure 3.11.

The diffusion profiles of gallium can be fitted with Gaussian functions having a depth offset, which unfortunately complicates the comparison between the profiles. In the cases of the samples diffused at 1500°C and 1600°C, the concentration of Ga^{3+} ions in the sapphire after diffusion may be calculated using number of gallium ions supplied by the source and the depth profile, if it is assumed that the fraction of gallium atoms which do not diffuse into the sapphire is insignificant. The peak gallium ion concentrations are then estimated, in terms of their ratio to the Al ion density in pure sapphire, to be approximately 4.8% and 3.7%, for the 1500°C and 1600°C diffusions, respectively. This calculation is complicated in the case of the sample diffused at 1400°C, because there is a thin source residue at the surface, so it cannot be assumed that all the gallium ions have entered the sapphire. Furthermore the diffusion depth is very similar to the original source film thickness, so that the material in the gallium-

doped region has a composition different to sapphire, which may change the SIMS etch rates. Omitting the region containing the residue of the thin source film, the maximum Ga:Al ion ratio for the sample diffused at 1400°C may be crudely estimated to be 50%.

Figure 3.9, Figure 3.10 and Figure 3.11 give the SIMS data for the 1400,1500 and 1600^{0}C samples fitted with Gaussian functions. As described, it is assumed that the first part of the data represents a “violent” evaporation of the diffusion source occurring during the cooling stage, a time period of approximately 1min.

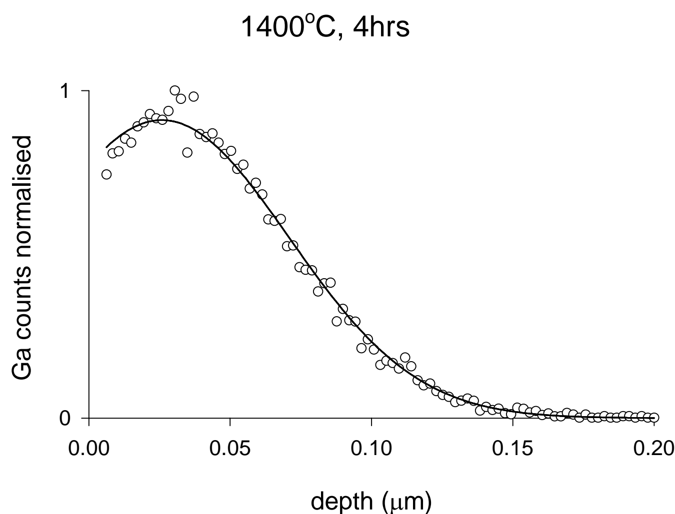

Figure 3.9 SIMS data for the 1400^{0}C, 4hrs sample with a gaussian fit for the diffusion profile.

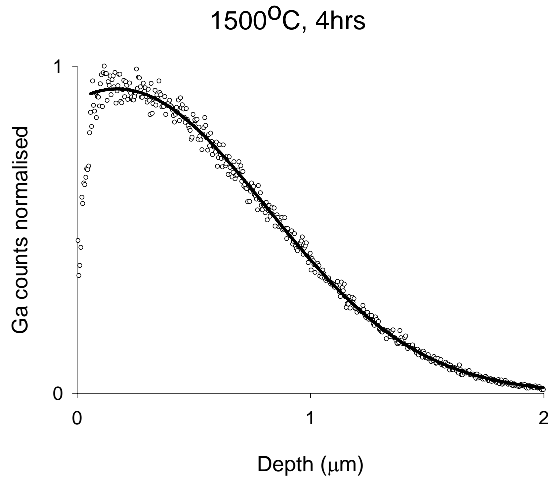

Figure 3.10. SIMS data for the 1500^{0}C, 4hrs sample with a gaussian fit for the diffusion profile.

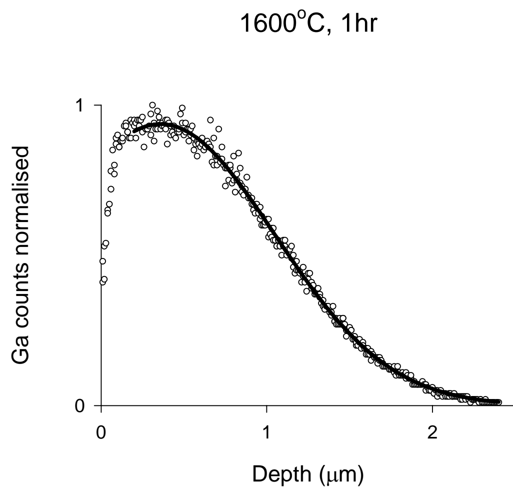

Figure 3.11. SIMS data for the 1600^{0}C, 1hr sample with a gaussian fit for the diffusion profile.

Table 3.2 gives the parameters of the Gaussian fits for the different samples and also the diffusion coefficients extracted from the diffusion depths. The results show that the diffusion coefficient of gallium ions in sapphire is approximately 3 orders of magnitude greater than the self-diffusion coefficient of Al^{3+} ions [13,22]. Ga^{3+} ions diffuse somewhat faster in the sapphire lattice than either Cr^{3+}or Y^{3+} ions, the difference in diffusion coefficients at 1500°C being approximately a factor of ten [23,26]. Cr^{3+} and other transition metal ions are reported to diffuse through aluminum

vacancies, whose concentration is related to the quality and the impurity content of the crystal, so that the diffusion coefficients obtained may differ from study to study [18,23,26]. All these ions have equal charge and different ionic radii. Although the size of the ion is expected to influence the rate of diffusion, it is generally accepted that the ionic size by itself cannot predict diffusion coefficients [26]. Conversely, the similarity of the diffusion coefficient of Ga^{3+} ions to those of Cr^{3+} and Y^{3+} ions may indicate that these ions diffuse through the same mechanism, although this may only be verified by further diffusion studies.

Temperature (^{0}C)	Time (hrs)	Diffusion depth (μm)	Centre of gaussian (μm)	Diffusion coeff. (m^2s^{-1})
1400	4	0.05±0.01	0.025±0.01	$(3.5\pm0.1)10^{-20}$
1500	4	0.65±0.05	0.17±0.01	$(7.2\pm0.1)10^{-18}$
1600	1	0.69±0.05	0.36±0.03	$(3.3\pm0.1)10^{-17}$

Table 3.2. Fabrication parameters of the characterized samples with the diffusion results.

3.5 Combined titanium and gallium diffusion in sapphire

3.5.1 Introduction

It will be shown in Chapters 4 and 6 that diffusion of gallium in sapphire can produce high quality passive waveguides and diffusion of titanium can provide a gain medium. The combined diffusion of the two cations may be an excellent way to fabricate active circuits in sapphire. The purpose of this section is to characterise if and how the two diffusion processes are interacting and affecting one another. The knowledge of the combined diffusion profiles is necessary for any future attempt to fabricate an active device that combines the two ions. This section reports the first investigation of

combined gallium and titanium diffusion in sapphire; quantitative results and informations about the mechanism of diffusion were obtained.

3.5.2 Fabrication of samples

The first fabrication step was the evaporation of thin films of titanium or gallium oxide using a standard thermal evaporator. The thickness of the gallium oxide films was approximately 150nm as this thickness gives optimum results for the fabrication of waveguides (Chapter 4). The thickness of the titanium films was approximately 10nm, this thickness was used because titanium has a low solid solubility in sapphire and if thicker films were used then the diffused samples would exhibit much surface residue (section 3.3.4). The annealing of all the samples was performed using the same furnace as that used for the diffusion of gallium. There is a specific point of incompatibility between the two diffusion processes. This is that in order to have gallium waveguide, oxygen atmosphere is necessary, conversely for the incorporation of titanium ions in the 3+ state (titanium sapphire crystal with a high figure of merit) a reducing atmosphere, namely argon, should be used. The temperature of the annealing was always 1600^{0}C, and the atmosphere was oxygen for gallium diffusion and argon for titanium diffusions. The time period was 16hrs for gallium annealing, and 1hrs for titanium, as according to previous measurements it was expected that the diffusion of titanium would be faster than the diffusion of gallium.

Four samples were fabricated and analysed using SIMS, and the fabrication parameters of each sample are described here. Sample 1 is the simple case of a titanium-diffused sample, where a thin film of titanium was evaporated and then the sample was annealed. This sample was fabricated to obtain as a reference for titanium diffusion; for gallium the reference is considered to be the diffusion coefficient that

was calculated in section 3.4.4. Sample 2 was prepared by evaporating a gallium oxide thin film followed by annealing (1600^0C, 16hrs, O_2), then a thin film of titanium is deposited and again the sample is annealed (1600^0C, 1hrs, Ar). Sample 3 is the reverse procedure for sample 2, where titanium diffusion is followed by gallium diffusion. Finally sample 4 is simultaneous titanium and gallium diffusion, a titanium film and then gallium oxide film is deposited and the sample is then annealed; an oxygen atmosphere was chosen in this case. In the following table, table 3.3, a summary of the fabrication parameters for the 4 samples is included for quick reference.

Sample #	Film	Diffusion conditions	Description
1	10nm Ti	Ti diffusion @ 1600^0C, 1hrs, Ar	Ti diffusion
2	150nm Ga_2O_3 10nm Ti	Ga diffusion @ 1600^0C, 16hrs, O_2 Ti diffusion @ 1600^0C, 1hrs, Ar	Ga diffusion followed by Ti diffusion
3	10nm Ti 150nm Ga_2O_3	Ti diffusion @ 1600^0C, 1hrs, Ar Ga diffusion @ 1600^0C, 16hrs, O_2	Ti diffusion followed by Ga diffusion
4	10nm Ti 150nm Ga_2O_3	Ti and Ga diffused together @ 1600^0C, 16hrs, Ar	Ti/Ga combined diffusion

Table 3.2 Fabrication parameters for the combined Ga/Ti diffusions.

3.5.3 Preparation of samples for analysis by bevelling.

The samples were expected to have diffusion profiles depths in the order of 10μm. Sapphire is a hard material that is etched slowly; according to measurements during the gallium diffusion characterisation, the SIMS equipment used would need approximately 45min to etch one micron of sapphire. This means that a profile of 10μm would be analysed in 7hrs. The analysis would be expensive and time-

consuming, furthermore over a period of 7hrs is difficult to maintain stable operation and constant etching rate. It is apparent that an indirect approach should be used for the analysis of the diffusion profiles. A simple, if time consuming method, is to polish the surface of the samples to a bevel. This means that a horizontal profile could be translated to a depth profile if the angle of the bevel is known. In Figure 3.12 a sapphire sample with a bevel is sketched to help in the understanding of the scheme. The horizontal resolution of the SIMS technique is about 50μm, the maximum expected depth profile, 40μm, and the required depth resolution 0.5μm. Taking into account these parameters, the required bevel angle was calculated to be 0.5 degrees.

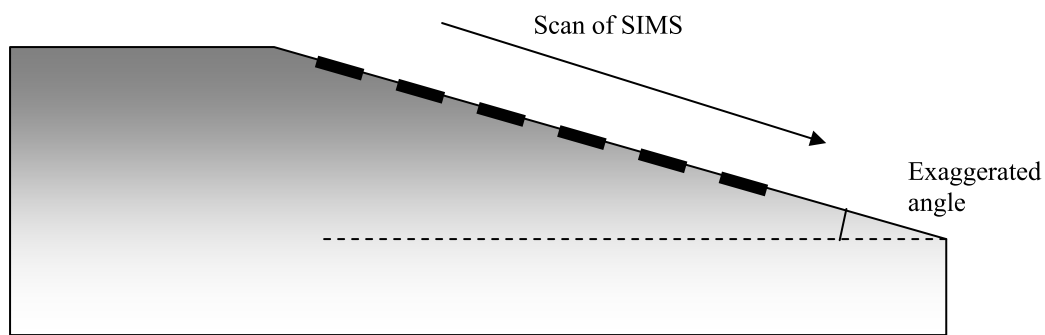

Figure 3.12. Sketch of a bevelled diffused sample with the craters that form the scan of SIMS.

An autocollimator was used with the appropriate polishing holder to define the bevel angle. The polishing process will not make a sharp angle but a curved region at the point that the bevel starts. This effect was reduced by depositing 8μm of a Ta_2O_5 film on top of the samples using sputtering. Ta_2O_5 as the buffer material was selected because it is mechanically hard, and good quality films were easy to be deposited.

3.5.4 Diffusion profiles of gallium and titanium diffused samples

The analysis of the samples was performed at Loughborough Surface Analysis ltd. The parameters used for the SIMS analysis are very similar to those described in section 3.4.3.

In order to have good precision in the conversion from horizontal to depth scale, interference microscopy was used. The basic principle of an interference microscope is that by interfering an incident laser wave with the reflected wave from the surface of the sample, on top of a normal microscope image, interference fringes are observed. Each fringe in the specific microscope translates to 273nm difference in depth. As an example images from the interference microscope used for sample 1 is depicted in Figure 3.13.

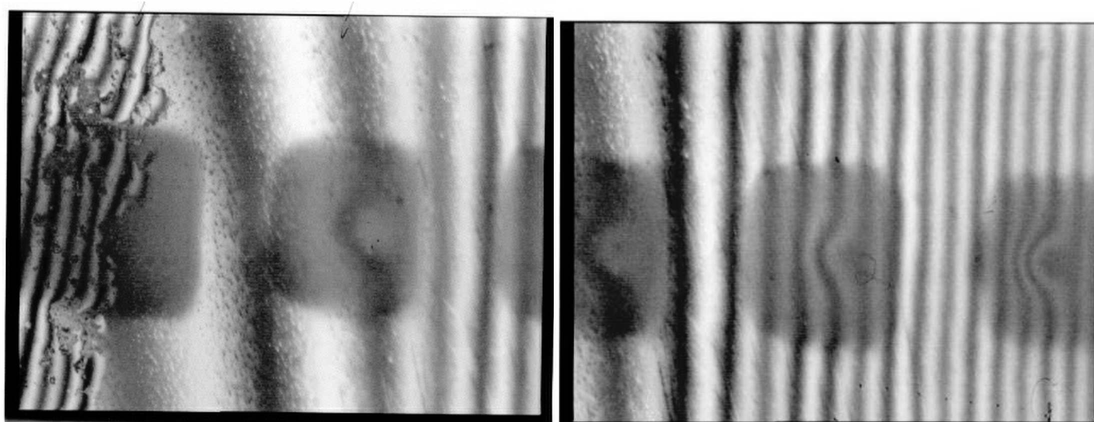

Figure 3.13. Interference microscopy pictures of the bevelled samples. The first picture is near the beginning of the bevel and shows the tantalum pentoxide film, also from the fringes the curvature of the sample can be seen.

i) Sample 1, Ti diffusion

The ratio of titanium to aluminium counts for the simple Ti diffusion (sample 1) is shown against depth in Figure 3.14. Generally in all the data for titanium ions, the

case of an infinite source is assumed because of the low solid solubility of titanium in sapphire. Therefore the functions fitted to the titanium diffusion profiles are complementary error functions (section 3.2.6). In all these graphs the first point or points give very high titanium concentrations that are caused by surface residue, which supports the assumption of the undepleted source. Nevertheless these points are omitted in the figures, because they do not offer significant extra information and they distort the results of the curve fitting. Conversely to titanium diffusion the fit for gallium profiles is always a Gaussian function; because gallium has an “infinite” solid solubility in sapphire the gallium source is assumed to be instantaneously exhausted. The assumption is again supported by the observation that no evidence of any gallium surface residue was found on the samples. The curve fitting was performed using the curve-fitting tool in Matlab.

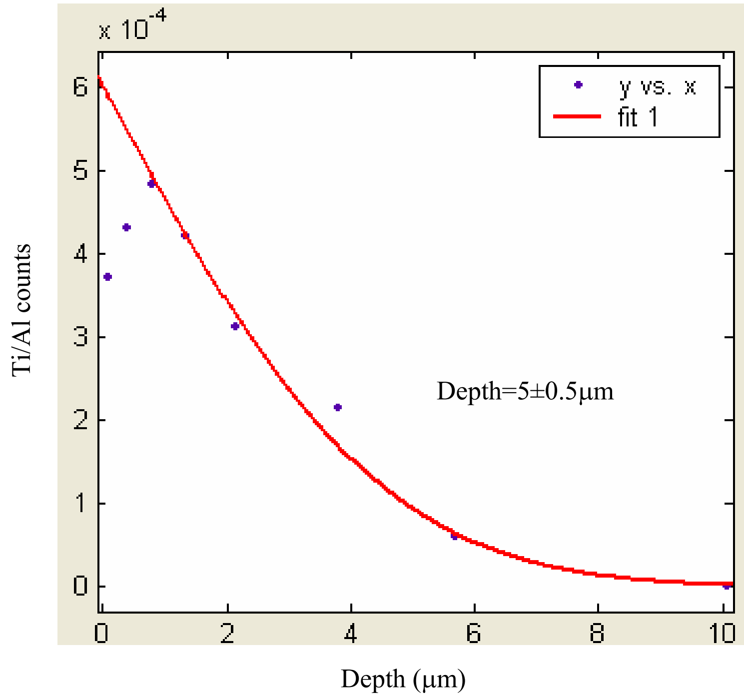

Figure 3.14. Ratio of titanium to aluminium counts versus depth

The depth of the fitted erfc function for sample 1 is 5μm yielding a diffusion coefficient for titanium at 1600^0C of (1.74±0.5) x 10^{-15} m^2s^{-1}. The value is close to the value found by Louise Hickey for diffusion of titanium (3±1) x 10^{-15} m^2s^{-1} (section 3.3.3) [9], this is an indication that the depth scale conversion used is correct and also indicates similar defect content of the sapphire crystals. Therefore the diffusion coefficient and depth values obtained for sample 1 will be used as reference for titanium diffusion in the analysis of the following samples. It is important to note that in this characterisation it was decided that all the fits (titanium and gallium) will be Gaussian or erfc functions centred at zero, even in the cases that an offset is apparent from the raw data. In the case of gallium diffusion characterisation, Gaussian functions with an offset were fitted, this was because an explanation of the mechanism of gallium diffusion was attempted. In the present case the main purpose is to explore the interaction of the cation diffusions and using fits without an offset

makes the comparison of the diffusion profiles easier by reducing the number of parameters. The reference values for gallium for 1600^0C and 1hour annealing, presented in the previous sections, should be recalculated assuming a gaussian fit centred at zero. Therefore using the same diffusion data as in section 3.4.4 a gaussian function is fitted, the diffusion depth was now found to be 1.17μm and the diffusion coefficient 9.5×10^{-17} m^2s^{-1}, and these values will be used as a reference data for gallium diffusion. The fit is depicted in Figure 3.15 and the physical meaning in selecting such a fit is to assume that the evaporated region near the surface is just a part missing from a normal Gaussian diffusion profile.

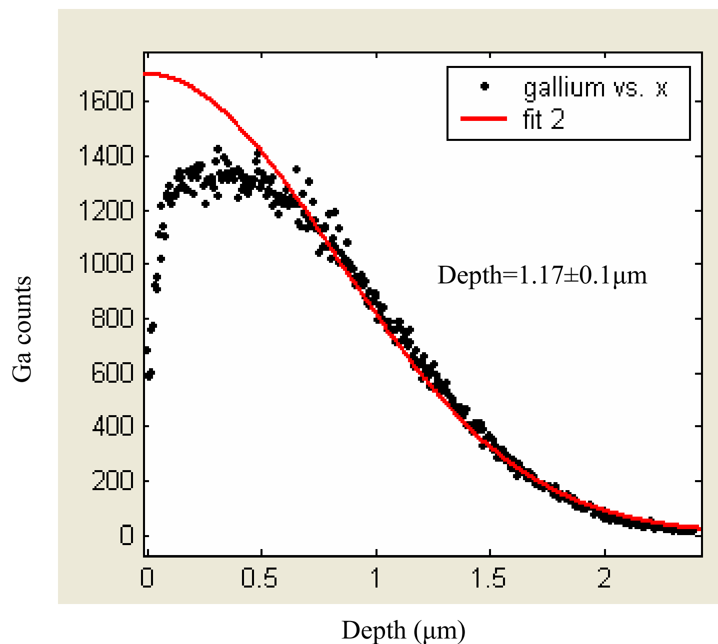

Figure 3.15. Reference Ga diffusion sample presented in section 3.4.4 with Gaussian fit.

ii) Sample 2, Ga diffusion followed by Ti diffusion

The fabrication procedure for sample 2 is gallium diffusion followed by titanium diffusion. The ratio of gallium to aluminium counts against depth is shown in Figure 3.16. The Gaussian fit also shown in the figure gives a diffusion depth of 5±0.5μm.

The total gallium diffusion time is 17hrs, therefore the expected depth is $1.17 \times \sqrt{17} = 4.81\,\mu m$, which is close enough to 5μm to safely assume that gallium diffusion was not affected by the titanium diffusion that followed.

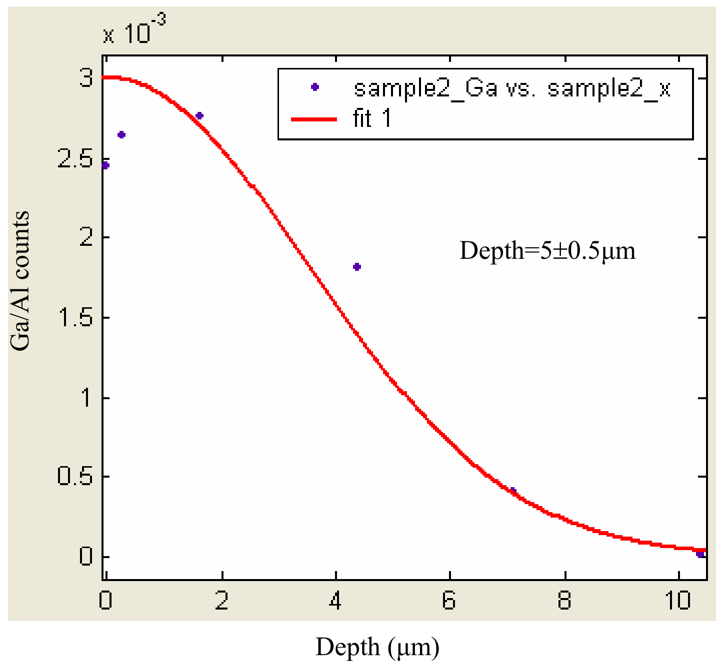

Figure 3.16. Ratio of gallium to aluminium counts for sample 2.

Figure 3.17 shows the diffusion profile of titanium in sample 2 along with an erfc function fit. The calculated depth of the diffusion is 8.6±0.8μm; the diffusion time for titanium was 1 hour and, according to the reference value, the expected depth would be 5±0.5μm if the gallium pre-diffusion did not affect the Ti diffusion. However, the diffusion depth is 1.7±0.1 times higher than that expected. This value, the ratio of the observed to the projected diffusion depth is named the “acceleration factor”. The difference is significant and leads to the assumption that the prediffusion of gallium accelerates the titanium ions diffusion in the sapphire crystal. A proposed explanation

is that gallium diffusion is increasing the concentration of defects in the crystal giving titanium ions increased mobility.

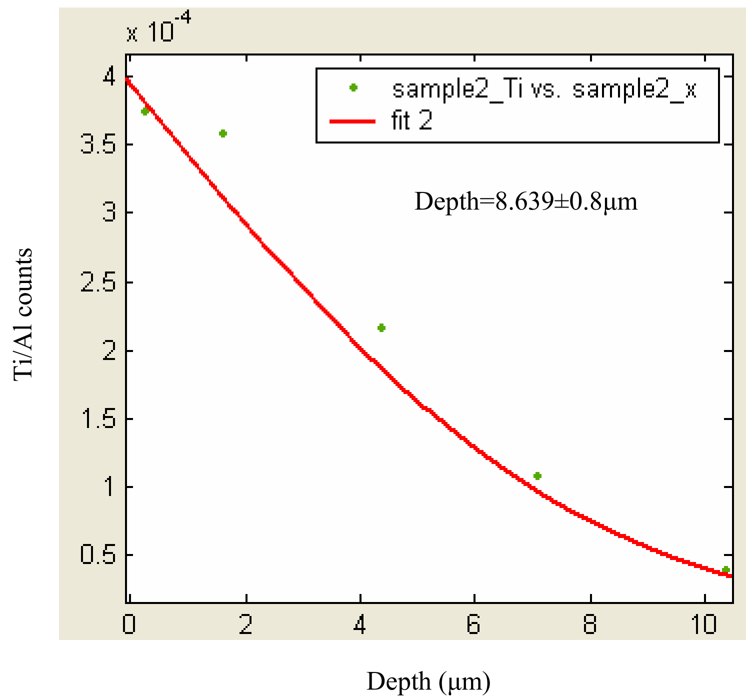

Figure 3.17. Ratio of titanium over aluminium counts versus depth, for sample 2.

iii) Sample 3, Ti diffusion followed by Ga diffusion

The next characterised sample is sample 3 which was fabricated with diffusion of titanium for 1 hour followed by gallium diffusion for 16hrs. Respecting the sequence of fabrication the titanium profile is presented first in Figure 3.18 with an erfc fit.

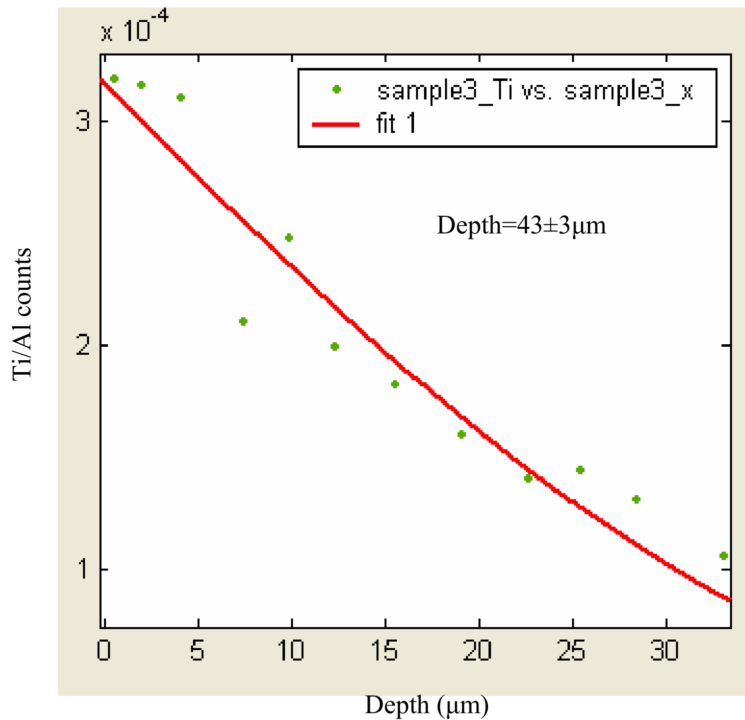

Figure 3.18. Ratio of titanium to aluminium counts versus depth for sample 3.

The expected depth for this sample since the total period of titanium diffusion is 17hrs is 20±2μm. The depth of the fitted function is 43±3μm, meaning that it is 2.1±0.1 times higher than the reference value. It is clear that titanium diffusion is significantly enhanced and it should be noted that the acceleration factor of 2.1 is similar to that found in sample 2 for Ga prediffusion.

The gallium profile for sample 3 is depicted in Figure 3.19 with a Gaussian fit. The expected depth for gallium for 16hrs of diffusion is 4.7±0.4 μm and here the observed difference is very significant as the Gaussian fit gives a depth of 18±2 μm that gives an acceleration factor of 3.9±0.3. It is proposed that the prediffusion of titanium is distorting significantly the crystal of sapphire giving a very high concentration of

defects. The diffusion coefficient of gallium using this diffusion depth is 1.5 x 10^{-15} m^2s^{-1}, which is two orders of magnitude higher than the reference.

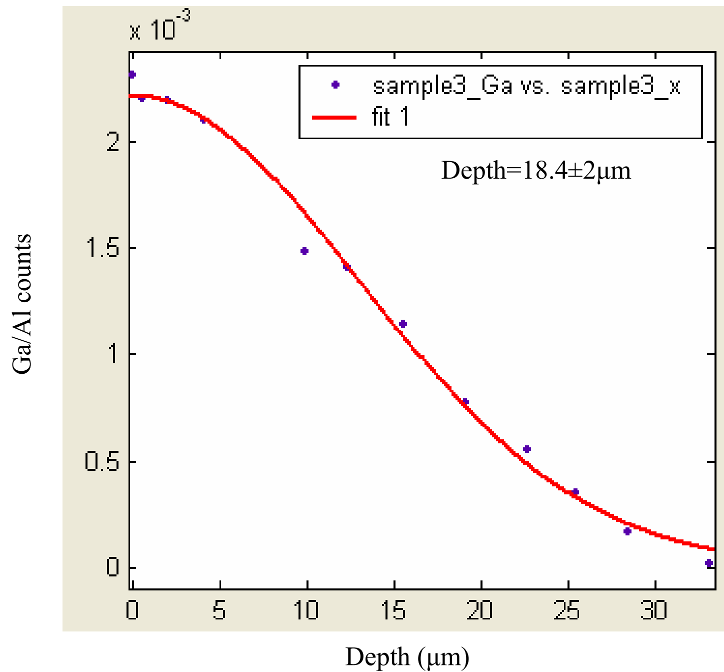

Figure 3.19. Ratio of gallium to aluminium counts versus depth for sample 3.

iv) Sample 4, Ga/Ti diffusion

Finally sample 4 is presented in which the two species are diffused together. Figure 3.20 shows the profile of titanium is depicted, the depth of the fit is 34±3μm; this means that the acceleration factor is 1.66±0.1. In Figure 3.21 the profile of gallium is depicted, the gaussian fit gives a diffusion depth of 15±2μm, which corresponds to an acceleration factor of 3.2±0.3.

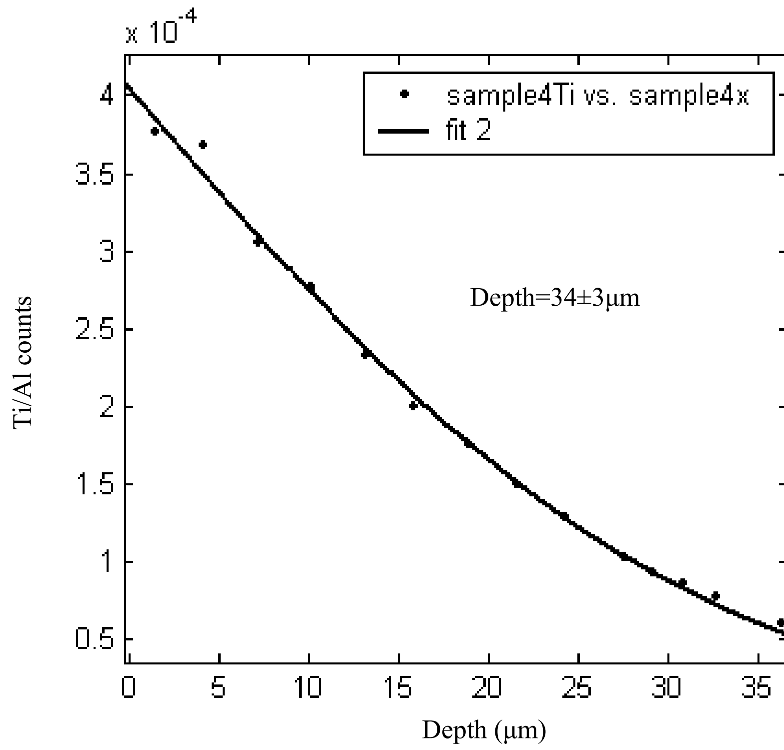

Figure 3.20. Ratio of titanium to aluminium counts versus depth for sample 4.

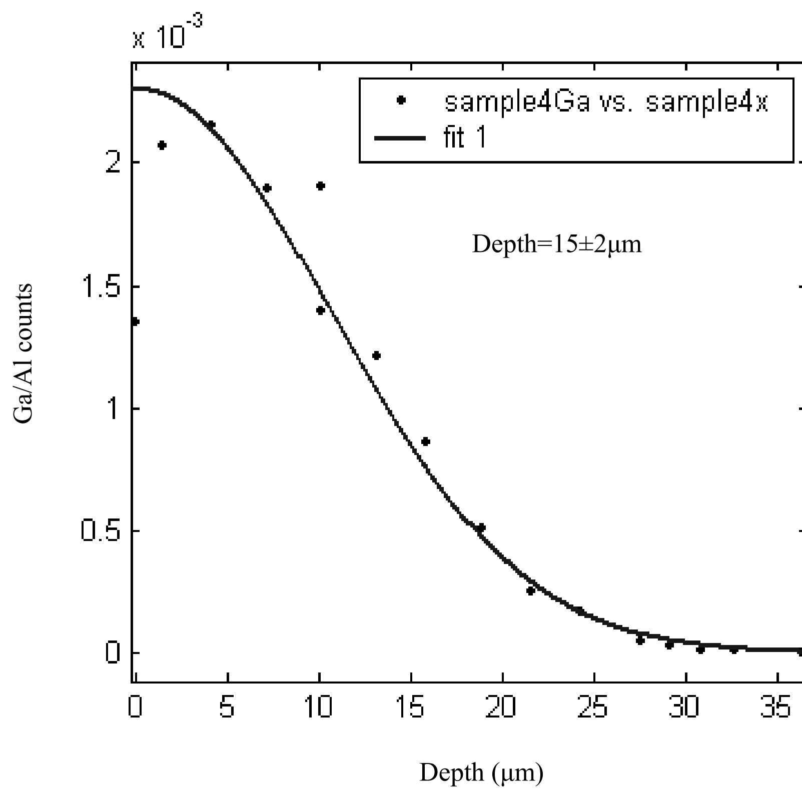

Figure 3.21. Ratio of gallium to aluminium counts versus depth for sample 4.

v) Overview of results for Ga/Ti diffusion

In table 3.3 all the results for the 4 samples and the gallium reference sample (sample 0) are summarised, in order to facilitate comparisons. From the diffusion coefficients given in the table it can be deduced that both species are accelerated. It is proposed that titanium diffusion increases significantly the defect concentration in the sapphire lattice. This can be seen by the diffusion coefficients of gallium; if titanium is previously diffused, the diffusion coefficient of gallium is increased by one or two orders of magnitude and is close to the diffusion coefficient of titanium. The acceleration factors in this case are approximately 3.5. On the other hand gallium pre-diffusion also enhances the diffusion of titanium having acceleration factors of approximately 2. The only diffusion sequence in which gallium and titanium are relatively unaffected is that in sample 2 in which gallium is followed by titanium diffusion. This is because the 16hrs Ga diffusion is followed by the shorter period, 1hrs, Ti diffusion. Ti diffusion is affected, with an acceleration factor of 1.7, but Ga diffusion is not significantly affected as the time period of 1hr in a total of 17hrs is sufficiently small.

Sample #	0	1	2	3	4
Description (diffusion sequence)	Ga reference	Ti diffusion	Ga followed by Ti	Ti followed by Ga	Ti/Ga combined
Ga depth (μm)	1.17		5	18.4	15
Ti depth (μm)		5	8.64	43	34.3
Ga acceleration factor			1	3.9	3.2
Ti acceleration factor			1.7	2.1	1.6
Ga diffusion coefficient (m^2s^{-1})	9.5×10^{-17}		1.02×10^{-16}	1.5×10^{-15}	9.77×10^{-16}
Ti diffusion coefficient (m^2s^{-1})		1.74×10^{-15}	5.2×10^{-15}	7.55×10^{-15}	5.11×10^{-15}

Table 3.3. Summary of the results for combined titanium and gallium diffusion.

3.6 Conclusions

The scope of this thesis is to use gallium and titanium ionic diffusion as the main fabrication processes for implementation of novel waveguide structures in sapphire. Titanium ionic diffusion creates an active region in sapphire that can be used for the fabrication of a laser and it will be seen in Chapter 4 that gallium diffusion is a successful fabrication technique for passive waveguides.

This chapter starts with an overview of the classical theory of diffusion. A review of cationic diffusion is presented, and results of titanium diffusion in sapphire from previous work carried out at Southampton University are included. Gallium diffusion results obtained are presented, to the best of our knowledge, for the first time for this range of temperatures. The diffusion coefficients obtained for the diffusion of gallium into sapphire indicate that sapphire substrates can be readily doped with gallium to diffusion depths in the order of microns. The procedure gives good quality samples with minimum roughness and considering also the high solid solubility of Ga into sapphire Ga diffusion is a promising procedure for the fabrication of waveguides. An interesting feature of diffusion in sapphire is revealed, the surface region of the substrates is depleted from doping ions, and an explanation is given based on the assumption of "recrystallisation" of sapphire's lattice during fast cooling.

It was not possible during the experiments to obtain data about the absolute concentration of Ga in sapphire from the SIMS measurements because it is very difficult to fabricate a sample with known concentration of gallium, nevertheless the high solid solubility of Ga was confirmed and concentration levels up to 50% were estimated. This diffusion study was performed in order to determine whether gallium is a suitable ion for doping sapphire by diffusion and this goal was met, giving a significant insight into the diffusion process itself.

Ionic diffusion in sapphire was further explored by the study of the combined diffusion of titanium and gallium. It is shown that gallium and titanium diffusions strongly affect each other, and there are indications that titanium diffusion in

particular creates a high concentration of defects in sapphire's crystal lattice. The results of the experiments are presented and the quantitative results are useful for any future research on combining active regions of sapphire with passive gallium waveguides.

References to Chapter 3

1. V.Apostolopoulos, L.M.B.Hickey, D.A.Sager, and J.S.Wilkinson. "Gallium diffused ridge waveguides in Sapphire". CLEO Long Beach, California. 2002.

2. V. Apostolopoulos, L. M. B. Hickey, D. A. Sager, and J. S. Wilkinson, "Gallium-diffused waveguides in sapphire," *Optics Letters* **26,** 1586-1588 (2001).

3. Louise M.B.Hickey. PhD thesis. "Ti:Sapphire waveguide laser by the thermal diffusion of Ti into sapphire", (Optoelectronics Research Centre, University of Southampton 1998).

4. D. A. Sager, V. Apostolopoulos, and J. S. Wilkinson, "Diffusion of neodymium into sputtered films of tantalum pentoxide," *Journal of the American Ceramic Society* **85,** 2581-2583 (2002).

5. V.Apostolopoulos. Mini-thesis. "Gallium diffused waveguides in Sapphire", (Electronics and Computer Science, University of Southampton, 2000).

6. Crank J, *Mathematics of diffusion* (Oxford University press, 2003).

7. Glicksman ME, *Diffusion in solids* (Wiley Interscience, 2000).

8. Richard J.Borg and G.J.Dienes, *An introduction to solid state diffusion* (Academic Press, 1988).

9. Louise MB Hickey. "Report on Activities in Southampton during the 1851 fellowship award". 1999.

10. BARON JEAN BAPTISTE JOSEPH FOURIER, *"Theorie Analytique de la Chaleur"* (French science academy, 1822).

11. Adolf Fick. *"Über Diffusion". Ann.Physik* , p.59. (1855).

12. Dr.Ron Fleming. "Secondary Ion Mass Spectrometry Theory Tutorial", http://www.cea.com/cai/simstheo/caistheo.htm, Charles Evans & Associates (2000).
13. Palandino A E et al. "Aluminum ion diffusion in aluminum oxide". *Journal of Chemical Physics*. **37**, 957. (1962).

14. Lloyd K I et al. "Iron tracer diffusion in aluminum oxide". *J.Am.Ceram.Soc* **64**, 744. (1981).

15. Lesage B et al. "Transport phenomena in undoped and chromium or yttrium doped-alumina". *Radiation effects* **75**, 283. (1983).

16. Stubican VS et al. "Grain-boundary and lattice diffusion of ^{51}Cr in alumina and spinel". *Advances in Ceramics* **10**, 406. (1984).

17. V. S. Stubican, G. Huzinec, and D. Damjanovic, "Diffusion of Cr-51 in Surface-Layers of Magnesia, Alumina, and Spinel," *Journal of the American Ceramic Society* **68,** 181-184 (1985).

18. L. Badrour, E. G. Moya, J. Bernardini, and F. Moya, "Bulk Diffusion of Ag-110 Tracer in Al_2O_3," *Scripta Metallurgica* **20,** 1217-1222 (1986).

19. L. Badrour, E. G. Moya, J. Bernardini, and F. Moya, "Fast Diffusion of Silver in Single and Polycrystals of Alpha- Alumina," *Journal of Physics and Chemistry of Solids* **50,** 551-561 (1989).

20. F. Moya, E. G. Moya, D. Juve, D. Treheux, C. Grattepain, and M. Aucouturier, "Sims Study of Copper Diffusion Into Bulk Alumina", *Scripta Metallurgica et Materialia* **28,** 343-348 (1993).

21. E. P. Macey and V. S. Stubican, "Diffusion of Co-57 in Surface-Layers of Nickel-Oxide and Alumina," *Journal of the American Ceramic Society* **76,** 557-559 (1993).

22. Legall M et al., "Self-Diffusion in a-Al_2O_3 I. Aluminum diffusion in single crystals", *Phil Mag A* **70**, 761. (1994).

23. E. G. Moya, F. Moya, A. Sami, D. Juve, D. Treheux, and C. Gratttepain, "Diffusion of Chromium in Alumina Single-Crystals" *Philosophical Magazine A-Physics of Condensed Matter Structure Defects and Mechanical Properties* **72,** 861-870 (1995).

24. E. G. Moya, F. Moya, D. Juve, and C. Grattepain, "Impurity diffusion in single crystal aluminium oxide" *Defect and Diffusion Forum* **143,** 1207-1212 (1997).

25. Fung S et al. "Gallium/aluminum interdiffusion between n-GaN and sapphire". *Journal of applied physics* **84**, 2355. (1998).

26. E. G. Moya, F. Moya, B. Lesage, M. K. Loudjani, and C. Grattepain, "Yttrium diffusion in alpha-alumina single crystal," *Journal of the European ceramic society* **18,** 591-594 (1998).

27. E. G. Gontier-Moya, G. Erdelyi, F. Moya, and K. Freitag, "Solubility and diffusion of cobalt in alumina," *Philosophical Magazine A-Physics of Condensed Matter Structure Defects and Mechanical Properties* **81,** 2665-2673 (2001).

28. E. G. Gontier-Moya, J. Bernardini, and F. Moya, "Silver and platinum diffusion in alumina single crystals," *Acta Materialia* **49,** 637-644 (2001).

29. Levin E, "Phase diagrams for ceramists" (Am. Ceram. Soc, 1964).

30. L. M. B. Hickey and J. S. Wilkinson, "Titanium diffused waveguides in sapphire," *Electronics Letters* **32,** 2238-2239 (1996).

31. V. S. Stubican, "Diffusion of Isotopes in Surface-Layers of Some Oxides," *Philosophical Magazine A-Physics of Condensed Matter Structure Defects and Mechanical Properties* **68,** 809-818 (1993).

32. V. S. Stubican, "Grain-Boundary Diffusion in Oxides," *Journal of the Electrochemical Society* **132,** C364 (1985).

33. Richard Syms and John Cozens, *Optical guided waves and devices* (McGraw Hill, 1992).

34. Charles Kittel, *Introduction to solid state physics* (7th ed. Wiley, 1996).

CHAPTER 4

GALLIUM DIFFUSED WAVEGUIDES IN SAPPHIRE

4.1 Introduction

The gallium ion was selected among other ions such as chromium and yttrium as the most promising candidate for the fabrication of passive waveguides in sapphire. Gallium was expected to have high solid solubility, as shown by the diffusion study presented in Chapter 3 and also by other work [1,2]. This corresponds to a wide selection range of dopant concentration and is also expected to result in low surface roughness. Furthermore, the gallium ion has higher electronic polarizability than the aluminium ion [3], this is an indication that Ga-doping would increase the refractive index of sapphire. Finally, Ga^{3+} has the same valence state as the Ti^{3+} ion; therefore, in the case of co-diffusion, it is not expected to increase the concentration of the Ti^{4+} ion which adversely affects the performance of a Ti:Sapphire laser. In the previous chapter the diffusion of gallium into sapphire was characterized and presented. The results show that annealing at 1600^{0}C creates diffusion profiles with a depth of some microns in reasonable diffusion periods. Gallium diffused waveguides in sapphire were realised for the first time during the course of this work and detailed characteristics are given in this chapter [4,5].

The chapter begins with the description of the waveguide fabrication, following this, the experimental optical characterisation process is described and the results of the experiments are given. The guided modal intensity profiles of slab gallium sapphire

waveguides were obtained at different wavelengths and for different fabrication parameters. The optimization of the waveguides was performed, based on the minimization of the modal waists. Channel waveguides were also fabricated using a patterned diffusion source and modal intensity profiles are given. Simulation results are included, based upon the slab waveguide model, the WKB method and commercial BPM packages. The experimental and modelling results are compared to obtain the peak index change that Ga diffusion creates in sapphire.

4.2 Waveguide fabrication

4.2.1 Fabrication of slab waveguides

The fabrication of the samples is similar to the fabrication procedure described in section 3.4.2. The samples were cut from c-cut sapphire wafers and had dimensions of $1x1cm^2$. For the fabrication of slab waveguides a thin film of gallium oxide was evaporated on the polished surface of the substrates followed by a thermal diffusion; the diffusion was carried out at 1600^0C for times of 6 to 16hrs. The annealings were performed in oxygen atmosphere, in contrast to the samples used for the diffusion characterization, which were diffused in an argon atmosphere. Studies of argon-diffused samples showed no evidence of waveguiding at a wavelength of 633nm. Therefore, oxygen atmosphere during annealing is necessary for the fabrication of gallium waveguides; lack of oxygen during diffusion could create an oxygen deficient layer of sapphire and therefore a localised refractive index decrease. Nevertheless, further studies should be performed comparing the composition of samples that are diffused in oxidizing and reducing atmospheres to reveal the origin of this effect. If The necessity of oxygen atmosphere during gallium diffusion is contrary to the need

for the titanium diffusion to be performed in an argon atmosphere in order to successfully create an active region.

The only variables in the fabrication were the diffusion time and the gallium oxide thickness. The temperature was always fixed at 1600^0C, which is close to the highest temperature that most furnaces can safely achieve when an oxygen atmosphere is used. The first set of samples to be fabricated were slab waveguide samples with the same gallium oxide source thickness (60nm) diffused for different times (6-16hrs). The second set of slab samples were all diffused for the same time (16hrs) and the variable was the thickness of the gallium oxide deposited on the samples (60-200nm).

4.2.2 Fabrication of channel waveguides

The third set of samples to be fabricated was designed to realize channel waveguides, so that each sample had stripes of different widths (2 to 11μm mask openings) and also a slab region. Photolithography with a light-field mask was used, using lift-off as described below:

- The surface of the sample was coated with a layer of positive photoresist (S1813, Shipley) and then the sample was baked at 90^0C for 30min.
- The sample was exposed to UV light with the mask being in contact with the sample.
- The sample was soaked in chlorobenzene to harden the photoresist surface.
- The sample was developed for 1min and rinsed in deionised water.

This procedure leaves a layer of patterned photoresist on the surface of sapphire. The next step was to evaporate the coating of gallium oxide on the surface of the sample. The photoresist was subsequently removed by rinsing the sample with acetone thereby washing away any diffusion source that is not in direct contact with the

surface of sapphire (lift-off). After the lift-off procedure the sample is ready for diffusion.

4.2.3 Overview of fabrication parameters

Based on the SIMS data that are described in the previous chapter the characteristics of gallium diffusion at 1600^0C are known and the diffusion depths of the samples can be estimated. While this approximation is reasonable, there are a number of parameters which insert a considerable error that is not yet quantified. The first difference in the parameters is that for waveguide fabrication an oxygen atmosphere is used instead of argon. Another difference is that the SIMS results refer to samples with gallium oxide thickness fixed at 50nm while here the thickness varies from 60 to 200nm. Diffusion coefficients can be dependent on concentration and this may insert another error that cannot be theoretically approximated. According to the results of the study of Ti and Ga co-diffusion (section 3.5.4, sample 2) it can be assumed that the atmosphere and the concentration do not strongly affect the diffusion coefficients. In section 3.4.4 a diffusion depth of 0.7μm is calculated for a sample diffused at 1600^0C for 1hr. The classical theory of diffusion (section 3.2) states that the diffusion depth has square root dependence with time and using this relation the diffusion depth of the samples is approximated. The offset of the Gaussian fit was 0.35μm and although it increases with time or temperature the exact dependence is not known thus inserting an error in the estimation of the diffusion profiles.

Table 4.1 shows the fabrication data, for the complete set of samples fabricated; a number is assigned to each sample for easy reference. The temperature is omitted as it is always 1600^0C. The predicted diffusion depth, also included in the table, has been

calculated and an error for the calculations is estimated taking into account uncertainties in the parameters.

Sample #	Time (hrs)	Thickness (nm)	Depth (μm)	Remarks
1	6	60±5	1.72±0.3	Planar samples
2	9	60±5	2.1±0.3	
3	10	60±5	2.2±0.3	
4	16	60±5	2.8±0.3	
5	16	60±5	2.8±0.3	
6	16	90±5	2.8±0.3	
7	16	130±7	2.8±0.3	
8	16	200±10	2.8±0.3	4 identical channel samples with a planar part

Table 4.1. Fabrication parameters of the gallium diffused waveguide samples.

4.3 Characterisation of Ga:Sapphire waveguides

4.3.1 Introduction

The characterization of gallium:sapphire waveguides was first performed using the slab samples; mode intensity profiles were obtained for different wavelengths and for different fabrication parameters. The experiments were designed in order to reveal the optimum fabrication conditions for minimization of the mode dimensions. The purpose of the gallium waveguide fabrication apart from the direct interest that exists in the fabrication of novel waveguides is the future possibility to use them for implementation of complex active integrated circuits, which requires small modal spotsizes for low-loss bends and low threshold lasers.

First the modal intensities profiles for samples 1, 2, 3 and 4 were measured using a commercial Ti:Sapphire laser operating at wavelengths between 700 and 850nm and a silicon CCD camera for imaging. For these samples the only variable is the diffusion time (consequently diffusion depth and peak concentration), therefore this experiment relates mode dimensions to the depth of the diffusion, and index change. A Ti:Sapphire laser was used because it allows the determination of mode size versus wavelength.

The second experiment was based in the fabrication of samples with identical diffusion parameters but with increasing peak concentrations of gallium inside sapphire (samples 5, 6, 7 and 8). For these samples a He-Ne and an Ar:Ion laser were used in order to determine the dependence of the mode profile upon gallium concentration. Two lasers were used to complement the data with wavelength dependence information; the diffused channel waveguide mode profiles were also obtained using the same experimental configuration.

4.3.2 Experimental procedure for optical measurements

Following diffusion, the end-faces of the samples were polished. This makes it possible to launch light, directly with a microscope objective or a fiber, into the waveguides and image the distribution of light at the output end-face. The light coming out of the waveguide was imaged onto a silicon CCD camera using a microscope objective lens. The images were stored in a computer and were analysed with the commercial package Vision XL to obtain quantitative data for the mode profiles. The configuration of the experiment is depicted in Figure 4.1.

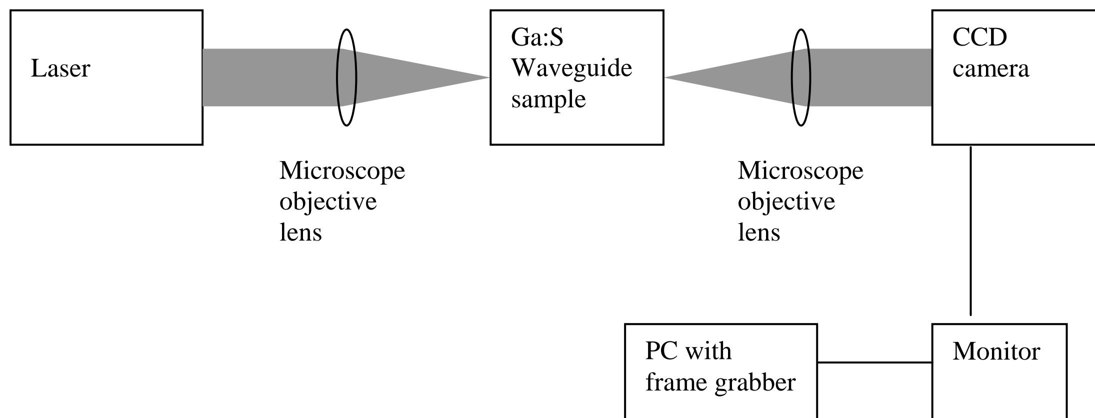

Figure 4.1. Experimental apparatus used for the mode profile characterisation of the gallium diffused waveguides.

4.3.3 Mode profiles of samples 1 to 4 between wavelengths of 700 and 850nm.

i) Experimental results

The Ti:Sapphire laser used was set up to operate in the range of 700 to 850nm, samples were tested with diffusion times from 6 to 16hrs and the same diffusion source thickness. In Figure 4.2 the mode profiles at 700 and 850 nm for sample 4 (16hrs) are shown. It is calculated for the numerical data obtained in the images that the size of the mode at 700nm is 4μm and at 850nm is 12μm. In all calculations the lateral size of the mode is defined by the 1/e value of the peak intensity and is referred to as mode size or mode waist. Figure 4.3 shows the modal intensity profiles for all the samples as they are calculated by the guiding images. Samples 3 and 4, in the range of wavelengths used, did not reach cutoff. Figure 4.4 gives the mode size of all the samples against wavelength.

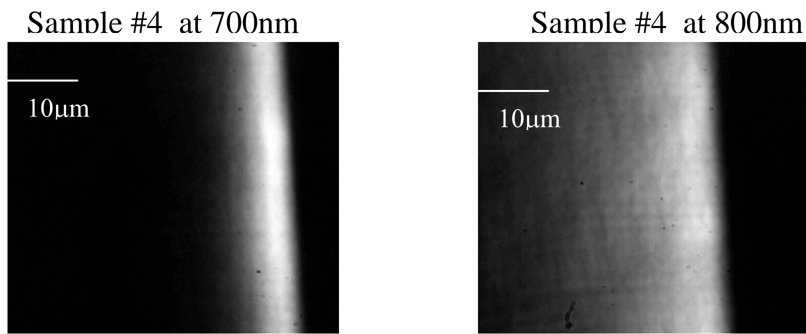

Figure 4.2. Images for the mode profiles of sample 4 at 700 and 850nm.

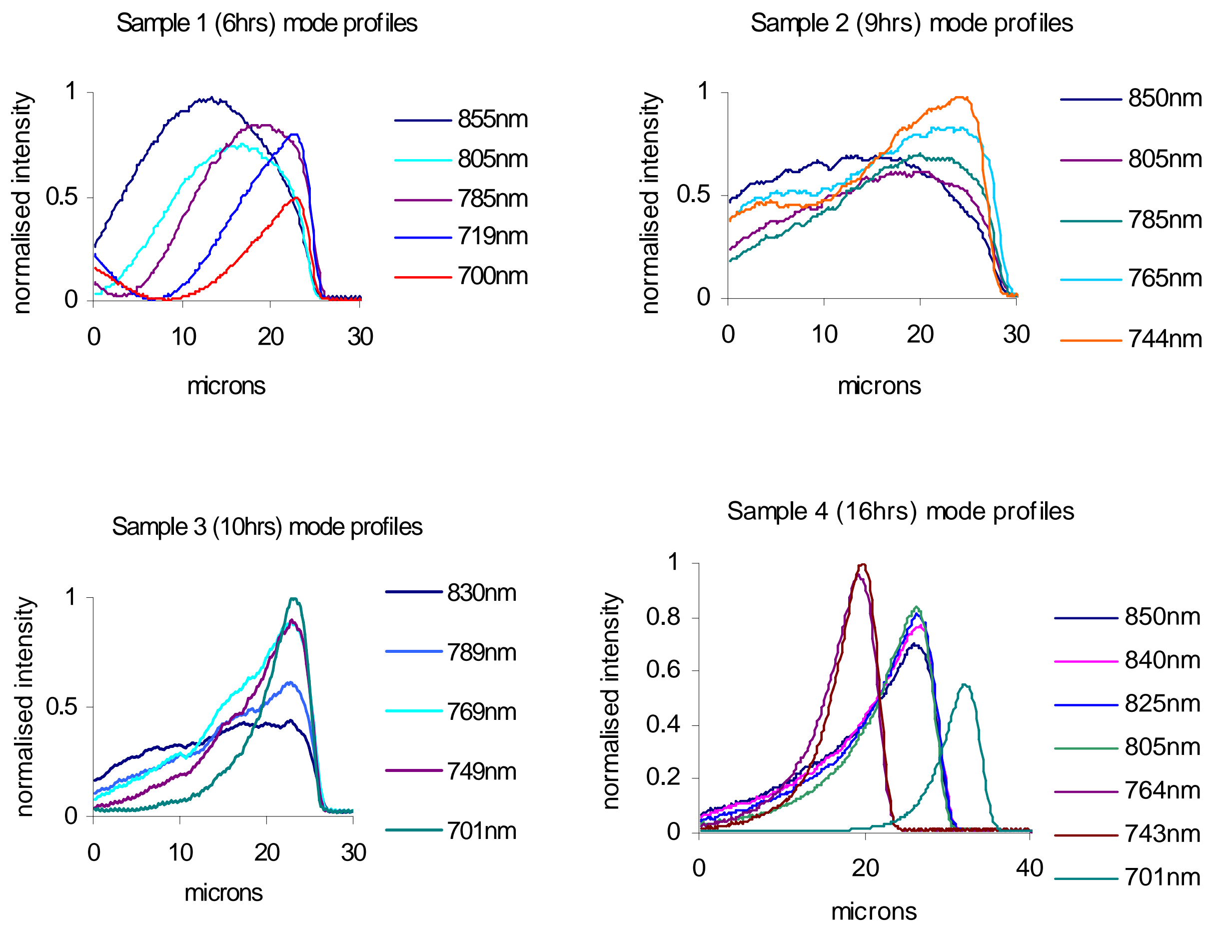

Figure 4.3. Modal intensity profiles for samples 1 to 4 between wavelengths of 700 and 850.

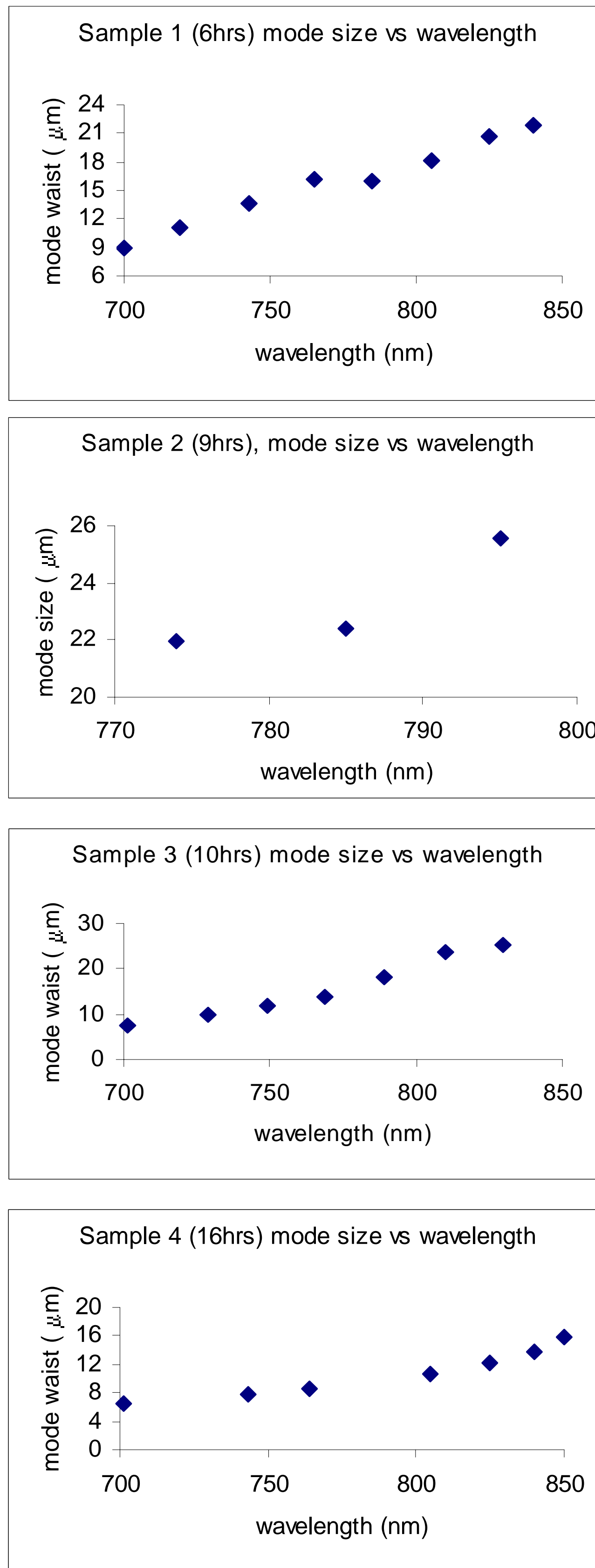

Figure 4.4. Wavelength dependence of the lateral mode size for samples 1 to 4.

A graph giving the asymmetry of the profiles versus wavelength is also shown in Figure 4.5. As a measure of asymmetry two mode half widths are calculated either side to the position of peak intensity of the profile. The ratio of the two widths is calculated so that as the ratio approaches unity the profile becomes symmetrical. Figure 4.5 shows the asymmetry ratio of the modes of sample 1 against wavelength, sample 1 is selected because it exhibited cutoff at this range of wavelengths. The graph of sample 1 is compared with the same graph for sample 3 which is selected because it is not close to cutoff.

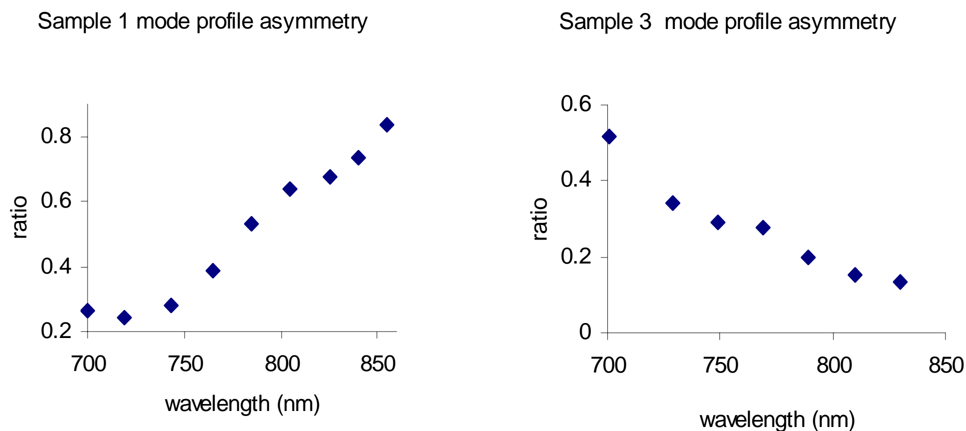

Figure 4.5. Mode profile asymmetry for samples 1 and 3.

ii) Discussion of results

It is expected that the index change due to the introduction of gallium into sapphire will be approximately proportional to the concentration of gallium into the sample. As the depth of diffusion is increasing in the samples, the peak concentration of gallium is decreasing. The cutoff wavelength of a waveguide increases with the diffusion

depth and with dopant concentration. In these samples these two parameters are driving the cutoff wavelength in opposite directions.

It is theoretically expected that the mode size of a waveguide increases with wavelength. This relation can be observed in Figure 4.3 and Figure 4.4. The experiment showed that samples with higher diffusion times and consequently larger diffusion depths have a better confined fundamental guided mode; this is clearly shown in Figure 4.3. Samples 1 and 2 exhibited cutoff in the range of wavelengths used in contrast to samples 3 and 4. Sample 1 exhibited cutoff near 780nm and in Figure 4.3 it can be seen that the shape of the mode profiles is changing rapidly near this wavelength. It can also be observed in this figure that the profiles become more symmetrical as they approach cutoff. Comparing the two graphs in Figure 4.5 that refer to the same range of wavelengths for sample 1 and sample 3 it can be deduced that the mode asymmetry gives an indication that the sample is near to the cutoff wavelength. The shape of the mode profiles gives an important indication that a sample is approaching cutoff, nevertheless an accurate rule based on the asymmetry ratio could not be deduced.

This experiment investigates the dependence of modal intensity profiles with diffusion depth, index change and wavelength. The results qualitatively were as theoretically expected and quantitative data for the mode size and for the cutoff wavelength for sample 1 were obtained. For sample 2 the cutoff could not be obtained with good precision. The data obtained for the cutoff wavelengths will be used later in this chapter in order to estimate the index rise of Ga:Sapphire waveguides by comparison with modelling results.

4.3.4 Mode profiles of samples 5 to 8 at 488 and 633nm

i) Experimental results

This set of measurements was performed using an Argon ion and a Helium Neon laser on samples 5 to 8 (experimental configuration in Figure 4.1). Samples 5, 6 and 7 had no residue on the surface after the diffusion, in contrast to sample 8 (200nm thickness). Sample 7 was double-moded at 488nm and sample 8 was double-moded at 633nm. Figure 4.6 gives the mode sizes as a function of thickness (samples 5, 6, 7) for the two wavelengths studied.

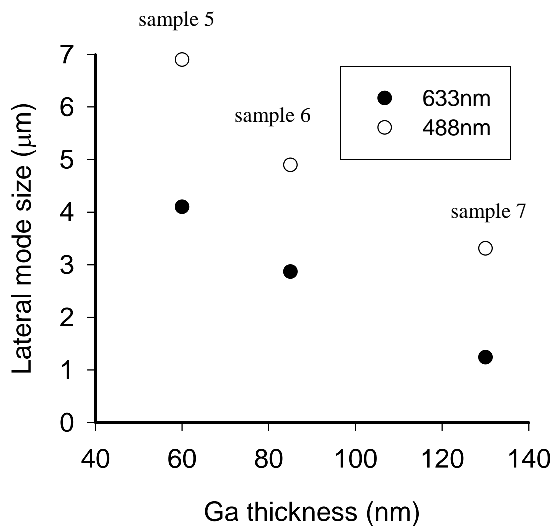

Figure 4.6. Mode sizes vs. gallium source thickness for He:Ne and Ar:ion laser.

ii) Discussion of results

The samples used are identical in all parameters except for the initial gallium oxide thickness. This is expected to correspond to different Ga concentrations inside the waveguides. Therefore as the film thickness is increased it is expected that the index change will increase, resulting in a reduction of the modal width. This experiment

confirmed this theoretical expectation as can be observed in Figure 4.6 and gave the anticipated small mode depths. Using the results obtained by these measurements the maximum index change obtained with gallium doping can be found by comparison with waveguide models. Furthermore the maximum thickness of gallium oxide that can be diffused into sapphire without leaving any residue, for this diffusion time and temperature, was found to be approximately 150nm. With this experiment the characterisation of slab Ga:Sapphire waveguides was completed as the mode size of the waveguide and its dependence upon fabrication condition had been established.

4.3.5 Channel waveguide mode profiles

i) Experimental results

Following the optimization of the mode dimensions of the planar waveguides four identical channel samples were prepared (sample 8). Figure 4.7 shows the image of a channel waveguide mode with opening 10μm. Figure 4.7 also shows an image of the end-face of the sample when light was launched in-between the channel waveguides; 50μm away (along the sapphire surface) from a gallium source.

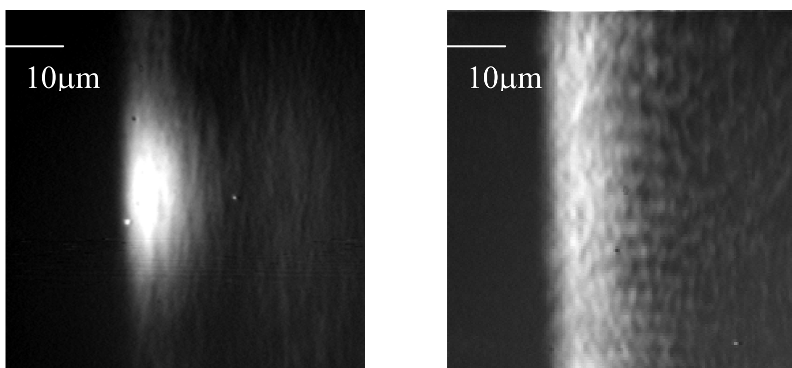

Figure 4.7. Mode image at He-Ne wavelength for a 10μm opening channel waveguide, also another image depicting a part of the sample 50μm away from the diffusion source that seems to guide.

ii) Discussion of results

The channel waveguides diffusion exhibited a strong lateral diffusion effect. It can be seen in Figure 4.7 that a part of the sample that had no diffusion source seems to guide like a slab waveguide. This effect was known to exist in sapphire from previous studies with titanium diffused waveguides [6,7]. The origins of the lateral diffusion according to previous research [8,9] are related to the increased concentration of defects near the surface which accelerate locally diffusion. Although the fabrication of channels was successful, the lateral diffusion poses a significant problem for the optimization of channel waveguide fabrication as it was difficult to control repeatably. Experimental work presented in chapter 5 avoids the problem of lateral diffusion by micromachining the surface of sapphire for creation of ridge waveguides.

4.4 Maximum index change of the Ga:Sapphire waveguides

In this section experimental data about the cutoff wavelengths of the fundamental or higher order modes are used in order to calculate the maximum index increase of the samples. The refractive index profiles of the waveguides are proportional to the diffusion profiles of Ga which are known from the diffusion characterisation presented in Chapter 3. The maximum index change is the only variable in the reconstruction of the refractive index profile and is calculated by matching the modelling with the experimental results as the waveguide simulations calculate the cutoff wavelengths versus the maximum index change. For sample 1 is known that it exhibited cutoff of the fundamental mode at 780nm, for sample 7 that it is double-mode at 488nm, finally for sample 8 that it is double-mode at 633nm. For samples 7 and 8 is assumed that the cutoff of the second order mode occurred at 488 and 633nm

therefore the calculated maximum index change of samples 7 and 8 is a minimum estimation.

Three different modelling methods (presented in Chapter 2) are used in order for the results to be confirmed. The first model to be used was the slab waveguide model. In the case of Ga:Sapphire waveguides the refractive index profile is not a step function but the slab waveguide model can be used as an approximation for calculating the maximum index change (Section 2.3.1, Figure 2.7). The width of the guiding layer input to the model is the approximated diffusion depth in addition to the Gaussian offset (Table 4.1).

The next model used in order to confirm the results was the WKB model. The refractive index profile used for the WKB is created with a Gaussian and a logistic function with the appropriate profile depths and Gaussian offsets for each sample (Section 2.3.2, Figure 2.7).

Finally a commercial BPM package called Selene Pro was used but only to obtain results for sample 1 as it was not readily usable to analyse higher order mode waveguides in graded index profiles. The input refractive index profile given to the BPM model was similar to the one used in the WKB metod. Giving to the program as variable the maximum refractive index, the effective refractive index of the modes could be calculated at a given wavelength. In Table 4.2 includes the results of the waveguide models for the maximum refractive index change of samples 1, 7 and 8.

Sample #	Fabrication conditions		Maximum refractive index change		
	Ga thickness (nm)	Time (hrs)	Slab	WKB	BPM
1	60	6	$2.5x10^{-3}$	$2x10^{-3}$	$2.45x10^{-3}$
7	130	16	$4x10^{-3}$	$4x10^{-3}$	
8	200	16	$6x10^{-3}$	$6x10^{-3}$	

Table 4.2. Model results for the maximum refractive index of Ga:Sapphire waveguides.

The maximum index change of the Ga:Sapphire waveguides was calculated using three different modelling techniques. The results obtained in all the models were in close agreement, thus, giving conclusive data on the index change that gallium creates as a diffusion dopant in sapphire. The maximum index change that was achieved was $6x10^{-3}$ and the mode sizes close to 1μm at 488nm. In the case of titanium diffusion for waveguide fabrication the mode sizes were approximately 5μm and the peak index change was lower than 10^{-3}. This difference is partly due to the fact that the Ti concentration into sapphire was kept at the optimum levels for laser operation [6].

4.5 Conclusions

In this chapter a novel waveguide fabrication method using thermal diffusion of gallium into sapphire has been presented. The mode profiles of the waveguides were obtained for a range of different wavelengths and also for different fabrication conditions. The optimization of the waveguides was based on the minimization of the mode profiles and consequently led to the maximization of the index change that

gallium can cause as a dopant into the lattice of sapphire. The index change and the mode sizes are appropriate for the implementation of devices with adequately sharp bends with low losses (curvature radius of approximately 30mm, see section 2.5.2).

One important issue to be resolved for successful channel waveguides fabrication is the lateral diffusion. The next chapter describes a technological solution which bypasses the problem and produces successful channel waveguides in sapphire.

References to Chapter 4

1. Levin E, "Phase diagrams for ceramists," (Am. Ceram. Soc, 1964).

2. Fung S et al., "Gallium/aluminum interdiffusion between n-GaN and sapphire". *Journal of Applied Physics* **84**, 2355. (1998).

3. Tessman R.Jack and Kahn A.H. "Electronic polarizabilities of ions in crystals". *Physical Review* **92**, 890. (1953).

4. V. Apostolopoulos, L. M. B. Hickey, D. A. Sager, and J. S. Wilkinson, "Gallium-diffused waveguides in sapphire," *Optics Letters* **26**, 1586-1588 (2001).

5. V.Apostolopoulos, L.M.B.Hickey, and J.S.Wilkinson, "Gallium diffused waveguides in sapphire," *European Conference in Integrated Optics, Paderborn, Germany* (2001).

6. Louise M.B.Hickey, PhD thesis, "Ti:Sapphire waveguide laser by the thermal diffusion of Ti into sapphire", (Optoelectronics Research Centre, University of Southampton, 1998).

7. Louise MB Hickey. "Report on activities in Southampton during the 1851 fellowship award." 1999.

8. V. S. Stubican, G. Huzinec, and D. Damjanovic, "Diffusion of Cr-51 in Surface-Layers of Magnesia, Alumina, and Spinel," *Journal of the American Ceramic Society* **68**, 181-184 (1985).

9. Stubican VS et al. "Grain-boundary and lattice diffusion of ^{51}Cr in alumina and spinel", *Advances in Ceramics* **10**, 406. (1984).

CHAPTER 5

GALLIUM-DIFFUSED RIDGE WAVEGUIDES IN SAPPHIRE

5.1 Introduction

In the previous chapter Ga^{3+} was identified as an appropriate ion to form waveguides in sapphire and it was demonstrated that gallium may be diffused into sapphire to create planar optical waveguides with an index change up to 6×10^{-3} [1,2]. These waveguides were characterised and gave very promising characteristics for integration. Nevertheless there is an innate difficulty in fabricating channel titanium or gallium waveguides in sapphire by patterning the diffusion source using photolithography [3,4]. The reason is that ionic diffusion in sapphire exhibits a strong component of lateral diffusion. This has been described in other studies of sapphire diffusion [5] and is probably due to an increased concentration of surface defects e.g. due to the mechanical stresses of cutting and surface polishing. This diffusion characteristic renders the fabrication of successful channel waveguides difficult to achieve because the confinement in the horizontal direction is degraded. In this chapter the implementation of a successful alternative route was followed that comprises the realization of gallium-diffused channel ridge waveguides in sapphire, for the first time.

The chapter starts with the description of the fabrication method of the ridge waveguides in sapphire. In this section the photolithographic process is described and details of the selection of photoresist that was found to be appropriate for this task are given. The ion beam milling technique used for the micromachining of the substrates is also described. The fabrication parameters of the produced samples are included. The next section focuses on the optical characterisation of the ridge waveguides performed using mode profile measurements, prism coupling and loss measurements. Finally the results of a BPM model used for the ridge structures are described for comparison with the experiments.

5.2 Fabrication

5.2.1 Overview of the process

Gallium oxide of thickness 150nm was deposited on sapphire samples by thermal evaporation, and each sample was annealed in oxygen at 1600°C for 16hrs. According to the diffusion coefficient of gallium into sapphire (diffusion data for gallium are presented in section 3.4) the resulting diffusion profile has a diffusion depth of approximately 4μm. Following the fabrication of the planar diffused waveguides, a photoresist pattern is created on the surface of the samples using standard photolithography. Then the pattern is transferred to the substrate with the use of Argon Ion Beam Milling (IBM), which is a fabrication tool used for surface micromachining. In the IBM apparatus a beam of argon ions is accelerated towards the surface of the sample to etch away material. A photoresist pattern is used as a protecting mask on the surface of the substrate to define the unetched areas. A schematic of the fabrication process, from diffusion to IBM, is shown in Figure 5.1.

The process is similar to the photolithography used for the fabrication of channel Ga waveguides that is described in section 4.2.

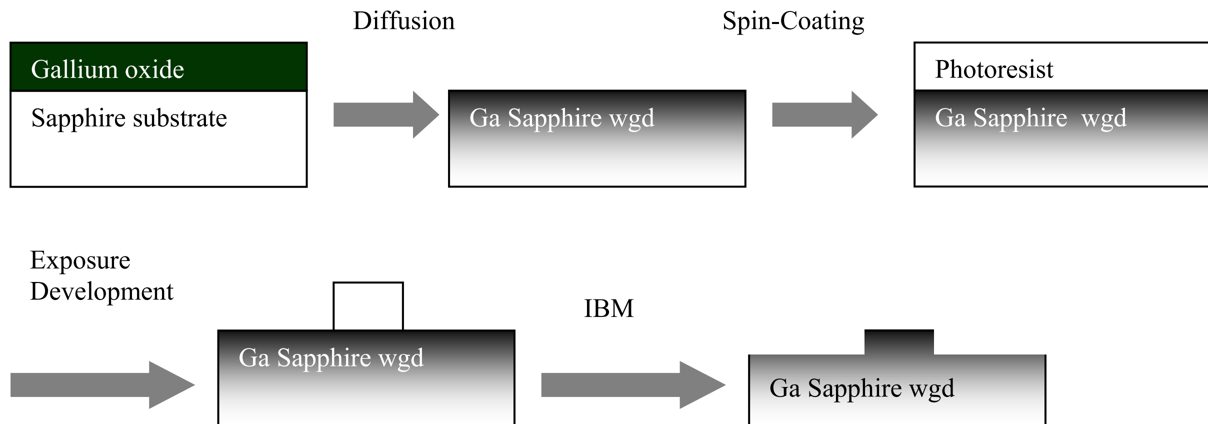

Figure 5.1 Schematic of the fabrication process for the ridge Ga waveguides

The relative etch rate, in IBM, of sapphire and photoresist is subject to the conditions used in the etching process and on the type of the photoresist. Nevertheless it has been found that most photoresists etch approximately 2-3 times faster than sapphire. In order to achieve good lateral mode confinement, the height of the ridge waveguides was estimated to be between 2 and 5μm, using a BPM model for which the results are given in Section 5.4. This fabrication requirement corresponds to a photoresist height between approximately 6 and 15μm, and aspect ratios that reach 3 to 1. These specifications cannot be achieved using common photoresists such as Shipley 1813 and 1828.

SU-8 is a negative, epoxy-type, near-UV photoresist based on EPON SU-8 epoxy resin (from Shell Chemical) that was originally developed and patented by IBM co. [6]. The resist is supplied as a liquid consisting of an epoxy resin, a solvent (GBL or cyclopentanone depending on formulation) and a photo-acid generator. The chemical

composition of the cross-linked photoresist is shown in Figure 5.2. The substrate is coated using a conventional photoresist spinner, with the film thickness controlled by the spin speed and the solvent content of the epoxy solution. A baking stage removes excess solvent from the layer. Upon exposure to UV radiation, a strong acid ($HSbF_6$) is generated which causes the epoxy resin to form a ladder-like structure with a high cross-linking density when heated above a critical temperature provided in a post-exposure bake. The unexposed material is then removed with a solvent in the development process [7,8].

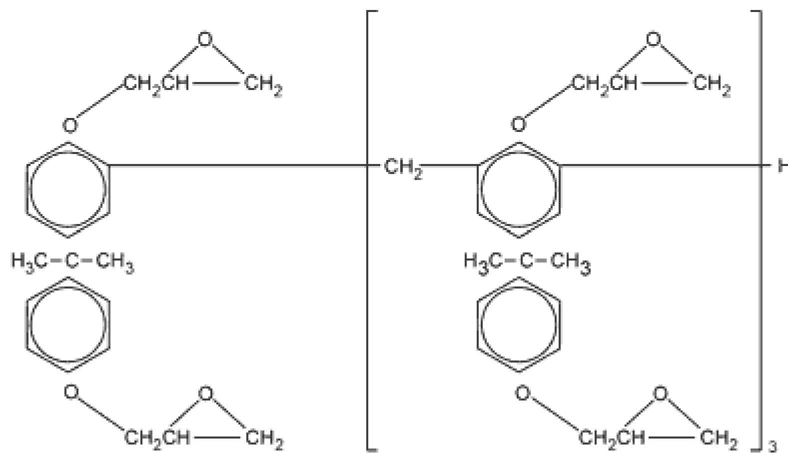

Figure 5.2 Sketch showing the chemical structure of cross-linked SU-8 photoresist, from [9].

This photoresist can be as thick as 2 mm and aspect ratios >20 have been demonstrated with standard contact lithography equipment. Figure 5.3 shows some spectacular results of SU8 photolithography (Microchem corporation [8,10]).These results are due to the low optical absorption in the UV range which allows thickness up to 2 mm for the 365nm-wavelength where the photo-resist is the most sensitive.

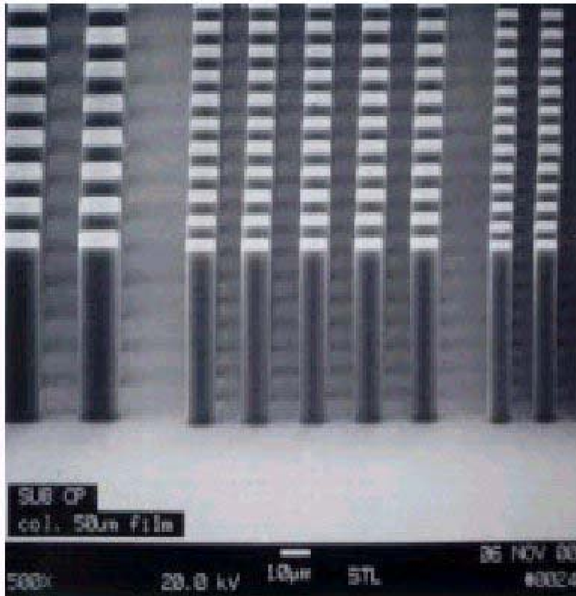

Figure 5.3. 5µm, 10µm and 20µm post arrays of SU-8 in a 50µm thick film, from [8].

5.2.2 Details of SU-8 application

Optimising the parameters for SU8 photolithography was time consuming due to the number of parameters that needed to be tuned and also due to the variety of problems that were encountered. In most photoresists the quality of the spin-coated film is degraded if the surface has roughness, is dirty or has moisture. SU-8 films are very sensitive to these parameters, therefore prior to spinning the resist, the surface of the sample was carefully cleaned using a strong acid, in most cases fuming nitric acid or sulphuric acid and hydrogen peroxide (a mixture called piranha). Subsequently the surface was cleaned of organic residues using acetone and isopropanol. The sample was then baked at 120^0C for 30min in order to remove any moisture. In the case of gallium diffused samples, surface roughness was usually not an important parameter because gallium diffusion leaves insignificant residue. The parameters of post and pre-exposure bake of SU8 were optimised in order to increase the adhesion of the sample while not inducing stress in the film. Figure 5.4 shows two common problems

that were encountered with non optimised fabrication. In Figure 5.4 (b) is a typical example of bad adhesion as after development all the SU8 has been washed away. If stressed, on the other hand, the SU8 film will behave as shown in Figure 5.4 (a).

A number of different conditions for the photolithographic processes were used, the one which was finally adopted, due to its simplicity as well as its success, was to bake for 20-30 minutes at 120^0C after spin-coating and then leave the sample at room temperature for at least 20 min before exposing in the mask aligner. After exposing for 40-50 s the sample was post exposure baked for 20 min at 120^0C and left again for 5min to cool before developing for 1min. During developing, rinsing and finally blowing dry, care was used to avoid challenging the adhesion of the SU8 stripes.

Finally another common disadvantage of SU-8 is that it is difficult to remove especially after hard baking. It is indicative of this, that companies that produce SU-8 are offering an award for finding a chemical etchant for SU-8 that does not also etch chrome, gold etc. [7]. However, sapphire is chemically inert and has an excellent mechanical strength, so SU-8 was removed when needed by chemical etching using fuming nitric acid or piranha; any SU-8 left on the surface was removed mechanically.

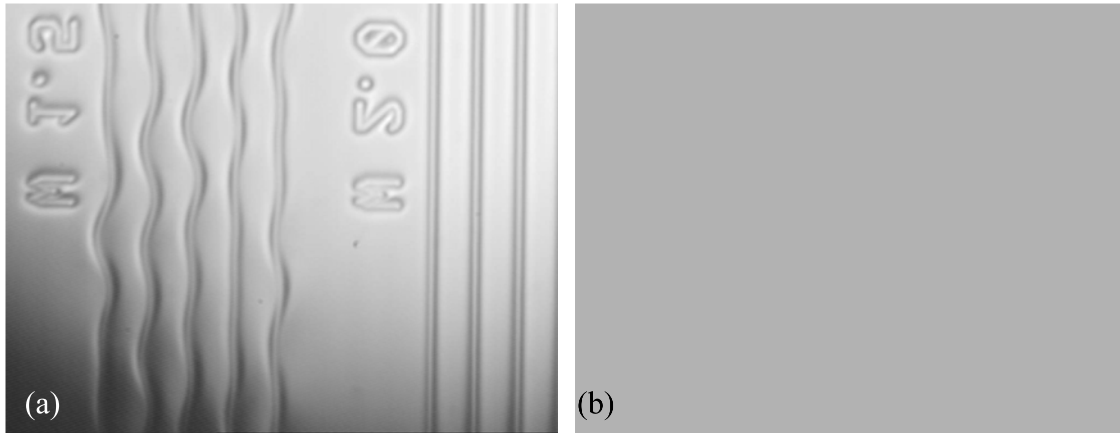

Figure 5.4. Photographs showing typical problems in the photolithography process using SU-8, from [11].

5.2.3 Fabricated samples

The samples were photolithographically patterned with stripes of SU-8 photoresist of width 3 to 15μm and height 5 to 15μm and then etched using argon ion beam milling to transfer the photoresist pattern to sapphire. The etch duration was varied for each sample, resulting in Ga:sapphire ridges with heights between 1.0 and 6.2μm. An SEM image of ridges of height 2.5μm is shown in Figure 5.5.

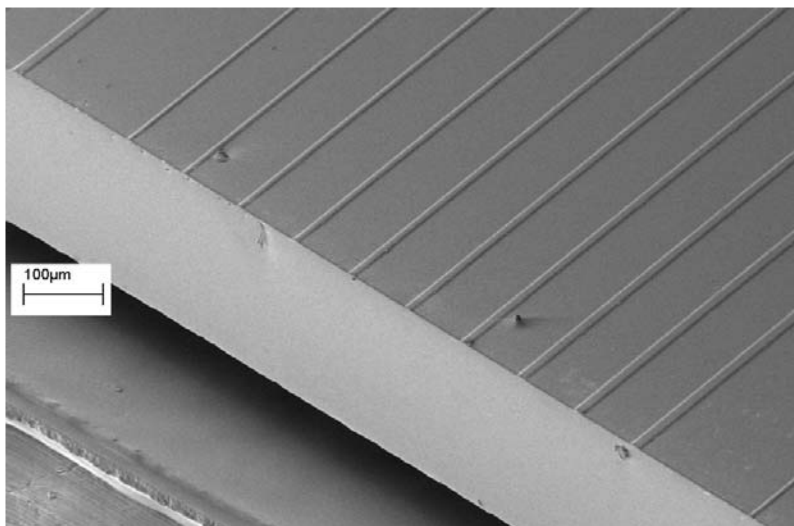

Figure 5.5. SEM photograph of the Ga:Sapphire waveguides. The height of the ridges is 2.5μm and the widths from 3 to 15μm.

5.3 Characterisation of gallium diffused ridge waveguides

5.3.1 Mode profiles

Following the fabrication process, the end-faces of the samples were polished. Light was launched into one end-face of the waveguide by coupling with a microscope objective lens or with a fibre. The modal intensity distribution at the other end-face was imaged onto a CCD camera using a microscope objective lens. The images were stored in a computer and quantitative data for the mode profiles were obtained using the commercial package Matlab. The response function of the imaging system used was obtained by imaging a photolithographically defined step. The point spread function of the system was deconvolved, using the Fast Fourier Transform (FFT) algorithm, from the waveguide mode data. The distortion caused by the imaging system was found not to be significant so that the mode size measurements presented have not been corrected. The modal intensity profiles for the samples were measured in both polarizations using a He:Ne laser operating at 633nm. The smallest mode profile obtained was for a ridge waveguide of both height and width 5μm and the mode waist was approximately 2μm (defined at 1/e of the peak intensity) in the horizontal and lateral direction. Figure 5.6 shows the image of this mode profile and a graph giving the size of the mode versus the height of the ridges for waveguides created using the same mask opening, of 2μm, for the TE polarisation. A height of 5μm was found to be optimum for the fabrication of small mode-size waveguides. The diffusion profile of gallium and therefore the waveguide core also extends up to a depth of approximately 5μm; therefore etching more than this value will not result to waveguides with better mode confinement. However, the width of the resulting

waveguide depends on the waveguide height, so it must be noted that as the waveguide height is increased the width increases as well. For a mask opening of 2μm, the 1μm high ridge has a width which is approximately 3μm while for the 6.2μm high waveguide the width at the top of the ridge is approximately 5μm. As expected, above the height of 5μm there was not an improvement of the mode dimensions. Ridges higher than 5μm have small mode sizes but they have a very complicated mode structure. It must be noted that the mode size of the ridge waveguides presented here is significantly smaller than that obtained from channels fabricated by photolithographically patterning the diffusion source either using titanium or gallium as the waveguide ion. This is expected to result in the potential for bends with approximately 30mm radius of curvature and lasers with low thresholds.

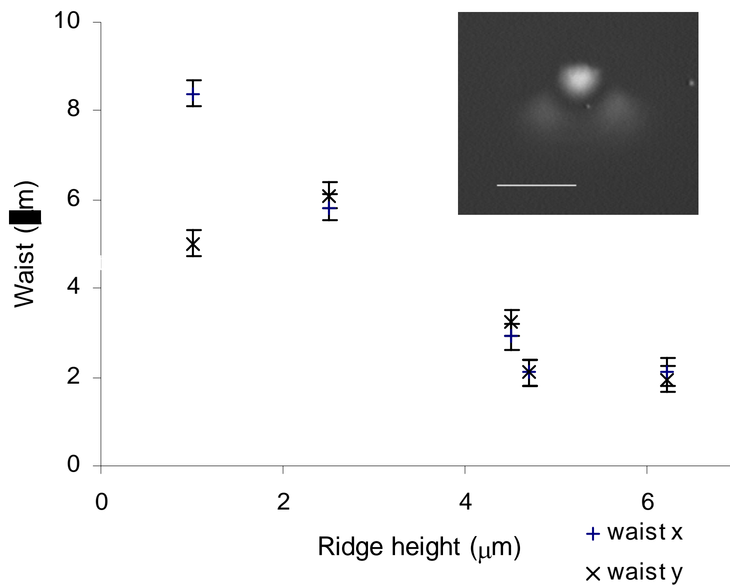

Figure 5.6. Vertical and horizontal mode waists versus the height of the ridge waveguides, also a mode profile of a ridge waveguide with height 4.7μm and width of 5μm.

5.3.2 Prism coupling

Modal effective indices were measured by prism coupling. The samples were held in close contact with a rutile prism and light from a He:Ne laser was coupled in the

waveguide. The sample and prism were held on a rotation stage and measuring the angle at which the laser beam is incident on the prism, as well as the refractive indices of the prism and substrate, the effective indices of the waveguide modes were estimated. Figure 5.7 shows the effective indices of the channel waveguide modes versus the width of the channels, for a sample with 2.5μm high ridges. It is expected in this graph that the curve of effective index versus width should saturate, as the width increases, to the effective index of a hypothetical planar structure. The polarization used in this measurement is TM, in order to have access to the ordinary refractive index (~2.6) of the rutile prism. This is due to the fact that the extraordinary refractive index of rutile (~2.9) in combination with the index of sapphire (1.766) give incident angles that cannot be accessed by the experimental configuration employed.

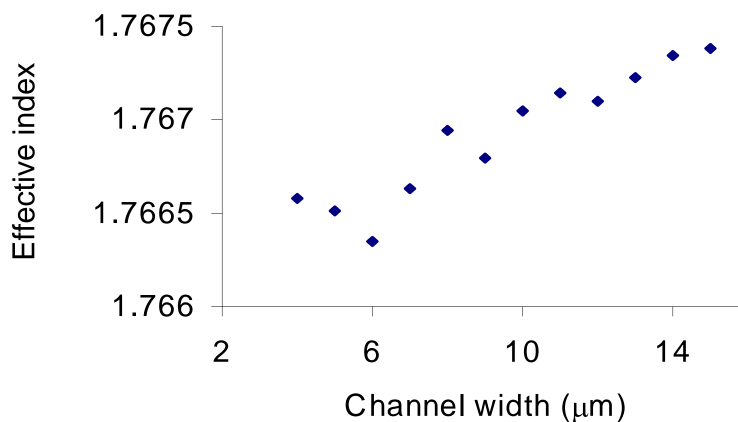

Figure 5.7. Effective index of channel waveguides versus the width of the channels. Height of the ridges is 2.5μm and the polarization is TM.

5.3.3 Propagation loss and spectral attenuation measurements

The total loss of the waveguides, propagation and coupling loss was measured using end-fire launching and calculating the ratio of input and output power. For a 5μm high and 13μm wide waveguide, this maximum possible propagation loss was calculated to

be 4dB/cm. For this estimation, it was assumed that the only coupling loss is due to reflections at the end-faces. It is expected that the coupling loss is usually in order of 3dB, therefore it can be safely assumed that the ridge waveguides have lower propagation loss than 2dB/cm. The insertion losses were measured as a function of wavelength and this measurement also reveals the cutoff wavelengths of the waveguides. For the spectral attenuation measurement light from a tungsten lamp was launched in a fiber that was end-coupled to the ridge waveguides, the output of the waveguides was spectrally analysed using a monochromator. Because the coupling efficiency of radiation from a white light source into a fiber is very low, a lock-in amplifier is used to amplify the signal of the detector; the experimental set-up is computer controlled. Figure 5.8 shows spectral attenuation measurements for the TE polarization of the sample with ridge height of 5μm and widths of 5 to 14μm. It can be observed, as expected, that as the width of the waveguide increases the cutoff wavelength becomes longer. Another observation is that the loss in the guiding regime decreases as the waveguide width increases, which is because the wider waveguides have lower coupling loss. For the 13μm wide waveguide the coupling loss is approximately 5dB, which confirms the value of 4dB/cm that was given at the beginning of this paragraph. In Figure 5.9, for the same sample the cutoff wavelengths are plotted as a function of the waveguide width. The same sample was used for the estimation of the loss and also exhibited the best mode confinement as mentioned above (mode size of 2μm).

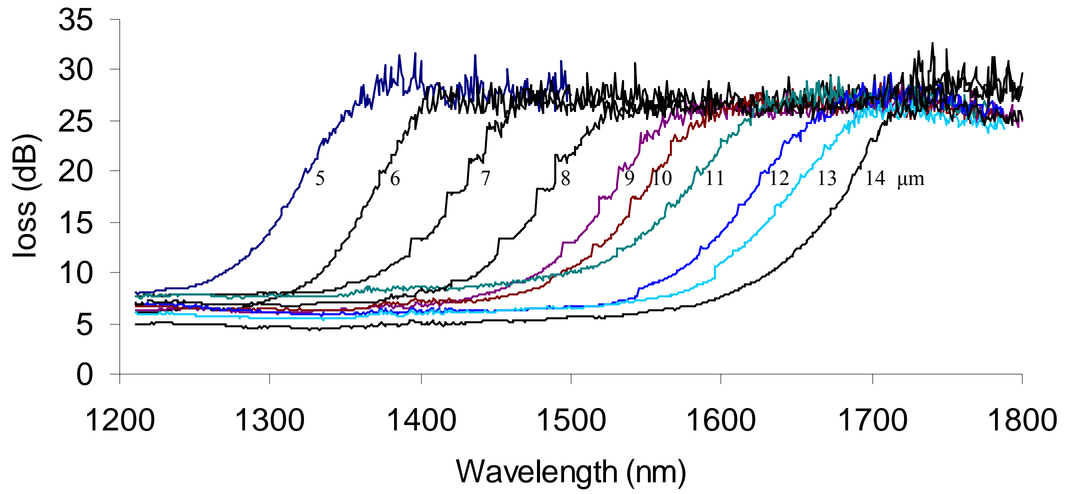

Figure 5.8. Spectral attenuation measurements for the TE polarization for a sample with ridge height of 5μm and widths of 5 to 14μm. As the width of the waveguides is increased, the cutoff wavelength of the fundamental mode is longer.

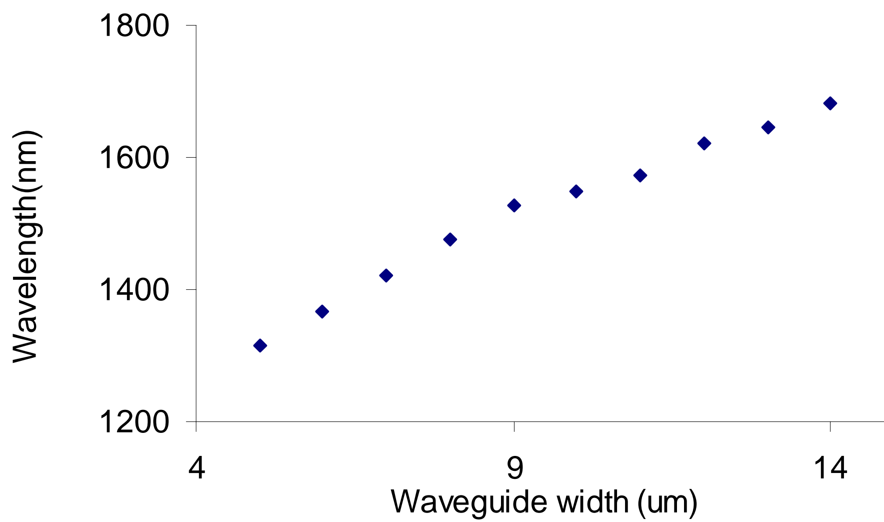

Figure 5.9. For a sample with ridge height of 5μm and widths of 5 to 14μm (same sample as in Figure 5.8) the cutoff wavelengths of the fundamental mode of the waveguides versus the waveguide width.

5.4 Beam Propagation Model.

A commercial modelling tool (BeamProp) was used in order to simulate the ridge waveguides in sapphire. The method used for the simulations is the beam propagation method which is described in Chapter 2. A ridge waveguide structure close to the structures that were fabricated was modelled. The refractive index profile was created using a Gaussian function proportional to the gallium diffusion profiles that are presented in Chapter 3. The following parameters were used in the computer aided design, the diffusion depth was 3.5μm and the offset of the gaussian was 0.5μm depth, the maximum refractive index was $6x10^{-3}$, which is the value calculated in Chapter 4. An example of the waveguide structure used in the model is shown in Figure 5.10. In the figure the width of the ridge is 5μm, stable for all the simulations presented here, and the height of the ridge is 1μm in this case. The variable used is the height of the ridge, in order to estimate the ridge needed in order to have good vertical and horizontal confinement. In Figure 5.11 images of the mode intensity profiles are given for ridges of different height, starting at 1μm and ending at 5μm. This parameter scan shows that the appropriate height is above 4μm; the confinement for ridges higher than 5μm stays approximately the same. These results give good agreement with the experimental data that are presented in the previous sections.

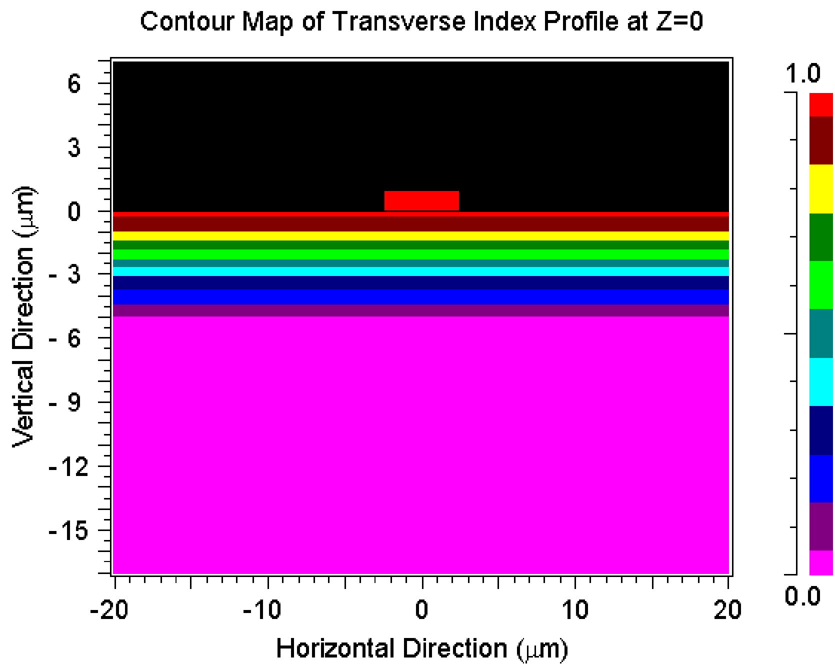

Figure 5.10 Ridge waveguide used for the simulations with height of 1μm and width of 5μm. The refractive index profile created by the diffusion can be seen according to the colour scale.

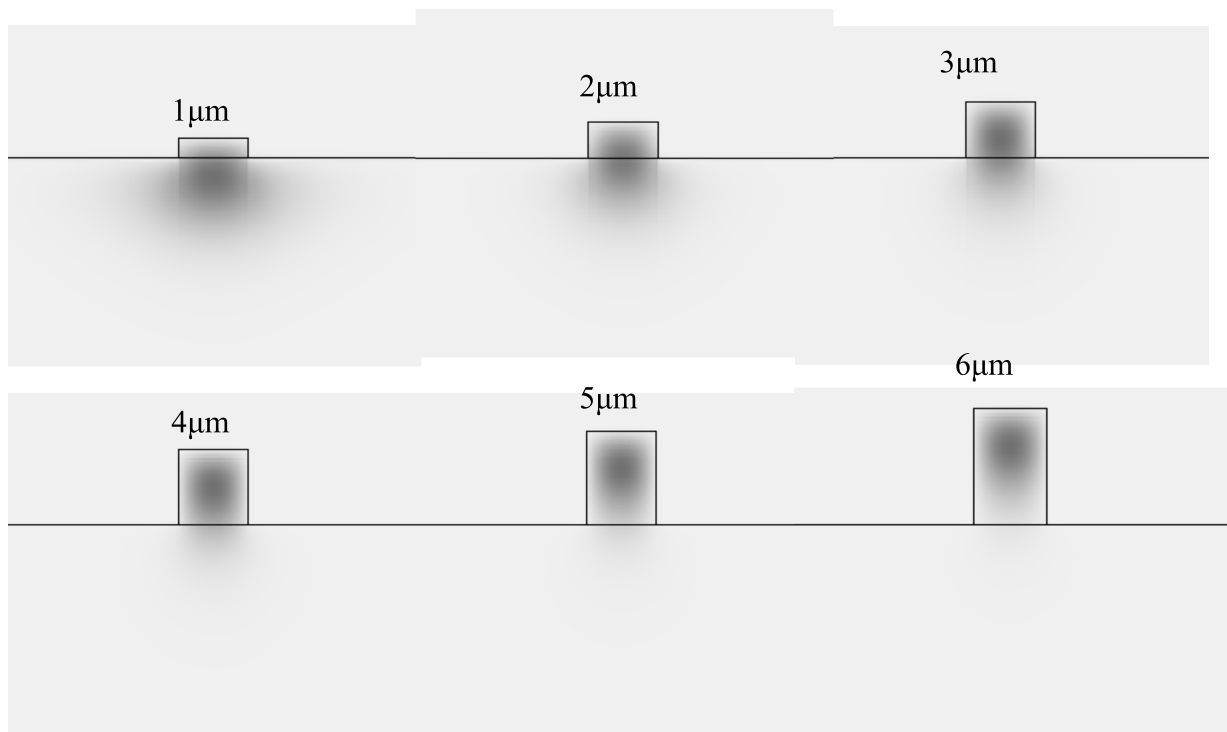

Figure 5.11 Simulated mode calculation using the BPM method.

5.5 Conclusions

In this chapter the characteristics of the gallium ridge waveguides are given. The chapter begins with the description of the fabrication process, describing in detail the photolithography of sapphire with SU-8 photoresist. Following this the characterisation of the channel waveguides is described, which was performed using mode profile measurements that show that the waveguides have very good mode confinement, exhibiting mode sizes of 2μm. The loss of the waveguides was also estimated to be less than 2dB/cm and the cutoff wavelengths of the ridges was measured. Finally, modelling results, using a BPM commercial package are shown that complement the experimental results.

For the first time the realization of gallium-diffused ridge waveguides in sapphire has been demonstrated. It has been shown that channel Ga:sapphire waveguides may be realized with small mode sizes and acceptable loss for the fabrication of Titanium sapphire lasers. The channel mode sizes are smaller than any result achieved by patterning the diffusion source, gallium or titanium, due to the restriction of the strong lateral diffusion. This work gives a general fabrication tool to micromachine the surface of sapphire in order to create waveguides and the same method is used for creating active titanium diffused waveguides which are presented in the next chapter.

References to Chapter 5

1. V. Apostolopoulos, L. M. B. Hickey, D. A. Sager, and J. S. Wilkinson, "Gallium-diffused waveguides in sapphire," *Optics Letters* **26**, 1586-1588 (2001).

2. V.Apostolopoulos, L.M.B.Hickey, and J.S.Wilkinson, "Gallium diffused waveguides in sapphire," *European Conference in Integrated Optics, Paderborn, Germany* (2001).

3. Louise M.B.Hickey, PhD thesis, "Ti:Sapphire waveguide laser by the thermal diffusion of Ti into sapphire", (Optoelectronics Research Centre, University of Southampton, 1998).

4. V.Apostolopoulos, Mini-thesis, "Gallium diffused waveguides in Sapphire" (Electronics and Computer Science, University of Southampton, 2000).

5. V. S. Stubican, G. Huzinec, and D. Damjanovic, "Diffusion of Cr-51 in Surface-Layers of Magnesia, Alumina, and Spinel," *Journal of the American Ceramic Society* **68**, 181-184 (1985).

6. H. Lorenz, M. Despont, N. Fahrni, N. LaBianca, P. Renaud, and P. Vettiger, "SU-8: a low-cost negative resist for MEMS," *Journal of Micromechanics and Microengineering* **7**, 121-124 (1997).

7. "Su-8: a thick photo-resist for MEMS", http://aveclafaux.freeservers.com/SU-8.html, 2003.

8. "SU-8 2-25 datasheet.", http://www.microchem.com/products/pdf/SU8_2-25.pdf., Microchem Corporation, 2003.

9. "SU-8 Photosensitive Epoxy". http://www.cnm.es/projects/microdets/su8.htm, National centre of microelectronics (Spain), 2003.

10. "SU8 photoresists", http://www.microchem.com/products/su_eight.htm. 2003. Microchem Corporation.

11. Dr.Richard Curry, (internal communication), "Pictures of SU-8 problems", 2003.

CHAPTER 6

ACTIVE TITANIUM-DIFFUSED RIDGE WAVEGUIDES IN SAPPHIRE

6.1 Introduction

This Chapter reports on the realisation of Ti:Sapphire diffused ridge waveguide lasers. In Chapter 3 the diffusion coefficients for gallium and titanium ions in sapphire have been given and in Chapter 4 the successful fabrication of gallium diffused waveguides has been established. Chapter 5 includes the realisation of gallium diffused ridge waveguides by photolithography and etching; the fabrication and characterisation of active titanium diffused waveguides is described here, using the same fabrication technique.

The chapter begins with the spectroscopic characterisation of combined titanium and gallium diffused samples. This section describes the potential of this scheme for realisation of an integrated laser device but also potential incompatibilities in the process which may inhibit the successful implementation of this co-doping approach.

The second part of the chapter presents the fabrication and characterisation of the titanium diffused ridge waveguide laser. The description of the fabrication of the titanium diffused ridge waveguides is given with detailed discussion of parameters which significantly affect the performance of the laser waveguides. The optical

characterisation of the waveguides starts with mode profile and coupling loss measurements. Following this, characterisation of the waveguide lasers is then presented with fluorescence measurements; spectral plots of the waveguides using different experimental configurations and pumping schemes show lasing action. Finally, discussion of the results is included with comparison of experimental and modelling results for the waveguide lasers.

6.2 Ga and Ti diffused ridge waveguides

The introduction of a second ion into sapphire by thermal diffusion in order to form a passive waveguide leads to greater design flexibility, as the waveguide and the gain medium characteristics can be independently controlled. This combined diffusion approach is used in waveguide lasers fabricated in lithium niobate where Erbium and titanium are the active and the waveguide ion respectively [1,2]. Gallium and titanium diffusion was studied for the fabrication of laser ridge waveguides. Ga was used to provide the waveguide and titanium to provide an active region. Diffusion of the Ga^{3+} ion in sapphire creates planar and ridge waveguides (Chapters 4 and 5) [3-5] with smaller mode sizes and higher index change than Ti-diffused waveguides [6], which is expected to lead to waveguide lasers with low threshold pump powers.

6.2.1 Samples fabricated for characterisation of Ti and Ga co-diffusion.

A set of samples was fabricated to estimate the effect of gallium and titanium co-diffusions on the fluorescence characteristics of an active device. The fabrication procedure is the same as that described in section 5.2 for the Ga:Sapphire ridge waveguides. The parameters of the samples are summarised in Table 6.1. Sample R1 is a c-cut sapphire sample (used as reference); sample R2 is a gallium diffused ridge waveguide. Samples R3 and R4 are titanium diffused ridge waveguides and finally

sample R5 is fabricated by gallium followed by titanium diffusion. This sequence of diffusion was used for sample R5 because as it was found in section 3.5.4 that gallium and titanium diffusions affect one another less when using this sequence. The tube furnace (Lenton) was used for all the samples with an argon atmosphere when titanium was diffused and an oxygen atmosphere when gallium was diffused.

Sample #	Gallium diffusion Thickness (nm)/ Temp.(^oC)/Time (hrs)	Titanium diffusion Thickness (nm)/ Temp.(^oC)/Time (hrs)	Height (μm)	Remarks
R1	-	-	-	Clean sapphire
R2	150/1600/16		4	Ga ridges
R3	-	10/1600/1	3	Ti ridges (thin film)
R4	-	150/1600/2	3	Ti ridges (thick film)
R5	150/1600/16	50/1600/1	3	Ga/Ti diffusion

Table 6.1. Fabrication parameters for samples used for the characterisation of Ga and Ti codiffusion.

6.2.2 Experimental fluorescence configuration

The purpose of the characterisation was to compare the fluorescence characteristics of samples R1-R5. The experimental setup that was used for this purpose was a micro-Raman spectrometer. Raman scattering is a form of inelastic scattering where the scattered photons have different energy than the incident photons [7] due to the vibrational states of the ions inside the crystal. As Raman scattering is usually very weak (1 in 10^7 photons), Raman and micro-Raman spectrometers are very sensitive

optical configurations and must be well calibrated. Figure 6.1 shows a general representation of a micro-Raman apparatus. A micro-Raman system combines a conventional Raman spectrometer with a microscope, giving a spatial resolution in the order of microns dependent on the spotsize of the microscope objectives that are used. Because of its sensitivity and precision a commercial micro-Raman setup was used for characterisation of the fluorescence spectra of the fabricated samples. Two pump lasers were used, an Argon ion (488nm) and a Helium Neon laser (633nm).

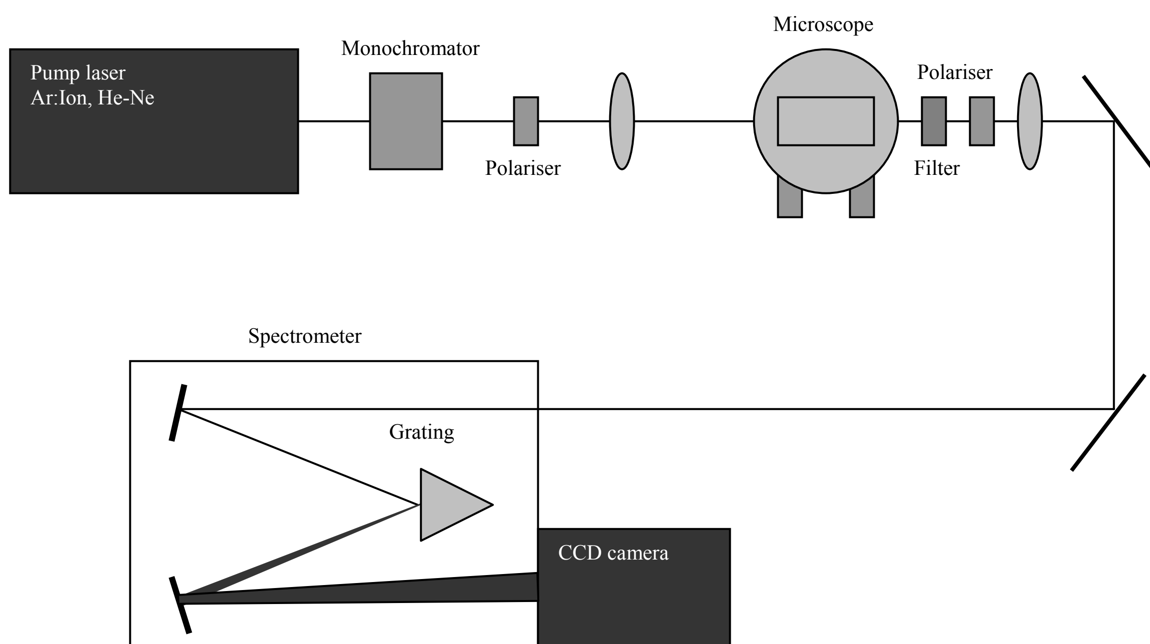

Figure 6.1. Schematic showing the general components of the experimental configuration used for the spectroscopic characterisation of the Ga:Ti:Sapphire samples.

6.2.3 Fluorescence spectra of samples R1-R5

A clean untreated c-cut sapphire wafer was characterised first to obtain a reference spectrum (sample R1). Sample R2, which is a gallium diffused ridge waveguide sample was also tested, as a reference and also to examine the effect of gallium diffusion on the spectroscopy of sapphire. Samples R3 and R4 are titanium diffused samples and are compared with sample R5 which is fabricated by gallium diffusion

followed by titanium diffusion. Figure 6.3 shows graphs with the fluorescence spectra of all the samples R1 to R5 and Figure 6.2 shows all the fluorescence spectra in one graph to facilitate comparisons.

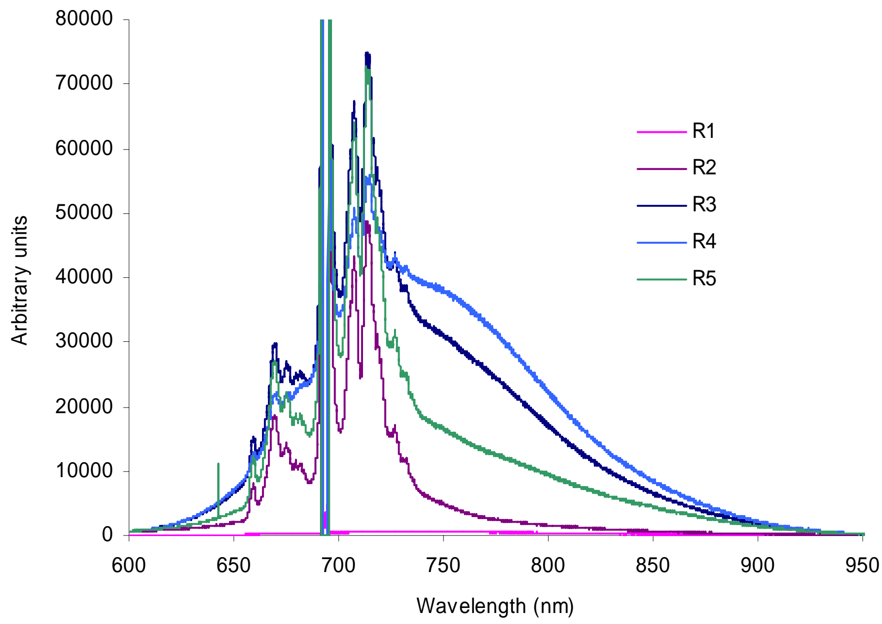

Figure 6.2. Fluorescence spectra of samples R1to R5 in the same graph for comparisons

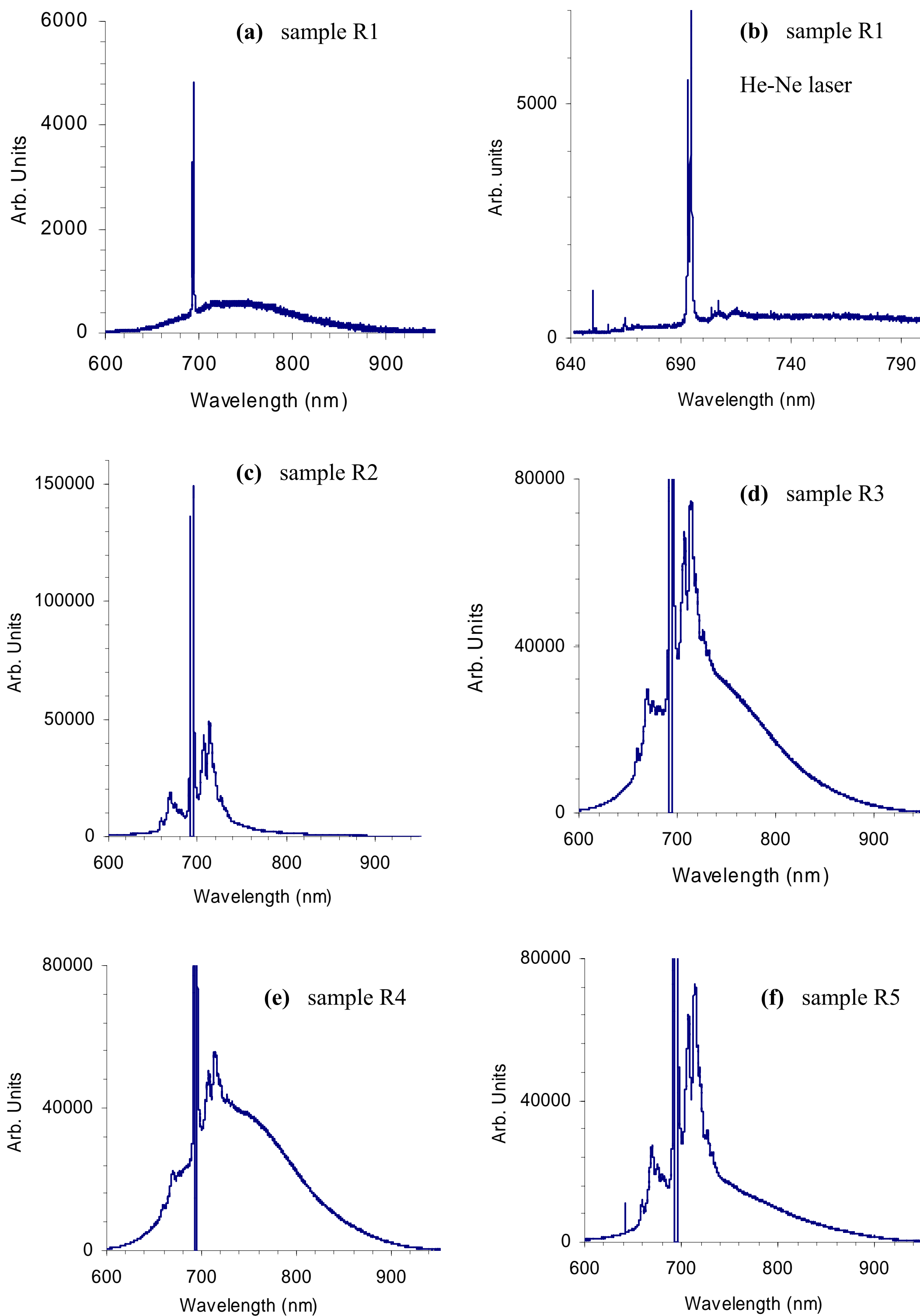

Figure 6.3. Graphs of fluorescence using a micro-Raman setup for samples R1 to R5. Graphs (a) and (b) give the spectrum of an untreated sapphire sample (sample R1) using as pump an Ar:Ion and a He:Ne laser. Graphs (c), (d), (e) and (f) give the spectrum of samples R2 to R5 all using as a pump the Ar ion laser

Figure 6.3 (a) shows the spectrum of undoped sapphire (sample R1), the spectrum shows Cr impurities in the substrates which are revealed by the double fluorescence line at 694nm. There are also traces of Ti ions in the undoped substrate as indicated by the characteristic broad fluorescence curve extending from approximately 650 to 900nm. Figure 6.3 (b) shows again the Raman spectra of undoped sapphire, using as a pump laser a Helium Neon laser emitting at 633nm instead of the usual choice of the Argon:Ion laser at 488nm. In this graph the Raman lines of sapphire can be seen at the wavelengths between 640 and 690nm and also two broader features just above 700nm. Figure 6.3 (c) shows the spectrum of Ga doped sapphire which exhibits the same lines at 694nm indicating the presence of Cr. The spectrum though is changed because features around this wavelength have appeared. Some of these features are present also in graphs (a) and (b) but are much weaker. This indicates that Ga doping is changing the lattice and the presence of Ga ions are activating or amplifying energy level transitions. Figure 6.3 (d) is the spectrum of sample R3 (diffusion of 10nm Ti film) and the fluorescence of the titanium ions can be easily distinguished, the spectrum also has the same features as the spectrum of Ga diffusion around the ruby lines. Figure 6.3 (e) is the spectrum of sample R4 (diffusion of 150nm Ti film), the fluorescence spectrum is stronger than that of sample R3 but the difference is not as significant as the thickness difference of the 10 and 150nm films would suggest. This is due to the fact that in both cases of samples R3 and R4, Ti diffuses following the case of the unlimited source (Chapter 3). Therefore the surface titanium concentrations of the two samples are approximately the same; dictated by the maximum solid solubility of Ti in sapphire. Sample R5 also has a diffusion source of Ti of 50nm, and would be expected to give similar fluorescence curve to samples R3 and R4. From Figure 6.3 (f) though, the fluorescence spectrum shows that the

fluorescence of Ti is weak; Figure 6.2 also shows this effect. As the setup is measuring the fluorescence of the ions situated near the surface this difference in fluorescence can not justified by difference in the diffusion characteristics (section 3.4.4). The fluorescence of titanium ions is most likely inhibited by the presence of Ga ions which are dominant in the lattice of sapphire due to the high solid solubility of gallium. More systematic tests are needed and future research could concentrate on revealing the origin of this effect.

6.3 Ti:Sapphire ridge waveguide lasers

6.3.1 Fabrication overview of the titanium diffused ridge samples

The fabrication sequence of the titanium-diffused ridges is identical to the sequence used for the gallium-diffused waveguides presented in section 5.2. A schematic of the whole fabrication process, from diffusion to Ion Beam Milling, is shown in Figure 6.4.

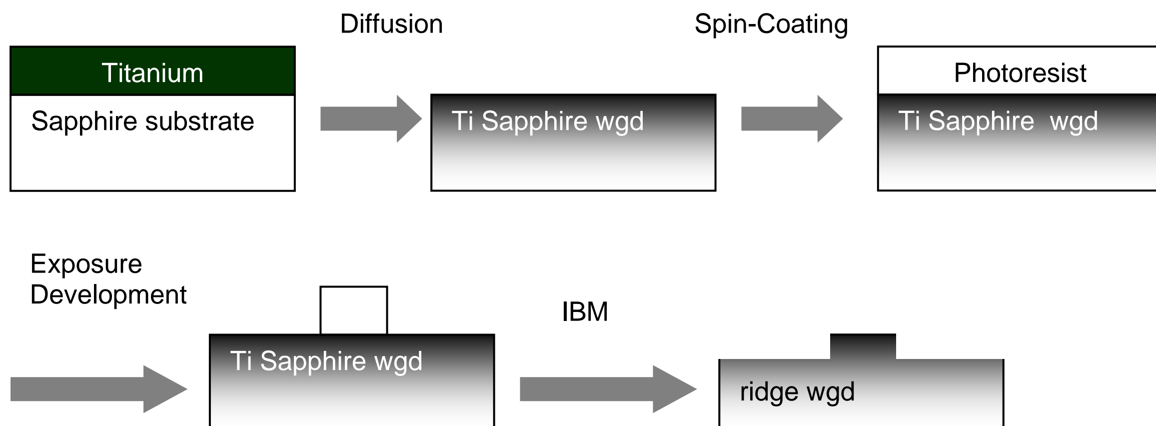

Figure 6.4. Schematic of the fabrication process for the ridge Ga waveguides

The fabrication starts with the thermal evaporation of a thin titanium film on sapphire, the thickness of the film is from 10 to 50nm. The samples were annealed at 1700^0C for durations of 1 or 2hrs using a reducing atmosphere (argon). For the annealing of samples L1-L3 a tungsten element high temperature furnace was used. The diffusion annealing for sample L4 was performed in the furnace which was also used for the fabrication of gallium waveguides (tube furnace, Lenton). Following annealing, the slab titanium sapphire waveguides were patterned using SU-8 photolithography and the pattern was transferred to the substrate using argon ion beam milling. The ridge height of the samples was 5.5-6.5μm. The width of the channels was defined by a mask with openings from 2 to 14μm and the resulting ridges exhibited widths from 5 to 20μm. Finally the titanium diffused ridge samples were end-face polished for optical characterisation. The sample parameters are summarised in Table 6.2.

Sample #	Temperature (^{o}C)	Time (hrs)	Thickness (nm)	Height (μm)	Width (μm)	Furnace
L1	1700	1	10±2	6±0.5	5-20	High temp.
L2	1700	1	30±5	6±0.5	5-20	High temp.
L3	1700	2	50±5	6±0.5	5-20	High temp.
L4	1600	2	15±2	4.5±0.5	5-20	Lenton

Table 6.2. Fabrication parameters of the laser titanium diffused ridge waveguide samples

6.3.2 Discussion of the fabrication procedure of the Ti-diffused ridge waveguides

i) Titanium diffusions

A thin diffusion source is generally used in titanium diffusion (<50nm) because of the low solid solubility of titanium in sapphire. In order to increase the refractive index change samples with more than approximately 60nm thick titanium films in sapphire were fabricated. The resulting samples had high surface roughness which increases propagation loss and causes poor adhesion of the photoresist film. Furthermore, the probability of the formation of Ti^{3+}-Ti^{4+} pairs is increased as is the probability of titanium ions situated in defect sites and not fluorescing; this leads to a material with poor figure of merit and low fluorescence.

The annealings for titanium diffusion need to be performed in a reducing atmosphere (usually argon) [8,9]. An oxygen atmosphere increases the concentration of the Ti^{4+} ions thereby adversely affecting the performance of a titanium diffused sapphire laser. A high temperature tungsten element furnace (up to 2200^0C) was used, capable of maintaining a pure argon atmosphere during the diffusions. Fast cooling increases the fluorescence of Ti:Sapphire waveguides so after the diffusion period the power to the tungsten elements was set to zero and the system was cooled down to room temperature. The thermal mass of the system permits a cooling time of approximately 3mins from 1700^0C to 100^0C.

ii) SU 8 photolithography of the planar Ti:Sapphire waveguides

The parameters for the photolithography are the same as in the case of the gallium ridge waveguides (section 5.2.2). The only difference in the case of the titanium diffused samples is that there is the extra problem of surface roughness which results

in a great difficulty in achieving a good quality SU-8 film. The samples were baked for 20-30 minutes at 120^0C after spin-coating and then left at room temperature for at least 20 min before UV exposure. After exposing for 40-50 s the sample was post exposure baked for 20 min at 120^0C and left again for 5min to cool before developing for 1min.

iii) Alignment and end-face polishing for active devices

Another characteristic of the photolithographic process for active waveguides is that the samples should be precisely aligned on the mask aligner during exposure in order for the waveguides to be normal to the end-faces. Any deviation from normality causes an increase in the loss of the waveguide laser cavity which increases the threshold and reduces the slope efficiency. The same accuracy should be applied when cutting and polishing the samples so the waveguides will be again normal to the end-faces.

6.3.3 Characterisation of the titanium sapphire ridges

i) Mode profiles and loss measurements

The coupling loss of the waveguides was measured using a He:Ne laser operating at 633nm in order to avoid any absorption due to Ti ions. Further, the measurements were performed in the same optical apparatus as that used for the laser experiments. For samples L1 to L3 the incident and output power of the waveguides was measured and the total loss (coupling and propagation losses) was found always to be more than 7dB. These samples were 3mm long and even if a 3dB/cm propagation loss is assumed, which is most likely an overestimate, the coupling loss is estimated to be 6dB. In all the measurements the waveguides exhibited coupling loss from 6 to 9dB.

Conversely the sample fabricated by the Lenton furnace, sample L4, in argon at 1600^{0}C for 2hrs, had a 3-4dB coupling loss. In Figure 6.5 the mode of a ridge waveguide of sample L3 is depicted with horizontal mode size of 18μm and vertical mode size of 7μm. The ridge waveguide measured is 18μm wide and 6μm high. As the diffusion profile of the titanium ions extends several microns more than the height of the ridges, the waveguides were leaking into a planar mode for some coupling conditions.

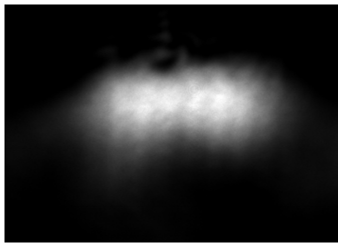

Figure 6.5 Image of a mode of a ridge waveguide of sample L3, 18μm wide and 6μm high

ii) Fluorescence measurements

The fluorescence from samples L1-L3 was measured; these samples were diffused at 1700^{0}C for 1hr and had films of titanium of 10, 30 and 50nm. Two different pump lasers were used (i) a frequency doubled solid state laser (Nd:YLF) that emits at 532nm up to 5.5W and (ii) an Argon ion laser which emitted at 488 and 514nm up to 30W. The laser beam was coupled in the waveguides using a microscope objective and micromanipulators; the output of the waveguide is collected in a monochromator using an aperture. Because the pump beam is very strong compared to the signal of the laser a series of filters is used, a cold mirror and a high-pass colour glass filter. The optical signal is detected by an avalanche photodiode and a lock-in amplifier is used to amplify the signal. For the use of the lock-in amplifier an optical chopper is

placed in the path of the optical beam, another significant use of the chopper is to avoid heating up of the sample due to the pump radiation, which significantly degrades the laser performance. The chopper blade was set to give an off:on ratio of 20:1. The experimental apparatus used is depicted in Figure 6.6.

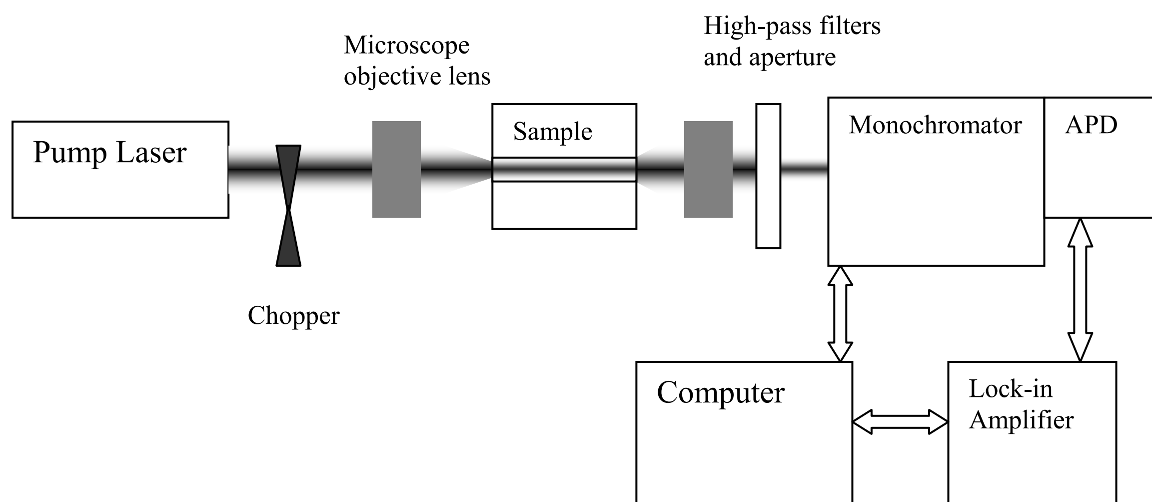

Figure 6.6. Experimental configuration used for fluorescence and laser measurements.

The measurements taken using this configuration must be corrected for the system response. In order to obtain a correction curve a white light source (tungsten lamp) was measured using an Agilent optical spectrum analyser that was recently calibrated by the manufacturer and then the same white light source was measured in the apparatus above. By dividing the two measurements a correction curve was obtained for the experimental apparatus.

Sample L3 exhibited the strongest fluorescence and the spectrum is shown in Figure 6.7. The graph is corrected for the response of the system and, as expected from theory of titanium sapphire bulk lasers, the spectrum peaks near 750nm. It is also

interesting that there is not a peak near 695nm which would be an indication of chromium impurities in the sapphire substrate. The peak near 1064nm is from the Nd:YLF crystal of the pump laser.

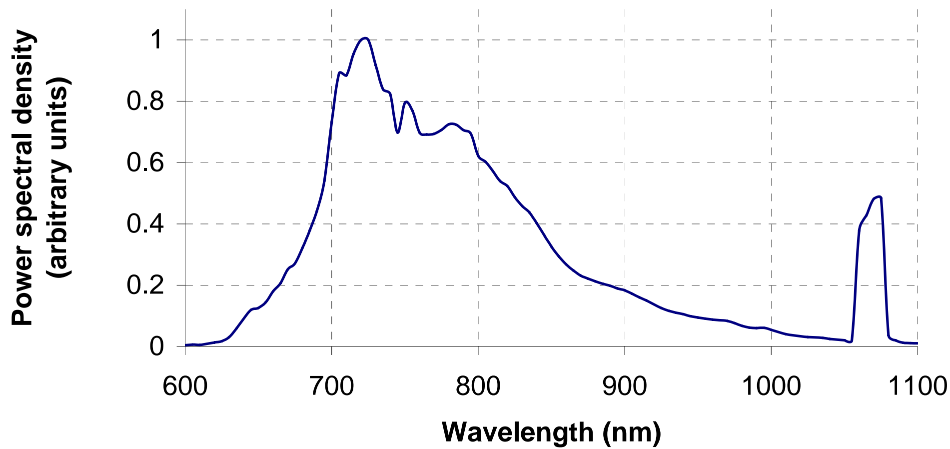

Figure 6.7. Fluorescence power spectral devsity of sample L3.

iii) Laser measurements

Following the fluorescence measurements, custom-made mirrors with thin dielectric coatings were butt-coupled to the end-faces of the samples using fluorinated liquid or a simple commercial adhesive. The mirrors used had very high reflectivity, approximately 99.9%, at the signal wavelengths from 700 to 900nm and high transmission, approximately 90%, at the pump wavelengths near 500nm. The reason for using high reflectivity mirrors is to reduce the threshold of the device as indicated from modelling of the laser threshold (included in Chapter 2). The transmission spectrum of the mirrors is shown in Figure 6.8. Figure 6.8 (a) shows on a semi-logarithmic scale the transmission of the mirrors from 400 to 1000nm and Figure 6.8 (b) shows the transmission of the mirrors over the range of wavelengths of the expected lasing output, from 700 to 900nm, in linear scale. The reflection in the signal

ranges from 99.999% to 99.7% with abrupt changes in the reflectivity which complicate the interpretation of the transmission spectrum of the device.

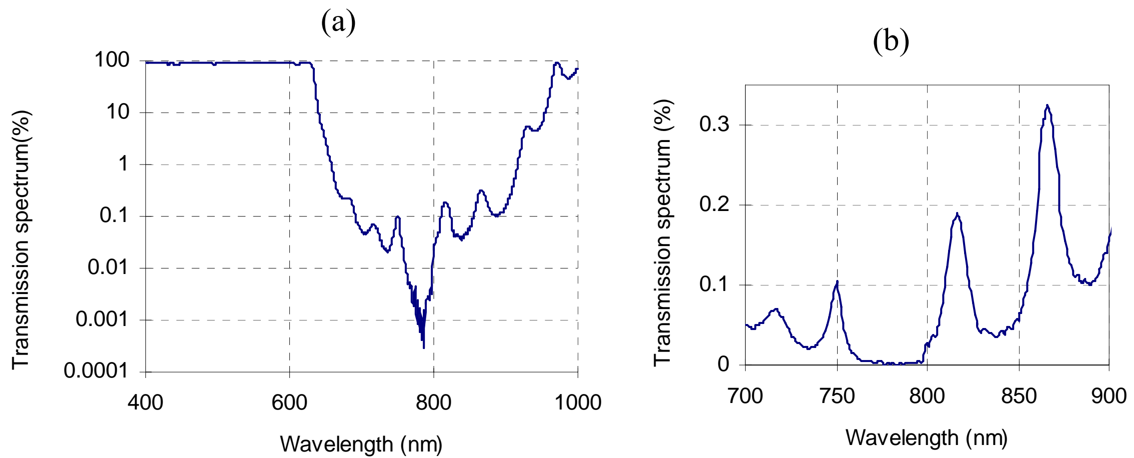

Figure 6.8. Transmission of the mirrors versus wavelength. Graph (a) shows the transmission of the mirrors in semi-logarithmic scale from 400 to 1000nm, graph (b) shows the transmission of the mirrors in the laser signal part of the spectrum (700-900nm) in linear scale.

The samples were cut and polished to a length of 3mm and the waveguides were found to be approximately 1 degree from normal. The mirrors were butt-coupled to the waveguides and the samples were tested for lasing in the apparatus shown in Figure 6.6. The pump laser power was set to be approximately 5W and the fluorescence from the waveguides was measured. Figure 6.9 shows fluorescence intensity spectra for sample L3, the graphs indicate that fluorescence could be detected in the wavelength windows where the mirrors showed higher transmission. These peaks that define the high transmission windows of the mirrors are at 750, 820 and 865nm as shown in Figure 6.8.

Following these measurements the pump power of the laser was increased to approximately 6W, which is very near the limit of this source, and coupling was optimised. The ridge waveguide measured was of sample L3, the ridge height was

6μm and the ridge width approximately 15μm. The power of the pump in the waveguide has been estimated to be between 800±100mW. In Figure 6.10 the spectrometer output for this measurement is included. A strong peak emerged near 800nm that is not at a maximum in the mirror transmission window and therefore is a strong indication of lasing action.

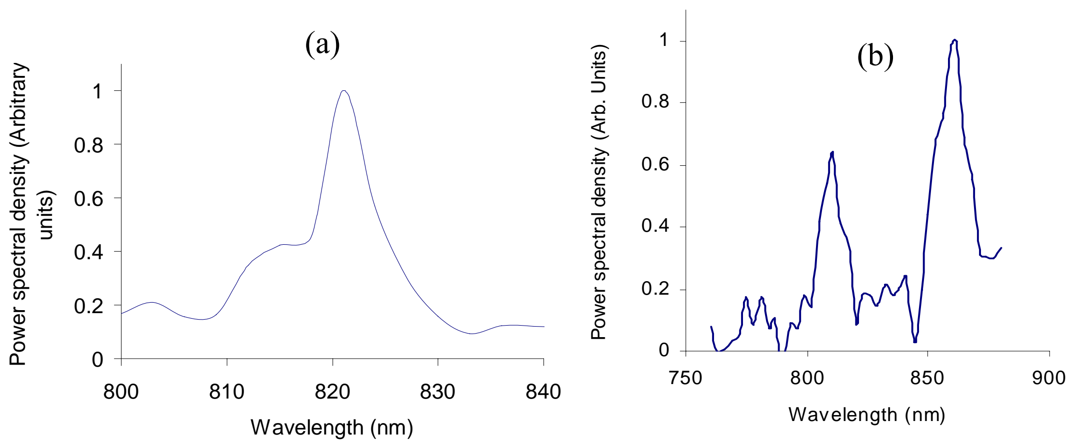

Figure 6.9. Fluorescence measurements for sample L3 with 5W of pump power on a ridge 15μm wide and 6μm high (below threshold).

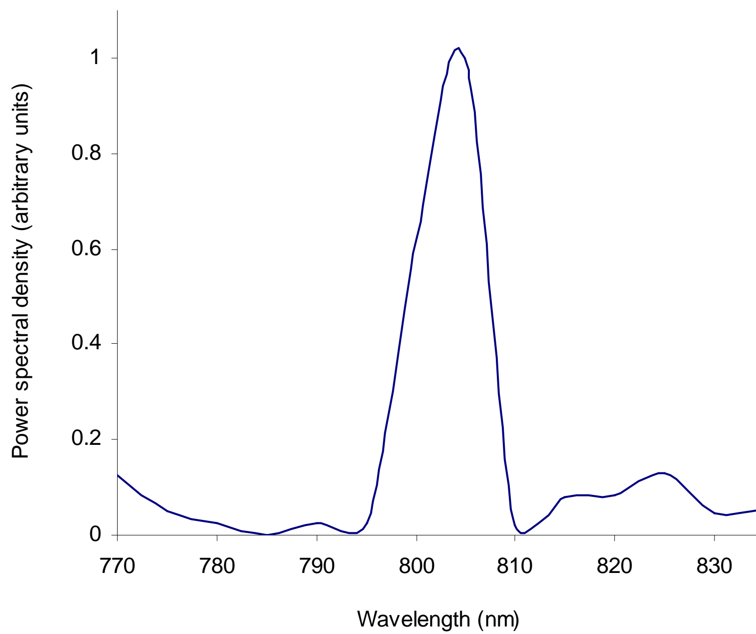

Figure 6.10. Strong peak at 800nm of sample L3, 6W of pump power on a ridge 15μm wide and 6μm high.

The spectral characterisation measurement was repeated using a similar experimental configuration. The optical part of the configuration was the same but the pump laser was an argon ion laser emitting at all lines, primarily at 488 and 514nm, and the spectrometer was a grating spectrometer using a liquid nitrogen cooled CCD camera. The spectral measurement, for a 16μm wide channel waveguide of the same sample and 8W of pump power is depicted in Figure 6.11.

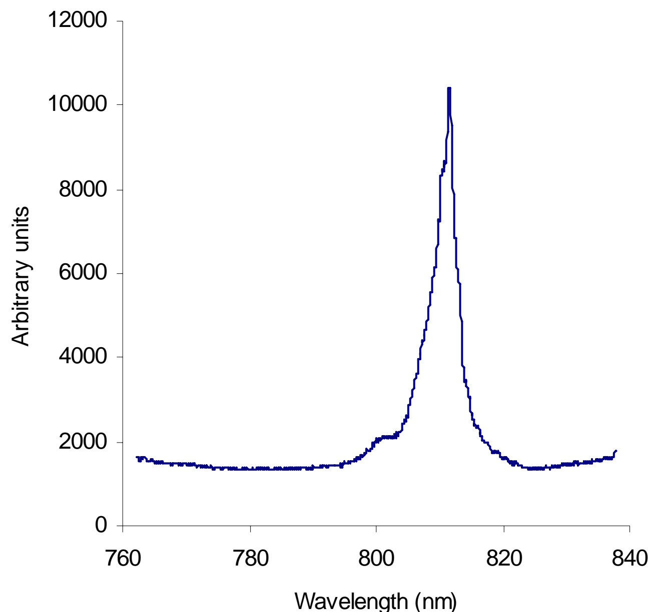

Figure 6.11 Measurement of sample L3 using an Argon:Ion laser delivering 8W of pump power and emitting at all lines. The ridge is 16μm wide and 6μm high.

6.3.4 Summary and discussion on the results of the waveguide lasers

In section 6.4.3 experimental results of the diffused Ti:Sapphire waveguide ridges were presented, which show strong evidence of lasing action. The apparatus depicted in Figure 6.6 was used for testing the samples and sample L3 exhibited a strong peak at approximately 805nm (Figure 6.10, Figure 6.11). The minimum incident pump power used in this case was 6W and according to the measured coupling loss of 8dB the power in the waveguide was calculated to be 800±100mW. The high incident

pump power causes heating in the waveguide which affects the properties of the waveguide and the gain medium. Sample L3 was the sample with the highest doping levels of Ti (50nm thick diffusion source) which resulted in a higher index change and better waveguide characteristics compared to samples L1 and L2. Sample L4, fabricated in the tube furnace exhibited lower coupling loss (3-4dB) and better waveguide mode confinement but the fluorescence characteristics were inhibited by the presence of oxygen during the annealings.

The difference in the annealing conditions between the tube furnace and the high temperature furnace is that the tube furnace has a poor control of atmosphere so oxygen is present during the annealings and also it has a much higher maximum cooling rate. Therefore the difference in the waveguide characteristics between the samples fabricated in the high temperature and the tube furnace may originate from the presence of oxygen or the higher cooling rate. Oxygen cannot be used because even if it is beneficial to the waveguide characteristics it has a detrimental effect in the fluorescence characteristics of Ti:Sapphire. A higher cooling rate though will be beneficial to both fluorescence and waveguide characteristics of the samples and may lead to samples with better lasing characteristics (section 3.3.3).

A laser simulation for a waveguide titanium sapphire device presented in Chapter 2 that relate the laser threshold to device parameters is presented here for a device using parameters as close as possible to the ones of sample L3. The mode sizes were assumed to be 15μm in the horizontal and 10μm in the vertical direction, the FOM of the samples to be approximately 100, the concentration of titanium to be 0.2wt% and the reflection of the mirrors to be 99.9%. Figure 6.12 shows the results of the

simulation regarding the threshold for a device with the aforementioned parameters. There are 4 curves having as variable the propagation loss of the device starting at 0dB/cm and reaching 3dB/cm with increments of 1dB/cm. As expected in the case of zero propagation loss, the length of the device is not affecting the threshold; all the other curves show that the optimum length of the device is approximately 0.3mm. Sample L3 gave a laser peak at a pump power of 800±100mW and had a length of 3mm corresponding to a simulated Ti:sapphire waveguide with 2dB/cm loss which gives a threshold of 700mW for a cavity length of 3mm (trace 3). The optimum length of the threshold curve is less than 0.5mm but the task to polish samples and preserve normality of the waveguides to the end face is becoming increasingly difficult as the length of the samples is reduced.

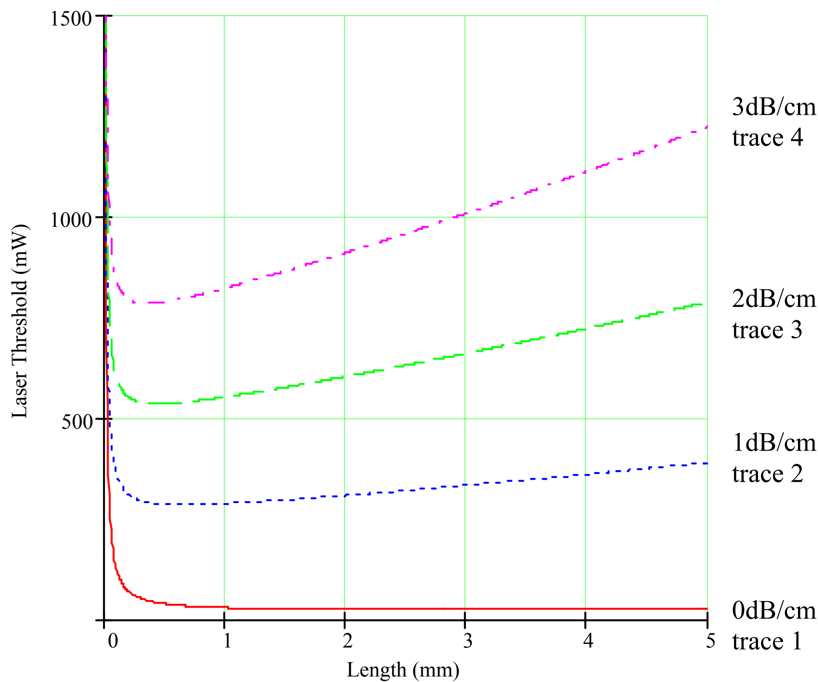

Figure 6.12 Simulation showing the threshold of the ridge waveguide laser versus the length of the device for different loss values ranging from 0 to 3dB/cm in increments of 1dB/cm.

The propagation losses of the Ti:Sapphire waveguide can be reduced by surface polishing after the annealing; minimising the roughness will have a beneficial impact to the propagation loss of the waveguides and additionally to the adhesion and the quality of the SU-8 film.

6.4 Conclusions

In this chapter, co-doping of sapphire was attempted with Ti and Ga, the first results indicate that the fluorescence of the active ions is inhibited. Further systematic study would be necessary to test the feasibility of titanium and gallium co-doping and identify a method for the realisation of Ga:Ti:Sapphire integrated devices.

The fabrication, modelling and characterisation of titanium diffused ridge waveguides in sapphire is described and the onset of laser action has been demonstrated in these structures. The active waveguides showed a strong peak at 805nm with a threshold of approximately 800mW in the waveguide. In the chapter many technological issues are identified which if resolved the quality of the waveguide and the gain medium characteristics would be greatly improved. The optimisation of these fabrication parameters can lead to a novel high potential fabrication technique for Ti:Sapphire waveguide lasers.

References to Chapter 6

1. P. Becker P et al., "Er-Diffused Ti-LiNBO3 Wave-Guide Laser of 1563 and 1576 NM emission wavelengths". *Applied Physics Letters* **61**, 1257. (1992).

2. R. Brinkmann, W. Sohler, and H. Suche, "Continuous-Wave Erbium-Diffused Linbo3 Wave-Guide Laser," *Electronics Letters* **27**, 415-417 (1991).

3. V.Apostolopoulos, "Mini-thesis," (Electronics and Computer Science, University of Southampton, 2000).

4. V. Apostolopoulos, L. M. B. Hickey, D. A. Sager, and J. S. Wilkinson, "Gallium-diffused waveguides in sapphire," *Optics Letters* **26**, 1586-1588 (2001).

5. V.Apostolopoulos, L.M.B.Hickey, D.A.Sager, and J.S.Wilkinson. "Gallium diffused ridge waveguides in Sapphire". CLEO Long Beach California. 2002.

6. Louise MB Hickey. "Report on activities in Southampton during the 1851 fellowship award." 1999.

7. "Raman tutorial". http://www.kosi.com/raman/applications/ramantutorial/ . Kaiser Optical Systems Inc., 2003.

8. L. M. B. Hickey and J. S. Wilkinson, "Titanium diffused waveguides in sapphire," *Electronics Letters* **32**, 2238-2239 (1996).

9. Louise M.B.Hickey, PhD thesis, "Ti:Sapphire waveguide laser by the thermal diffusion of Ti into sapphire", (Optoelectronics Research Centre, University of Southampton, 1998).

CHAPTER 7

CONCLUSIONS

7.1 Introduction

The work described in this thesis charts the progress towards identifying novel methods for successful fabrication of active sapphire waveguides. Ionic diffusion of Ga and Ti in sapphire was characterised and used as a doping method for the realisation of waveguides in sapphire. Ga^{3+} was identified as a metal ion which can be diffused in sapphire for the realization of passive waveguides. Further, a technological solution was developed for overcoming the problem of lateral diffusion and gallium diffused ridge waveguides were realized. Titanium diffused laser ridge waveguides were also fabricated and characterised and the potential for integration of gallium and titanium ions was investigated.

7.2 Summary of the presented work

Passive and active waveguides were fabricated by incorporation of gallium and titanium ions in sapphire by thermal diffusion. A theoretical analysis of the Ti:Sapphire waveguide laser is given in Chapter 2. A summary of theoretical principles is included that were used as design guidelines for this project. Furthermore, theoretical simulations were established which outline the potential of Ti:Sapphire lasers fabricated by thermal ionic diffusion. A grating and a coupled caivity design which are expected to lead to line-narrowed operation in an integrated device were proposed and modelled.

The diffusion study of gallium, titanium and gallium/titanium co-doping is presented (Chapter 3) with the prospect of realising titanium and gallium integrated devices. The diffusion coefficient of gallium ions in sapphire was calculated to be 3.3×10^{-17} m^2s^{-1} at 1600^0C and the diffusion coefficient of titanium ions in sapphire at 1600^0C was found to be 1.7×10^{-15} m^2s^{-1}. The diffusion coefficients obtained, for the diffusion of gallium and titanium into sapphire indicate that sapphire substrates can be readily doped to diffusion depths in the order of microns.

The fabrication and characterisation of Ga diffused sapphire passive waveguides is presented in Chapter 4 [1,2]. The optimization of the waveguide was achieved giving maximum index change of 6×10^{-3} and mode sizes of ~1μm at 488nm. These characteristics underline the potential of these devices for fabrication of active integrated circuits.

The realisation of Ga:Sapphire ridge waveguides was achieved by diffusion of gallium, photolithography and ion beam milling. The channel mode sizes obtained (as small as 2μm at 633nm) are smaller than any result achieved by patterning the diffusion source, gallium or titanium, due to the restriction of the strong lateral diffusion. Therefore the developed fabrication procedure is a general technological tool for micromachining the surface of sapphire, which solves the problem of lateral diffusion [3].

The same fabrication procedure is used for the realisation of the first Ti:Sapphire ridge waveguide laser (Chapter 6). Furthermore, sapphire laser circuits were

fabricated with titanium and gallium co-doping and the fluorescence charaterisation of the waveguides is given.

In summary, this thesis presents the successful realisation of gallium passive waveguides in sapphire, micromachining of the substrate surface for the implementation of channel waveguides and finally the first titanium sapphire ridge waveguide laser.

7.3 Proposed future research directions

7.3.1 Improvement of the Ti:Sapphire ridge waveguide laser

The work presented creates the possibility of diverse future activity as the realization of fully integrated miniature titanium sapphire laser becomes closer. The active Ti-diffused sapphire ridge waveguides showed a laser peak at 805nm and a threshold of approximately 800mW in the waveguide. Future work should target the improvement of the presented devices by identifying methods to improve the characteristics of the waveguides. The fabrication conditions should be optimised for smaller waveguide mode size and also decreased surface roughness, this will lead to lower propagation losses and therefore lower threshold and higher slope efficiency lasers.

7.3.2 Gallium and titanium co-doping

Co-doping of sapphire with Ti and Ga was realised and fluorescence measurements were carried out with the aim of characterizing the effect of co-diffusion on the spectroscopic properties of Ti:Sapphire. The first results indicate that the fluorescence of the active ions is inhibited. A further systematic study would be needed to fully

establish the feasibility of titanium and gallium co-doping and to identify a method for the realisation of Ga:Ti:Sapphire integrated devices. The feasibility of gallium and titanium co-doping needs to be pursued further as this is may be the only way to implement a truly integrated waveguide laser. Titanium diffusion in sapphire yields a small index change at the optimum concentrations for the laser [4]. Waveguides created with diffusion of the Ga^{3+} ion [2,3,5] can give smaller mode sizes which would decrease significantly the laser threshold. Design flexibility with the introduction of a second ion into sapphire will be increased as the waveguide and the gain medium characteristics can be independently controlled. Furthermore, a passive waveguide formed by introducing another ion can deliver pump power in waveguide circuits, since it would not absorb at pump wavelength. The active region could be localised in the centre of the sapphire chip which would benefit the thermal management of the device. This combined diffusion approach has been with great success in waveguide lasers fabricated in lithium niobate where erbium and titanium are the active and the waveguide ion respectively [6,7].

7.3.3 Wavelength selection and tunability

Implementing the Ti:Sapphire laser in waveguide geometry gives the opportunity of integrating wavelength selection components and realizing an all integrated narrow linewidth laser. If gallium and titanium co-doping is successful then wavelength selection mechanisms can be readily incorporated on a chip. A coupled cavity design and a grating design were modelled in Chapter 2 and both configurations are believed to be ideally suited for implementation with gallium diffused waveguides. Further, the potential of integrating tuning components such as acousto-optic or thermo-optic

elements can be investigated. The result is expected to lead to an all integrated miniature tunable laser with applications in spectroscopy and sensing.

References to Chapter 7

1. V.Apostolopoulos, L.M.B.Hickey, and J.S.Wilkinson, "Gallium diffused waveguides in sapphire," *European Conference in Integrated Optics, Paderborn, Germany* (2001).

2. V. Apostolopoulos, L. M. B. Hickey, D. A. Sager, and J. S. Wilkinson, "Gallium-diffused waveguides in sapphire," *Optics Letters* **26**, 1586-1588 (2001).

3. V.Apostolopoulos, L.M.B.Hickey, D.A.Sager, and J.S.Wilkinson. "Gallium diffused ridge waveguides in Sapphire". Conference on Lasers and Electro-Optics, Long Beach California. 2002.

4. Louise MB Hickey. "Report on Activities in Southampton during the 1851 fellowship award". 1999.

5. V.Apostolopoulos, Mini-thesis, "Gallium diffused waveguides in Sapphire" (Electronics and Computer Science, University of Southampton, 2000).

6. Becker P et al., "Er-Diffused Ti-$LiNbO_3$ Wave-Guide Laser of 1563 and 1576 nm emission wavelengths." *Applied Physics Letters* **61**, 1257. (1992).

7. R. Brinkmann, W. Sohler, and H. Suche, "Continuous-Wave Erbium-Diffused $LiNbO_3$ Wave-Guide Laser," *Electronics Letters* **27**, 415-417 (1991).